Sol-Gel Alumina Nano Composites for Functional Applications

THESIS SUBMITTED TO

COCHIN UNIVERSITY OF SCIENCE AND TECHNOLOGY
IN PARTIAL FULFILMENT OF THE REQUIREMENTS
FOR THE DEGREE OF

DOCTOR OF PHILOSOPHY
IN CHEMISTRY

UNDER THE FACULTY OF SCIENCE

BY

JAYASANKAR M.

Under the Supervision of
Dr. K.G.K. Warrier

Materials and Minerals Division
NATIONAL INSTITUTE FOR INTERDISCIPLINARY SCIENCE AND TECHNOLOGY
(Formerly Regional Research Laboratory)
Council of Scientific and Industrial Research
Thiruvananthapuram, Kerala, India – 695 019

DECEMBER 2009

DECLARATION

I here by declare that the work embodied in the thesis entitled **"Sol-Gel Alumina Nano Composites for Functional Applications"** is the results of the investigations carried out by me at Materials and Minerals Division, National Institute for Interdisciplinary Science and Technology, (formerly Regional Research Laboratory), CSIR, Trivandrum under the supervision of **Dr. K. G. K. Warrier** and the same has not been submitted elsewhere for any other degree.

J. Sankar M

Jayasankar M.

Thiruvananthapuram

December 2009

राष्ट्रीय अंतर्विषयी विज्ञान तथा प्रौद्योगिकी संस्थान
National Institute for Interdisciplinary Science and Technology
(पहले क्षेत्रीय अनुसंधान प्रयोगशाला) (formerly Regional Research Laboratory)
An ISO 9001 Certified Organisation
वैज्ञानिक एंव प्रौद्योगिकी अनुसंधान प्रयोगशाला
Council of Scientific and Industrial Research

Dr. K. G. K. Warrier Ph.D., F.IICer
Deputy Director
Head, Materials & Minerals Division
Ceramic Technology

इन्डस्ट्रियल इस्टेट डाक घर, तिरुवनन्तपुरम ६९५०१९, भारत
Industrial Estate P.O., Thiruvananthapuram - 695 019, INDIA
Phone : +91- 471- 2490674, 2515280 (O)Fax : +91- 471- 2491712
E-mail:warrier@niist.res.in Website : www.niist.res.in, http//kgkwarrier.tripod.com

CERTIFICATE

This is to certify that the work embodied in the thesis entitled **"Sol-Gel Alumina Nano Composites for Functional Applications"** has been carried out by **Mr. Jayasankar M.** under my supervision at Materials and Minerals Division, National Institute for Interdisciplinary Science and Technology, (formerly Regional Research Laboratory), CSIR, Thiruvananthapuram, in partial fulfilment of the requirements for the award of the Degree of Doctor of Philosophy in Chemistry, under the faculty of science, Cochin University of Science and Technology, Cochin and the same has not been submitted elsewhere for any other degree.

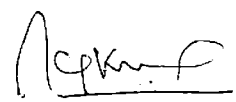

K. G. K. Warrier

(Thesis Supervisor)

Thiruvananthapuram

December 2009

राष्ट्रीय अंतर्विषयी विज्ञान तथा प्रौद्योगिकी संस्थान
National Institute for Interdisciplinary Science and Technology
(पहले क्षेत्रीय अनुसंधान प्रयोगशाला) (formerly Regional Research Laboratory)
An ISO 9001 Certified Organisation
वैज्ञानिक एंव प्रौद्योगिकी अनुसंधान प्रयोगशाला
Council of Scientific and Industrial Research

Dr. K. G. K. Warrier Ph.D., F.IICer
Deputy Director
Head, Materials & Minerals Division
Ceramic Technology

इन्डस्ट्रियल इस्टेट डाक घर, तिरुवनन्तपुरम ६९५०१९, भारत
Industrial Estate P.O., Thiruvananthapuram - 695 019, INDIA
Phone : +91- 471- 2490674, 2515280 (O)Fax : +91- 471- 2491712
E-mail:warrier@niist.res.in Website : www.niist.res.in, http//kgkwarrier.tripod.com

CERTIFICATE

This is to certify that the work embodied in the thesis entitled **"Sol-Gel Alumina Nano Composites for Functional Applications"** has been carried out by **Mr. Jayasankar M.** under my supervision at Materials and Minerals Division, National Institute for Interdisciplinary Science and Technology, (formerly Regional Research Laboratory), CSIR, Thiruvananthapuram, in partial fulfilment of the requirements for the award of the Degree of Doctor of Philosophy in Chemistry, under the faculty of science, Cochin University of Science and Technology, Cochin and the same has not been submitted elsewhere for any other degree.

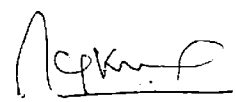

K. G. K. Warrier

(Thesis Supervisor)

Thiruvananthapuram

December 2009

CONTENTS

ACKNOWLEDGEMENTS

I have great pleasure to express my deep sense of gratitude to Dr. K. G .K. Warrier, my thesis supervisor, for suggesting the research problem and for his valuable guidance, leading to the successful completion of this work, I am greatly indebted to him for his keen interest in my work. I also wish to remember him here as the one who has lead me to this fascinating world of sol-gel science and as a never ending source of encouragement. He has been more than a guide and philosopher to me.

I express my sincere thanks to Dr. Suresh Das, Director, NIIST, Thiruvanathapuram for allowing me to use the facilities in the institute. I wish to acknowledge former Acting Director Dr. B.C.Pai and former Directors of NIIST Prof. T. K. Chandrashekar, Dr. Vijay Nair and Dr. Javed Iqbal at this juncture.

I extend my thanks to Dr. S. K. Ghosh, Dr. S. Ananthakumar, Mr. P. Krishna Pillai and Dr. S. K. Shukla for their help and support during the course of my work. I am immensely thankful to Mr. P. Mukundan for supporting my work with the instrumental facilities. Thanks are also due to Mr. P. Perumal for his kind co-operation.

I am equally indebted to Dr- Ing. Rolf Janssen, Advance Ceramics Group, Technical University of Hamburg-Harburg, Germany, for accommodating me in his group as a DAAD fellow and for providing technical and intellectual support. I thank him for his constractive suggestion, and encouragement. I would like to place on record my indebtedness to Prof. Dr. G.A. Schneider, Head of the department, Advance Ceramics Group, Technical University of Hamburg-Harburg, Germany, for his valuable suggestions and also extending to me all facilities in the department.

I wish to acknowledge the technical support from Mr. M. Geerken, Ms. A. Borchert, Mr. H. Ozcoban, Mr. R. P. Fernandes, Mr. H. Mgbemere, Mr. C. Chang, Mrs. A. Engert, Mrs. C. Neusel, Mrs. S. F. Ang, and Mrs. S. Bechtle, of Advance Ceramics Group, Technical University of Hamburg-Harburg, Germany,

I value the sincere support and encouragement rendered by my former colleagues Dr. C. P. Sibu, Dr. Rajesh Komban, Dr. K.V. Baiju, Dr. P.R. Aravind, Dr. P. Pradeepan, Mr. B. B. Anil Kumar and Mr. R. Rohith.

I wish to thank my present colleagues Mrs. Smitha Ajith, Mr. Anas, Mr.Vinod Kumar, Mr. Sanoop, Mr. Sankar Sasidharan, Mr.Mirash, Mr. Divish, Ms. Sumalatha, Ms. Athria, Mrs. Smitha, Mrs. Manju, Ms. Jaimy, Mrs. Jyothi, and Ms. Sreeremya, who helped me directly or indirectly during the tenure of my work. I am thankful to all my

friends especially, Mr. P. Shajesh and Mrs. P. N. Remya for their friendship and help during my days at NIIST.

I always cherish the warm friendship of Dr. Surendran, Dr. Mahesh, Dr. Shayam Krishnan, Dr. Suboth and Dr. Jyothish. I would like to express my sincere thanks to former project student Ms K. P. Hima for providing value inputs to my work.

I extend my gratitude to Mr. Guruswamy, Mr. Chandran for instrumental support. I wish to acknowledge all scientists of MMD for their kind co-operation.

I acknowledge the financial assistance from the CSIR, DST, New Delhi and DAAD Bonn, Germany.

I am thankful to my wife Indu for her help and support for the thesis writing. Finally, I remember with gratitude my family members who were always a source of strength and support and all who are near and dear.

Jayasankar M.

Thiruvananthapuram

December 2009

friends especially, Mr. P. Shajesh and Mrs. P. N. Remya for their friendship and help during my days at NIIST.

I always cherish the warm friendship of Dr. Surendran, Dr. Mahesh, Dr. Shayam Krishnan, Dr. Suboth and Dr. Jyothish. I would like to express my sincere thanks to former project student Ms K. P. Hima for providing value inputs to my work.

I extend my gratitude to Mr. Guruswamy, Mr. Chandran for instrumental support. I wish to acknowledge all scientists of MMD for their kind co-operation.

I acknowledge the financial assistance from the CSIR, DST, New Delhi and DAAD Bonn, Germany.

I am thankful to my wife Indu for her help and support for the thesis writing. Finally, I remember with gratitude my family members who were always a source of strength and support and all who are near and dear.

Jayasankar M.

Thiruvananthapuram

December 2009

Preface

Ceramic matrix composites combine reinforcing ceramic phase with a ceramic matrix to create materials with new and superior properties. The primary goal of the ceramic reinforcement is to enhance characteristics such as toughness, hardness, electrical conductivity, thermal conductivity, thermal expansion coefficient and thermal shock resistance. The combination of these characteristics makes ceramic matrix composites attractive alternatives to traditional processing industrial materials such as high alloy steels and refractory metals.

The properties of ceramics are determined by the properties of each phase present in the sample. There are several factors that determine the phase distribution and how they operate in ceramic systems. Preparation methods also play a key role in the properties of sintered ceramics. The increasing industrial application of nanocomposites related to thermal, electronic, machinable and bioceramics fields have generated considerable interest in developing nanocomposites through novel methods like sol-gel core shell approach in addition to solid state method.

The thesis entitled **"Sol-Gel Alumina Nano Composites for Functional Applications"** investigate sol-gel methods of synthesis of alumina nanocomposites special reference to alumina-aluminium titanate and alumina-lanthanum phosphate composites. The functional properties such as thermal expansion coefficient and thermal shock resistance, machinability of

composites as well as thermal protection are highlighted in addition to novel approach in synthesis of composites.

A general introduction of alumina matrix composites materials, followed by brief coverage of alumina-aluminium titanate and alumina-lanthanum phosphate composites is highlight of the first chapter. The second chapter deals with the sol-gel synthesis of aluminium titanate and alumina–aluminium titanate composite. The synthesis of machinable substrate, based on alumina and lanthanum phosphate forms the basis of the third chapter. The fourth chapter describes the sol-gel coating of mullite on SiC substrate for the possible gas filtration application.

Abbreviations

DTA	Differential Thermal Analysis
FTIR	Fourier Transform Infrared
PCS	Photon Correlation Spectroscopy
TGA	Thermo Gravimetric Analysis
TMA	Thermo Mechanical Analyser
TEM	Transmission Electron Microscopy
PVA	Poly Vinyl Alcohol
TEOS	Tetraethyl Ortho Silicate
SEM	Scanning Electron Microscopy

Chapter I

An Introduction to Alumina Matrix Composites, Sol-Gel Approach and the Present Work

1.1 Introduction to Composites: An Overview

Ceramic materials are generally high temperature inorganic compounds such as oxides, nitrides, carbides, boride and structurally stable system.[1,2] Ceramics are generally classified as conventional or traditional ceramics which consist of clay and clay based materials, and high-tech or advance ceramics which are from synthetic raw materials and having specific structural and functional properties.[3] The major attraction of structural ceramics has always been the capability of operating at temperatures far above those of metals. Structural applications include engine components, cutting tools and chemical process equipments. Electronic applications for ceramics with low coefficient of thermal expansion and high thermal conductivity include superconductors, substrates, magnets, and capacitors.[4]

Ceramic matrix composites were developed to overcome the intrinsic brittleness and lack of reliability of monolithic ceramic, with a view to introduce ceramics in structural parts used in severe environments, such as rocket and jet engines, gas turbines for power plants, heat shields for space vehicles, fusion reactor first wall, and heat treatment furnaces.[5] Ceramic matrices can be categorized as either oxides or non-oxides and in some cases may contain residual

metal after processing.[6,7] Some of the more common oxide matrix includes alumina, silica, and mullite. Of these, alumina and mullite have been the most widely used because of their in service thermal and chemical stability and their compatibility with common reinforcements.

Ceramic matrix composites combine reinforcing ceramic phase with a ceramic matrix to cerate materials with new and superior properties. The primary goal of the ceramic reinforcement is to enhance characteristics such as toughness, electrical conductivity, thermal conductivity, thermal expansion coefficient, thermal shock resistance and hardness of the composites.[8,9] The combination of these characteristics makes ceramic matrix composites attractive alternatives to traditional processing industrial materials such as high alloy steels and refractory metals. The properties of ceramics are determined by the properties of each phase present in the sample. There are several factors that determine the phase distribution and how they operate in ceramic systems. Preparation methods also play a key role in the properties of sintered ceramics. Secondary phases in ceramics have several advantages. Such phases can produce important microstructural modifications and change all the properties of the monolithic materials. For example, phases that form a strong interface with the matrix could drastically reduce the creep rate at high temperatures.

1.1.1 Composites-Definition

There is no universally accepted definition of composite materials. Definition in the literature differs widely. A working definition of composite

materials which can take into account both the structural form and composition of the material constituents follows. "A composite material is a material system composed of a mixture or combination of two or more macroconstituents differing in form and/or material composition and that are essentially insoluble in each other".[10]

1.1.2 Constituents of Composites

In principle, composite can be constructed of any combination of two or more materials, whether metallic, organic, or inorganic. Although the possible material combinations in composites are virtually unlimited, the constituent forms are more restricted. Major constituent forms used in composite materials are fibers, particles, laminae or layers, flakes, fillers and matrixes. The matrix is the body constituent, serving to enclose the composite and give it its bulk form. The fibers, particles, laminae, flakes and fillers are the structural constituent, they determine the internal structure of the composite. Generally, but not always, they are the additive phase.

1.1.3 Classification of Composites

Based on the nature and structure of composites, a working classification of composites can be made. Several classification systems have been used, including classification (1) by basic material combinations, e.g. metal-organic or metal-inorganic, (2) by bulk-form characteristics, e.g. matrix systems or laminates, (3) by distribution of the constituents, e.g. continuous or discontinuous and (4) by

function, e.g. electrical or structural. The classification system mainly used is based on the form of the structural constituents. This gives five general classes of composites **Figure 1.**

1. Fiber composites composed of fiber with or without a matrix.
2. Flake composites, composed of flat flakes with or without a matrix.
3. Particulate composites composed of particles with or without a matrix.
4. Filled (or skeletal) composites, composed of a continuous skeletal matrix filled by a second materials.
5. Laminar composites, composed of layer or laminar constituents.

The fiber type composite has evoked the most interest among engineers concerned with structural applications. Initially most work was done with strong, stiff fibers of solid, circular cross section in a much weaker, more flexible matrix. Then development work disclosed the special advantages offered by metal and ceramic fibers. In structural application flakes appear to offer several advantages over fibers. For example, as long as the flakes are parallel, flake composite can provide uniform mechanical properties in the plane of flakes. Flakes composites also have a higher theoretical modulus than fiber composites and can be packed closer and with fewer voids. Compared with fibers, flakes are relatively inexpensive to produce and can be handled in batch quantities.

Particulate composites have an additive constituent which is essentially one or two dimensional and macroscopic. Particulate composites differ from the fiber and flake types in that distribution of the additive constituent is usually random

rather than controlled. In the filled composites, there is a continuous 3D structural matrix, infiltrated or impregnated with a second phase filler material. The filler also has a 3D shape determined by the void shape. The matrix itself may be an ordered honeycomb, a group of cells, or a random sponge like network of open pores. Laminar or layered composites have been made up of films or sheets and they are easier to design, produce, standardize and control than other type of composites. The most successful application of the laminar principle has been the development of sandwich materials. Composite materials have many characteristics that differ from those of more conventional engineering materials. Most common engineering materials are homogeneous and isotropic. In contrast, composite materials are often both in homogeneous (or heterogeneous) and non isotropic (or anisotropic).

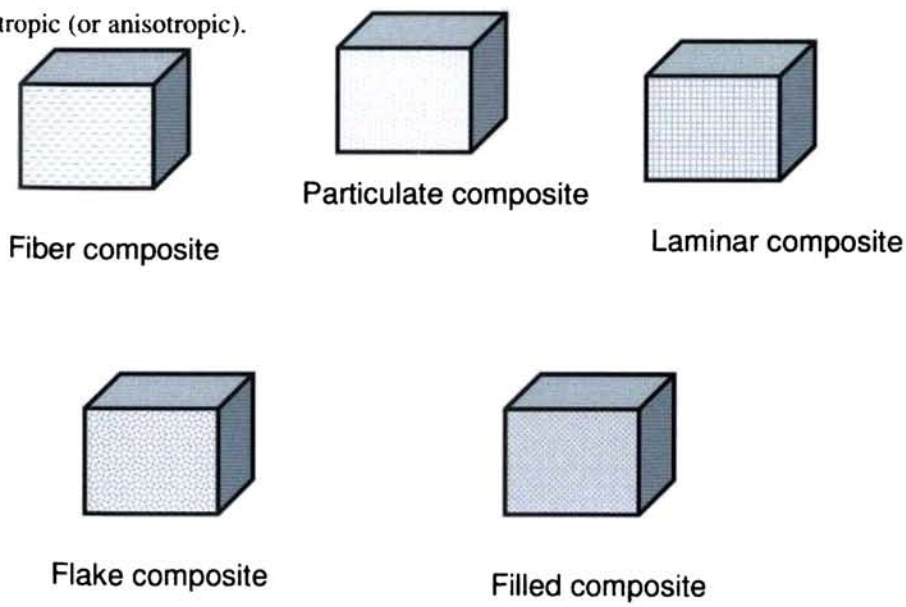

Figure 1. Classes of composites[10]

1.2 Alumina

Alumina (Aluminium oxide, Al_2O_3) is mostly prepared from mineral bauxite (Al_2O_3+ SiO_2+ TiO_2+ Fe_2O_3) by the Bayer process, which involves the selective leaching of the alumina by caustic soda, followed by the precipitation of aluminium hydroxide.[11] There are a lot of applications for alumina. Alumina is mainly used in ceramic, refractory and abrasive industries. High thermal conductivity, hardness, wear resistance and electrical resistivities are some properties of alumina that are considered better than other substances. Alumina (Al_2O_3) exists in various crystallographic forms α, β, δ and γ.[12] The most stable crystallographic form of alumina is α- Al_2O_3 which exists in corundum crystal structure.[13]

Table 1. Some of the properties of alumina[14]

Crystal structure	Hexagonal
Theoretical density	3.97 g/cm^3
Thermal expansion coefficients	7.2-8.6 × 10^{-6} /K
Thermal shock resistance	500 K^{-1}
Thermal conductivity	27.2 W/mK at 400K
Melting point	2000 - 2050 °C
Vickers Hardness	18-23 GPa
Facture toughness	2.7-4.2 MPa.m $^{1/2}$
Young's modulus	380 GPa

Some of the properties listed above can be varied according to the starting material and processing method.

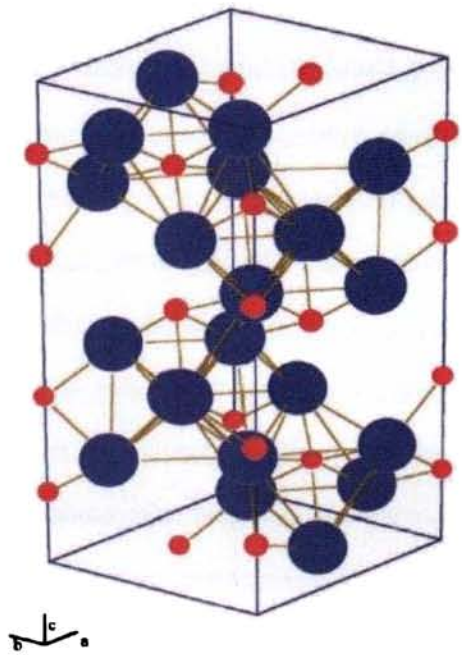

Figure 2. Crystal structure α-Alumina (α- Al_2O_3). The ionic radii are proportional to 0.55 A° for Al^{3+} (red) and 1.35 A° for O^{2-} (blue) (**Adopted from the reference: Acta. Crystallographica, B49, 1993, 937-980**)

The crystal structure of α- Al_2O_3 has hexagonal cell containing six formula units per unit cell with lattice parameters 'a' and 'c' of 4.754 and 12.982 A° respectively. The structure of α- Al_2O_3 consists of planes of close-packed oxygen ions in the **A-B-A-B** sequence interleaved with planes of aluminium ions in an **a-b-c-a-b-c** sequence. In each aluminium plane, the aluminium ions occupy only

two-thirds of the available octahedral sites. In this way, α- Al_2O_3 maintains charge neutrality with four Al^{3+} for every six O^{2-}. A hexagonal crystallographic cell is formed from the repeated sequence **A-a-B-b-A-c-B-a-A-b-B-c**.[15]

1.3 Literature Survey of Alumina Matrix Composites

Alumina ceramics are widely used as structural materials because of their high melting point and excellent mechanical properties, as well as electrical resistance and chemical durability.[16] The application of alumina range from high-speed cutting tools, dental implants, electrical and thermal insulators, wear resistance parts and coatings. It is anticipated that alumina-based nano-sized ceramic composites will demonstrate novel and favorable properties in comparison with their micro-sized crystalline counterparts.[17] Alumina forms composites with other materials ranging from metals, intermetallics, to ceramics. The starting materials for composites are carefully selected such that even if a reaction occurs between them, at least two phases must be distinct in the material and the interaction of these phases in the matrix would not affect the properties of the matrix. Some of the commonly used alumina matrix composites are described below.

To increase the fracture toughness of alumina, zirconia is added as a second phase material. Clausen et al. published the first work related to the high fracture toughness of composite in the Al_2O_3-ZrO_2 system by transformation toughening. The fracture toughness of alumina can be increased from 4 to 7 MPa $m^{1/2}$ by the

addition of ZrO_2 contents between 10 to 20 wt%.[18] A fine grained Al_2O_3-20%ZrO_2 composite showing super plasticity at 1500 °C was reported by Wakai et al.[19]

Alumina-SiC nanocomposite, having very high hardness and fracture toughness was prepared by Nihara.[20] This composite also show improvement in strength, creep resistance and wear resistance over monolithic alumina. The improvements in mechanical properties appears as a results of incorporation of the inert nanosized SiC particles by reducing the flaw size or by residual stress due to thermal expansion mismatch between the alumina matrix and the SiC inclusion. The conventional processing technique used is the solid state mixing of alumina and SiC. The synthesis of alumina-SiC by sol-gel route was reported by Haaland et al.[21] The processing of alumina-SiC composite by pre coating of SiC was also reported by Hareesh et al.[22] But the Al_2O_3 –SiC nanocomposite is a thermodynamically metastable system at elevated temperatures in air or in presence of oxygen the SiC will undergo oxidation at a temperature above 1000 °C by preferential formation of silica.

Alumina–cerium oxide nanocomposite electrolyte for solid oxide fuel cell application is also reported.[23] Kumar et al. reported synthesis of yttria and ceria toughened alumina composite for cutting tool application.[24] Gu et al. reported the synthesis of silica-alumina composite membranes for hydrogen separation by chemical vapour deposition method (CVD). A thin layer (30-40 nm) of a dual-

element silica-alumina composition was deposited on a porous alumina support by chemical vapour deposition in an inert atmosphere.[25]

Alumina- mullite nanocomposite has high strength, creep resistance, good thermal and chemical stability, and low dielectric constant.[26,27] Alumina–mullite ceramics with a low content of a glassy phase may have a high potential for armour and wear resistance applications.[28] In recent years research has been focused to reduce the inherent brittleness of the mullite ceramics. One way is to make alumina-mullite fiber composite. The important applications of such composite are components and structures for gas turbine engines, burner tubes and heat shields for re-entry space vehicles.[29]

The emergence of carbon nanotubes (CNTs) for toughening ceramics also needs to be mentioned, seeing the unsurpassed mechanical properties of CNTs. Efforts for reinforcing ceramics with CNTs are being made but significant improvements are still uncommon. Recent literature shows that there are few interesting studies of carbon nanotube reinforced ceramic matrix composites. Chang et al. fabricated the alumina matrix composites containing 5-20 vol% of multiwall carbon nanotubes. An improvement of 24% on fracture toughness compared with that of the single phase alumina was observed. The effective utilization of nanotubes in composite applications depends strongly on the ability to disperse CNTs homogeneously throughout the matrix. Sung et al. reported an effective way to improve the mechanical properties of alumina-carbon nanotube composite by adjusting the surface properties of alumina and that of carbon

nanotube by a colloidal processing route. The addition of only 0.1 wt % carbon nanotubes in alumina composites increases the fracture toughness from 3.7 to 4.9 MPa $m^{1/2}$, an improvement of 32% compared with that of the single-phase alumina.[30] Wang et al. reported the toughening effect of adding single-wall carbon nanotubes to Al_2O_3 composites.[31] More research needed in this area as well as to strengthen ceramic-CNT interface strength, dispersion and survival of CNT after high temperature sintering.

Alumina is widely used as a biomaterial because of its high bio-compatibility and its good mechanical properties except toughness. Al_2O_3-ZrO_2 composite is also used in orthopedics application. Alumina offers better tribological characterstics and high chemical-physical stability, but poor toughness. On the other hand, zirconia is tougher and less stable.[32] Zirconia toughened alumina has been regarded as the next generation orthopaedic graft material due to its excellent mechanical properties and biocompatibility. Porous ZTA (zirconia toughned alumina) is reported ceramics with good interconnectivity can potentially be used as bone graft for load bearing applications.[33] It was also reported that the mechanical properties of Al_2O_3 like strength and fracture toughness can be improved by the addition of TiN. This composite can be used as better wear resistance composite in the living environments.[34] Leivo et al. reported that osteoblast response to sol–gel derived high-purity aluminosilicate ceramic coatings, on alumina substrate.[35]

The thermal shock resistance of Al_2O_3 (500 °C) can be improved by the addition of TiC. You et al. studied the influence of Al_2O_3 and TiC, starting particle size on the thermal shock resistance of the Al_2O_3-TiC composite. Decreasing grain size can improve the thermal shock resistance and increase in density improves thermal shock resistance even further. The critical thermal shock temperature difference (ΔT_c) of Al_2O_3-TiC composite is 100 °C higher than the T_c of monolith alumina.[36]

Thermal shock behaviour of an alumina/zirconia functionally graded material is also reported which was prepared by electrophoretic deposition. Thermal shock resistance of particular layers was studied using indentation-quench method. The results were compared to those obtained from a reference non-layered composite material, prepared by the same fabrication technique.[37] The possibility of improving the thermal shock behaviour of alumina under mild thermal conditions by the addition of sub-micron-sized and homogeneously dispersed aluminium nitride (AlN) particles is reported by Nieto et al.[38] The thermal shock resistance of alumina-mullite (5-15 vol%) composites with 6 vol% tungsten carbide[39] have been studied and compared with reference alumina ceramic.[40]

The alumina- aluminium titanate (AT) composite offers high temperature stability and high thermal shock resistance. Alumina is excellent for mechanical properties but has poor thermal shock resistance. On the other hand, aluminium titanate is superior in thermal shock but lacks mechanical toughness. Generally,

the alumina- aluminium titanate composite can be prepared by solid-state reaction, infiltration, and sol-gel reaction methods.

1.4 Alumina-Aluminium titanate Composites

Aluminium titanate (Al_2TiO_5, AT) is a promising engineering material because of its low thermal expansion coefficient, excellent thermal shock resistance, good refractoriness, and nonwetting with most metals. AT has a high melting point of 1860 °C, and a highly anisotropic thermal expansion (i.e., widely differing expansions along the crystallographics axes) of about $\alpha_a = 10.9 \times 10^{-6}\ K^{-1}$, $\alpha_b = 20.5 \times 10^{-6}\ K^{-1}$, $\alpha_c = -2.7 \times 10^{-6}\ K^{-1}$.[41] AT exists in two allotropic forms α and β and the low temperature phase is β Al_2TiO_5.[42] The extreme anisotropy causes the formation of internal stress within large AT grains. This results in severe microcracking while cooling from high temperature which is attributed to its anisotropic coefficient of thermal expansion.[43] AT exhibits a bulk CTE ranging from about -3 to +9 $\times 10^{-7}$ / °C depending on the grain size and degree of microcracking. Larger grain growth and subsequent microcracking, however, produce a low strength material. Each Al^{3+} or Ti^{4+} cation is surrounded by six oxygen ions forming distorted oxygen octahedra. These AlO_6 or TiO_6 octahedral form (001) oriented chain is weakly bonded by shared edges. Such a structure is responsible for the thermal expansion anisotropy that leads to the generation of localised internal stresses and microcracking during cooling from the sintering temperature. This display of microcracking is believed to be grain-size dependent

and is responsible for imparting poor mechanical strength and low thermal expansion coefficient but outstanding thermal shock resistance.[44] Thomas and Stevens et al. in 1993 reported that the grain size of aluminium titanate can be controlled by the addition of MgO and ZrO_2.[45] The presence of spinel or zirconia serves to inhibit grain growth and reduce microcracking. Hamano et al. reported that introducing additives like MgO and SiO_2 could increase the strength of AT.[46] Addition of 5% MgO, Fe_2O_3 or ZrO_2 has also been shown to improve the bending strength of AT.[47]

Freudenberg et al. has studied the formation of Al_2TiO_5 in an equimolar Al_2O_3-TiO_2 powder mixture of small particle size and moderate purity. Two reaction stages were identified during isothermal treatment around 1580 K.[48] Stamenkovic prepared aluminium titanate in 1989 by heating single oxides (mechanically mixed) with an excess of 2 wt% MgO at 1450 °C. The composite ceramics built from aluminium titanate matrix and rutile as a dispersed phase was obtained by sintering at 1500 °C and hot pressing at 1350 °C. Hot pressed Al_2TiO_5-TiO_2 ceramics reached a density level of over 96% of the theoretical density, contained low intergranular porosity and a fine-grained structure, the mean grain diameter was 3-8 μm and no size change with TiO_2 content was noticed.[49] Wohlfromm et al. reported that Al_2TiO_5 formation in Al_2O_3/TiO_2 multilayer composites obtained by slip casting has been studied in the temperature interval ranging from 1200 to 1450 °C. It has been found that nucleation plays a fundamental role in Al_2TiO_5 formation.[50] Segadaes et al. reported the submicron

Al_2TiO_5 powders through combustion synthesis technique, using the corresponding metal precursors-urea mixtures.[51] Ibrahim et al. synthesied aluminium titanate via the urea formaldehyde route. Nano particle size of tialite (aluminium titanate) was prepared through resin formation of 1:2:2 urea, formaldehyde and ethylene glycol, respectively.[52]

Advanced AT ceramics have been prepared from nanosized reactive powders to improve thermal and mechanical properties and sinterability.[53,54,55] Takahashi et al. reported that AT ceramic doped with alkali feldspar ($(Na_{0.6}K_{0.4})AlSi_3O_8$), exhibited an extremely low thermal expansion coefficient, comparable to undoped AT ceramics and high thermal stability, high refractoriness up to 1800 °C and relative by large flexure strength (46.8 MPa).[56] Recently Korim reported effect of Mg^{2+} and Fe^{3+} ion on the formation mechanism of aluminium titanate.[57]

The alumina-aluminium titanate composite exhibits functional as well as structural properties for application such as thermal barrier coating, exhaust filter components for diesel engines and high temperature ceramic substrates.[58] Studies show that the addition of aluminium titanate to alumina results in improved flaw tolerance due to induced residual stresses by virtue of the thermal expansion mismatch between alumina and aluminium titanate.[59] Increasing content of aluminium titanate particles of controlled size would improve the thermo-mechanical response of the composite.[60]

Hasselman and co-workers reported synthesis of alumina-aluminium titanate composite made by directed metal oxidation process.[61] Aluminium alloy powder was blended with stiochiometric ratio of Al_2O_3 and TiO_2, in a proprietary composition incorporating stabilizers, which when reacted in air gave a porous alumina-reinforced aluminium titanate composite. The density was approximately 2.6 g/cm^3, with a pore content of about 50%. The mean grain size is of the order of 10 μm. The microstructure also shows the presence of microcracks.

Usually alumina-aluminium titanate composite is synthesised by solid state reaction between alumina and titania.[62,63] However, the high processing temperatures (> 1600 °C) result in heterogeneous microstructure and abnormal grain growth in addition to the presence of unreacted residual titania phase. Dense and microcrack-free Al_2O_3/Al_2TiO_5 composites (10, 30 and 40 vol.% of Al_2TiO_5) were prepared by colloidal filtration and reaction sintering, using alumina and titania as starting powders which was sintered at 1450 °C but the average grain size was above 5 μm for 10% addition of aluminium titanate.[64] Manurung et al. studied the effect of β spodumene (maximum 15 wt %) addition on the thermo-chemical reaction of alumina-aluminium titanate composite and concluded that β spodumene addition less than 5 wt% results in aluminium titanate formation commencing at 1380 °C.[65] Green compacts made of alumina powder covered by titanium isopropoxide precursor followed by heat treatment at 1300 °C resulted in high density alumina-20 vol % of aluminium titanate composite. However,

composites with larger second phase contents (20-40 vol%) gave lower densities (95% of theoretical).[66] Alumina-aluminium titanate was synthesized by in-situ reaction using Fe_2O_3+ $FeTiO_3$ as stabilizer for aluminium titanate decomposition, was sintered at 1450 °C.[67] Park et al. reported the effect of starting powder on the morphology and grain growth of alumina-aluminium titanate, depending on the composition of starting powders, various Al_2TiO_5 morphologies, such as rod-like, polyhedron-like, and irregular shape were observed.[68]

If alumina is present as an additive in the composite system, it will affects the microstructure and bending strength of aluminium titanate. Similarly if aluminium titanate is present as an additive in the composite system, the mechanical and thermal properties of alumina will be influenced. Also, the more efficient and flexible sol-gel method in view of the high order of homogeneity of phases has not been subjected to any detailed investigation for the preparation of these nanocomposites.

1.4.1 Thermal Properties

Investigation into other properties of alumina-aluminium titanate like thermal expansion coefficient and thermal shock resistance are reported and the data are provided in the **Table 2.**[69] Most of solid materials expand on heating and contract when cooled. In many material, linear coefficient of thermal expansion is anisotropic in nature. Aluminium titanate exhibits a bulk CTE range from about 1 $\times 10^{-6}$ / °C which is very low compared to alumina.

Table 2. Thermal expansion coefficient

Materials	Thermal expansion coefficient / °C X 10^{-6}
Silica	0.55
ZrO_2	10.33
SiC	4.0
Al_2TiO_5	1.0

1.4.2 Thermal Shock Resistance

Aluminium titanate shows better thermal shock compared to alumina due to the low thermal expansion coefficient. Thermal shock resistance depends on multiple parameters. It depends not only on size and shape of samples, but also on thermal, physical and mechanical properties of the material.[70] In order to increase thermal shock resistance of materials they can be reinforced by strong filament monocrystals (whiskers) or be strengthened by other methods.[71] The thermal shock resistance of ordinary alumina ceramics cannot withstand an 800 °C quench into a cold airflow.[72]

Despite these positive results, research aimed at increasing thermal shock resistance of ceramics by reinforcements suffers an obvious disadvantage, it does not seek to decrease the level of stresses from thermal shock. The level of thermal shock stresses that appear in a solid body is directly proportional to the thermal expansion coefficient (TEC) and Young's modulus and increases with the

Poisson's ratio.[73] Decreasing the last two values is neither easily accomplished nor desirable. Decreasing the TEC, on the other hand, is desirable in every respect, as long as it does not affect other properties, and can be achieved by introducing additives that possess low or negative values of TEC into the initial ceramic.

The maximum temperature increment that the material can stand without fracture, T_c is given by,

$$T_c = k\,\sigma_f/E\alpha$$

Where k= conductivity, σ_f = strength, E= Young's modulus, α= thermal expansion coefficient.

1.4.3 Mechanical Properties: Hardness, Young's modulus and Toughness

The problem which limits the use of aluminium titanate as a structural ceramic material is attributed to the extensive microcracking occurring during cooling the sintered material which also reduces the mechanical strength. Buch et al. explained that the microcracks were associated with thermal anisotropy.[74] Ohya et al. explained the grain boundary microcracking of AT by measuring the change in the length of the sample and acoustic emissions during heating and cooling.[75] They suggested that the critical grain size of AT is dependent on the sintering temperature and the critical grain size increases with temperature. The presence of extensive cracks severely lowers the mechanical strength of aluminium titanate, and the corresponding data are provided in the **Table 3**.

Table 3. Mechanical properties

Material	Strength (MPa)	Hardness (GPa)	Toughness (MPa.m $^{1/2}$) Indentation
Al_2O_3	364	19	3.9±0.3
Al_2TiO_5	15	5	1.5±0.3
Al_2O_3 -10 Al_2TiO_5	360	17	3.5±0.2
$LaPO_4$	130	5	1.0±0.1

1.5 Alumina-Lanthanum phosphate Composites

Alumina, an amphoteric oxide (exhibiting both basic and acidic properties), is chemically inert with a few oxides. $LaPO_4$ is monoclinic, it belongs to a large structural family which includes chromates, vanadates, selenates and other phosphates. In $LaPO_4$ phosphorus is 4 co-ordinated in a distorted tetrahedral environment, La is 9 co-ordinated by O in an unusual arrangement while O is 3 or 4 co-ordinated to 2 or 3 La and 1P.[76] The density of $LaPO_4$ is 5.13 g/cm^3. Interest in monazite ceramics during the eighties was due to its high temperature stability, high melting point (> 1900 °C) higher than that of alumina (Al_2O_3), low thermal conductivity and diffusivity.[77] Later, in mid nineties search for high temperature, oxidation resistant and weakly bonded interface materials for ceramic composites had also ended up in monazite ceramics, especially lanthanum phosphate

($LaPO_4$).[78] Due to the identical thermal expansion coefficients of Al_2O_3 and $LaPO_4$, their composites were widely investigated and were found to be chemically inert. The melting temperature and linear thermal expansion coefficient of monazite type monoclinic $LaPO_4$ were 2072± 20 °C and 10.0×10^{-6} / °C at 1000 °C respectively. These values are close to alumina ceramics (9.0×10^{-6} / °C at 1000 °C). Therefore $LaPO_4$ is suitable to fabricate composite with Al_2O_3.

$LaPO_4$ in the Al_2O_3 composites is quite stable and no reaction occurs between the two phases up to 1650 °C provided the La:P ratio in the monazite is close to 1. Recently, according to Davis et al. two-phase composites consisting of $LaPO_4$ or $CePO_4$ and alumina, mullite or zirconia were cut and drilled using conventional tungsten carbide metal-working tools.[79] Morgan et al. reported that monazite-type $LaPO_4$ was stable and phases were compatible with Al_2O_3 at 1750 °C in air, for use in high-toughness composites, the $LaPO_4$-Al_2O_3 interface was shown to be sufficiently weak interfacial debonding prevented cracks from growing from $LaPO_4$ in to Al_2O_3.[79]

$LaPO_4$ is also of interest for coating on films and for fiber-matrix interface debonding and to confer damage tolerance to oxide composites. Research has been conducted on developing monazite sol and solution based precursors that can be used either to produce monazite as a matrix constituent or as a discrete fiber coating. The advantages of incorporating monazite fiber coating into alumina-

based composites have been demonstrated via improved composite strength and strain to failure at elevated temperature.[80]

Usual procedures for synthesis of these composites utilize solid state and wet mixing methods and also reactive hot pressing has been attempted.[81,82,83] Even when nanosized precursors are used for the synthesis of the composite, sintered grain sizes approach micron range in most cases. Surprisingly, reports on Al_2O_3-$LaPO_4$ nanocomposites are rare. Also, the more efficient and flexible sol-gel method has not been subjected to any detailed investigation for the preparation and machinability of these nanocomposite, which is ideal for the preparation of nanocomposites and improved properties are expected for nanocomposites.

Flexible use of advance ceramic material is restricted due to high hardness which makes conventional machining very difficult or even impossible. Reduced hardness leads to good machinability. It has been reported that lanthanum phosphate has low hardness as 4.2 GPa[84] which is close to that of machinable mica glass-ceramic (3 GPa)[85] and layered ternary compound Ti_3SiC_2 (4-5 GPa).[86] Further Davis and co-workers demonstrated that two-phase composite containing $LaPO_4$ and alumina were cut and drilled using conventional tungsten carbide metal working tools. The Young's modules and toughness of lanthanum phosphate is also lower than alumina.

1.6 Sol-Gel Process in General

Sol-gel process is a wet chemical process which is superior to other preparation methods in view of its efficiency in intimate mixing of components

which ensures homogeneity of final product. Application from coatings to powders can be addressed with a single preparation scheme. A schematic representation of the sol-gel technique is presented in **Figure 3.** The sol-gel process, as the name implies, involves the evolution of inorganic networks through the formation of a colloidal suspension (sol) and gelation of the sol to form a network in a continuous liquid phase (gel).[87] A sol is a dispersion of solid particles in a liquid phase where the particles are small enough to remain suspended indefinitely by Brownian motion.[88]

Sol are classified as lyophobic if there is a relatively weak solvent/particle interaction and lyophilic if this interaction is relatively strong. Gel is a solid containing a liquid component and an internal network structure so that both the solid and the liquid are in a highly dispersed state. Not all sols can be converted to gels. An important criterion for gel formation is that there will be a strong particle/solvent interaction so that at least part of the solvent is bound. Gelation process influences structure, pore volume and gel pore size and depends on many factors like pH, concentration of the medium and chemical nature of the precursors.

1.6.1 Stability of Sol

Although sol is thermodynamically unstable, they can be made kinetically stable by electrostatic repulsion between the particles (electrostatic stabilisation) or by a screening envelope of organic molecules (steric stabilisation).

1.6.2 Electrostatic Stabilisation (DLVO Theory)

The stabilization of colloids by electrostatic repulsion is successfully described by the DLVO theory. The net force between particles in suspension is assumed to be the sum of the attractive Van der Waals forces and the electrostatic repulsion created by charge absorbed on the particles. The repulsive barrier depends on two types of ions that make up the double layer. Charge determining ions that control the charge on the surface of the particle and counter ions that are in solution in the vicinity of the particle and act to screen the charges of the potential determining ions. It is the value of zeta potential which largely determines whether the suspension will be flocculated or deflocculated.[88]

For hydrous oxides the charge determining ions are H^+ and OH^- which establish the charge on the particle by protonating the MOH bonds on the surface of the particle.

$$M\text{-}OH + H \longrightarrow M\text{-}OH^{2+} \qquad (1)$$

$$M\text{-}OH + OH^- \longrightarrow M\text{-}O^- + H_2O \qquad (2)$$

The ease with which the proton are added or removed from the oxide depends on the metal atom. The pH at which the particle is neutrally charged is called the Point of Zero Charge (PZC). At pH greater than PZC equation (2) predominates and the particle is negatively charged, whereas at pH less than PZC equation (1)

gives the particle a positive charge. The magnitude of the surface potential depends on the departure of the pH from the PZC, and that potential attracts oppositely charged ions (counter ions) that may be present in the solution.

According to the standard theory, from **Figure 4.** the potential drops linearly through the tightly bound layer of water and counter ions, called the stern layer. Beyond the Helmholtz plane h=H, that is, in the Gouy layer, the counter ions diffuse freely. In this region the repulsive electrostatic potential of the double layer varies with distance from the particle, h, approximately according to

$$V_R \alpha e^{-K(h-H)}, h \geq H$$

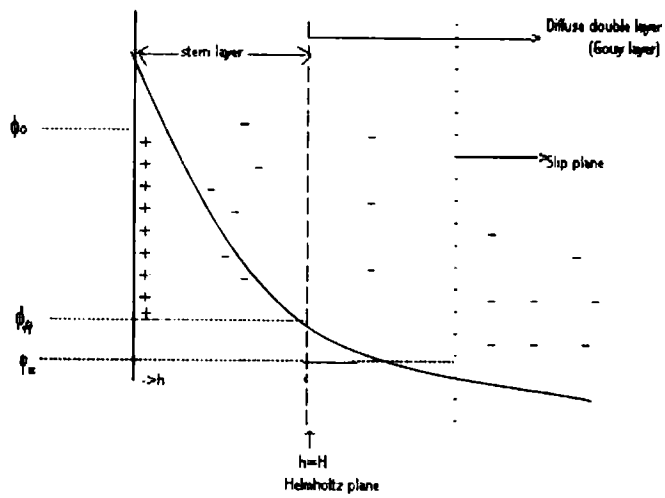

Figure 4. Schematic of Stern and Guoy layers. Surface charge on the particle is assumed to be positive

Where 1/K is called the Debye Huckel screening length. When the screening length is large (i.e. K is small), the repulsive potential extends far from the particle. This happens when the counter ion concentration is small. When counter ions are present, the potential drop more rapidly with distance. Since the repulsive force is proportional to the slope of the potential,

$$F_R = dV_R/dh \; \alpha \; K \, e^{-K(h-H)}$$

The repulsive force increases with small additions of electrolyte (i.e. FR increases with K). Large amount of counter ions collapse the double layer. As the concentration of counter ions increase, the double layer is compressed because the same number of charges are required to balance the surface charge and they are now available in a smaller volume surrounding the particle. On further increase in the concentration of counter ions, the double layer repulsions are reduced to the point that net particle potential is attractive and the colloid will coagulate immediately.

When an electric field is applied to a colloid, the charged particles move towards oppositely charged electrode, and this is called electrophoresis. When the particle moves, it carries along the adsorbed layer and part of the cloud of the counter ions, while the more distant portion of the double layer is drawn towards the opposite electrode. The slip plane (plane of shear) separates the region of fluid that moves with the particle from the region that flows freely. The rate of movement of the particle in the field depends on the potential at the slip plane .This potential is called the zeta potential. The pH at which zeta potential is

zero is called the isoelectric point (IEP). The stability of the colloid correlates with zeta potential to be around 30-50 mV.[88]

1.6.3 Steric Stabilisation

Steric stabilisation is due to the adsorption of sterically crowded organic molecules on the surface of colloidal particles. The adsorbed organic layer constitutes a steric barrier, which enthalpically and entropically discourage close approach of the particles and prevent them being coagulated.[89]

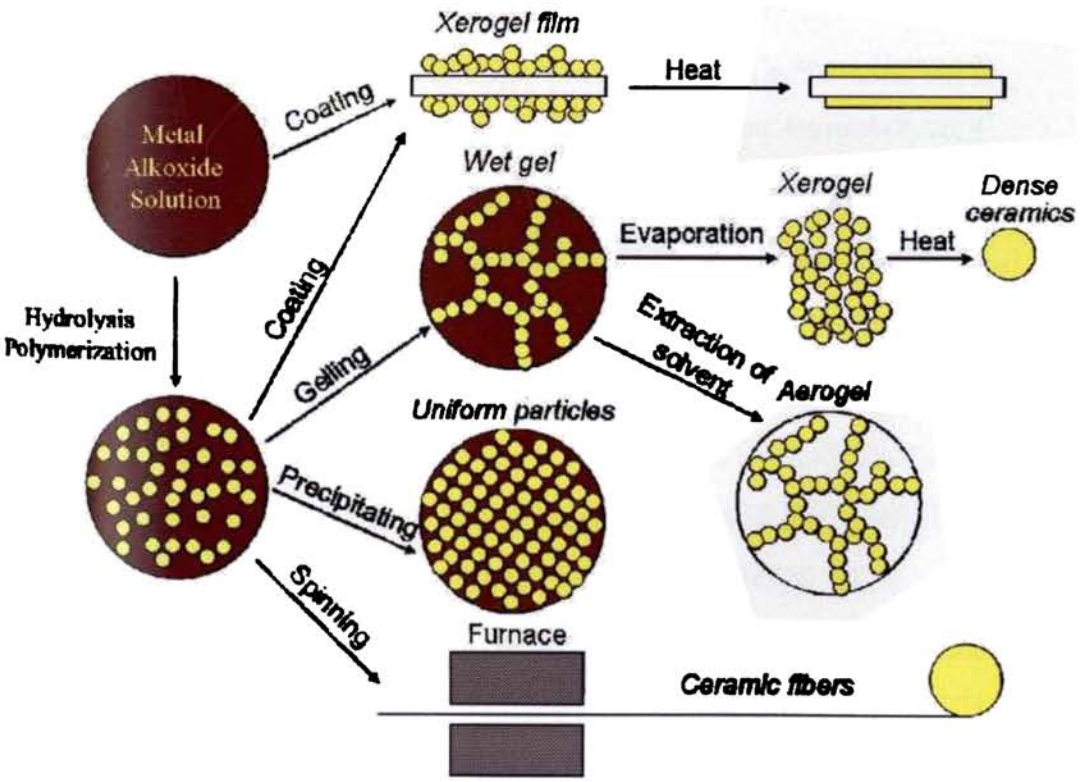

Figure 3. Sol-gel process and its various products

1.7 Sol-Gel Process as a Synthesis Tool for Composites

The worldwide goal of all sol-gel process has been ultra homogeneity, while this area has been switched in the early 1980's to the preparation of nanocomposites that exhibit ultra heterogeneity or nano heterogeneity. The concept of nanocomposite materials was a new direction for sol-gel research. The goal of ceramic material processing science via ceramic nanocomposite is to exploit the thermodynamics of metastable materials and in particular to utilize the heat of reaction of the discerete phases and the advantages offered by epitaxy. The term and concept of nanocomposite was formally adopted for ceramic materials by Roy, Komarneni and colleagues.[90,91] They developed hybrid ceramic metal nanocomposite material synthesised by sol-gel process. The concept of structural nanocomposite was proposed by Niihara in 1991 and can be seen as an adoption of the nanocomposite approach for nanostructural tailoring of structural ceramic composite.[92]

There are five major families of nanocomposites based on their material function, physical and chemical differences, and temperature of formation.[93]

1. Sol gel nanocomposites- Composites which are made at low temperature [<100 °C]. These nanocomposite precursors can lead to homogeneous single crystalline phase ceramics or multiphase crystalline ceramics upon high temperature heating.

2. Intercalation type nanocomposites- These can be prepared at low temperatures [<200 °C] and lead to useful materials upon heating to modest temperatures [<500 °C].

3. Entrapment type nanocomposites- These can be prepared from three dimensionally linked network structures such as zeolites which can also be synthesised at low temperature [<500 °C].

4. Electro-ceramic nanocomposites - These can be prepared by mixing nano phases of ferroelectric, dielectric, superconducting and ferric materials in a polymer matrix at low temperatures [<200 °C].

5. Structural ceramic nanocomposites - These are prepared by traditional ceramic processing at very high temperatures [1000 °C-1800 °C].

The sol-gel processing has been used for the preparation of different type of sol-gel nanocomposite, like mullite, alumina, and zirconia ceramic which have numerous technological application such as infrared transmitting material, refractory materials, substrate materials and high temperature structural materials. The sol-gel process has been extended to the preparation of new diphasic xerogel leading to new ceramic nano composite **Figure 5.** Two preparation routes are used in making ceramic nanocomposites. Method (a), Solution mixing of all components simultaneously. Method (b) uses a pre-made sol to which a further solution is added before gelation.

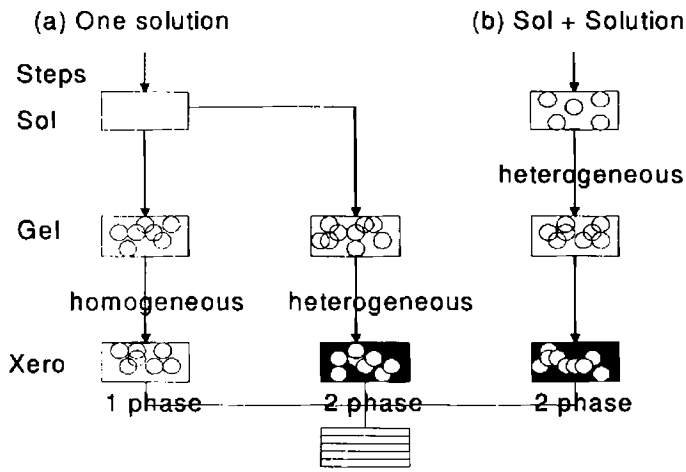

Figure 5. Flow chart for different type of synthesis procedure for the preparation of nanocomposites.

A new development in the processing of ceramic composites is through precoated powders. This can be accomplished by sol-gel and in situ solution precipitation process. The benefit of using coated powder is by achieving enhanced homogeneous distribution, fast densification and improvement of homogeneity of microstructure of the sintered material, and the reported high green compact strength. Sol-gel processing exhibits many significant advantages over conventional ceramic processing in terms of high purity, homogeneity and low temperature densification. The most outstanding advantage is in processing multicomponent systems where the chemical homogeneity of the individual constituents can be controlled down to the atomic level. This is quite often very difficult to achieve in simple mechanical mixing of powders. Moreover, the

nucleation and growth of the primary particles can be controlled in order to get particle of a given shape, size and size distribution.

Definition of the Present Research Problem

Alumina ceramics have been widely used as structural materials because of their high melting point and excellent mechanical properties, as well as electrical resistance and chemical durability. It is anticipated that alumina-based nano-sized ceramic composites will demonstrate novel and favourable properties in comparison with their micro-sized crystalline counterparts. Significant research efforts are reported on alumina matrix composite with special reference to alumina-aluminium titanate and alumina-lanthanum phosphate composites for the last few years due to a range of promising applications such as low thermal expansion, high thermal shock resistance and machinable ceramics. Earlier efforts for synthesis of alumina matrix nanocomposite were based on solid state reaction. This will result in high temperature sintering of the composites and grain growth. Synthesis of alumina-aluminium titanate composite through a sol-gel coating method is not investigated in depth for the preparation of alumina composites.

Therefore present work has been designed based on the following:

1) Aluminium titanate ceramic (AT) will be prepared at low temperature through sol gel synthesis using boehmite and titanium hydroxide precursors, by controlling the particle size at nano scale following in-situ peptisation of hydroxide precursors. The formation characteristics of AT phase, particle size distribution, sintering, microstructural features and thermal expansion behaviour will be studied.

2) Synthesis of alumina-aluminium titanate composite has been of considerable interest in recent years owing to great potential in low thermal expansion and high thermal shock resistance. Usually alumina-aluminium titanate was synthesized by solid state method which results in high temperature formation of aluminium titanate and grain growth. Hence alumina-aluminium titanate will be synthesized through a sol-gel core-shell method. Effect of sol-gel core-shell method on the formation temperature of aluminium titanate, and sintering of composite will be investigated.

3) The reports on machinability of Al_2O_3 - $LaPO_4$ nanocomposites are seldom found in the literature although this material is projected as a potential ceramic composite for easy shaping. Also the more efficient and flexible sol-gel method has not been subjected to any detailed investigation for the preparation of these nanocomposites, which is ideal for the preparation of nanocomposites and improved properties are expected for such nanocomposites. The synthesis of alumina-lanthanum phosphate will be carried out through sol-gel method. The mechanical properties of the sintered composites are also investigated.

4) Silicon carbide is a commonly used filter material because of its high temperature strength and thermal shock resistance. One potential barrier for such applications is their environmental durability. Mullite is highly compatible with

SiC because of close coefficient of thermal expansion. Mullite was coated on SiC by plasma spray coating techniques and contains metastable phases because of rapid cooling from high temperature. One key issue with plasma-sprayed mullite coating is phase instability. We attempt sol-gel coating of mullite on SiC substrate where mullite is being formed in-situ and its characterization using SEM, particle size and gas permeation analysis.

The thesis has been designed on the above objectives. The results obtained have been discussed and correlations have been derived between the experimental parameters and the properties.

References

1. Introduction to Ceramics, W. D. Kingery, H. K. Bowen, D. R. Uhlmann, John Wiley and Sons, New York, **1975.**
2. Fundamentals of Ceramic Powder Processing and Synthesis, T. A. Ring, Academic Press, Inc. San Diego, **1996.**
3. Composite Materials: Dream and Reality, G. Ondracek, I. Hochschule, 787-820, Advanced Structural Inorganic composites, edited by P. Vincenzini, Elsevier Science Publishers, Trieste, **1991.**
4. Ceramic Precursor Technology and its Application, C. K. Narula, Marcel Dekker, New York, **1995.**
5. K. Niihara, A. Nakahira, Structural Ceramic Nanocomposites by Sintering Method: Roles of nano-size particles. In Ceramics: Towards the 21st Century. Ceram. Soc. Japan, **1991,** 404.
6. C. Laurent, J. J. Demai, A. Rousset, K. R. Kannan, C. N. R. Rao, *J. Mater. Res.* **1994,** 9, 229.
7. E. Breval, G. Dodds, C. G. Pantano, *Mater. Res. Bull.* **1985,** 20, 1191.
8. K. Niihara, T. Hirai, *Ceramics.* **1986,** 26, 598.
9. M. Sternitzke, *J. Eur. Ceram. Soc.* **1997,** 17, 1061.
10. Composite Materials Handbook. MelM. Schwartz, Publisher McGraw-Hill Book Company, **1998.**
11. Alumina Production: Principles and Practice. Chemical Engineer, A.N. Adamson, London, **1970,** 239, 156.
12. Oxides and Hydroxides of Aluminium, K. Wefers, C. Misra, Alcoa Laboratories, Pittsburgh **1987.**
13. Alumina processing Properties and Application. E. D. H. Hubner, Springer-Verlag, New York, **1984.**
14. Engineered Materials Handbook. 4, S. J. Schneider, ASM International, **1994.**
15. R. G. Munro, *J. Am. Ceram. Soc.* **1997,** 80, 1919.
16. G. B. Kenny, H. K. Bowen, *Am. Ceram. Soc. Bull.* **1983,** 62, 590.

17. Particulate Strengthened Oxide Ceramics-Nanocomposites. K. Niihara, A. Nakahira in Advanced Structural Inorganic Composites, Edited by P. Vincenzini, Elsevier Science Publishers B.V. **1991,** 974.

18. N. Claussen, R. L. Cox, J. S. Wallance, *J. Am .Ceram. Soc.* **1982,** 65, C-190.

19. F. Wakai, S. Sakagusi, Y. Matsuo, *Adv. Ceram. Mater.* **1986,** 1, 259.

20. Strengthening of Oxide Ceramics by SiC and S_3N_4 dispersions, K. Niihara, and A. Nakahira in Proc. Third International Symposium on Ceramic Materials and Components for Engines, Edited by V. J. Tennery, Westerville, Ohio, **1998,** 919.

21. R. S. Haaland, B. I. Lee, S. Y. Park, *Ceram. Eng. Sci. Proc.* **1987,** 8, 879.

22. U. S. Hareesh, M. Semitzke, R. Janseen, N. Claussen, K. G. K. Warrier, *J. Am. Ceram. Soc.* **2004,** 87, 1024.

23. R. Chockalingam, V. R. W. Amarakoon, H. Giesche, *J. Eur. Ceram. Soc.* **2008,** 28, 959.

24. A. S. Kumar, A. R. Durai, T. Sornakumar, *Int. J. Refract. Met. H.* **2007,** 25, 214.

25. Y. F. Gu, P. Hacarlioglu, S. T. Oyama, *J. Membrane. Sci.* **2008,** 310, 28.

26. Mullite and Mullite Matrix Composite Edited by, S. Somiya, R. F. Davis, J. A. Pask, Am. Ceram. Soc, Westerville, **1990.**

27. J. Wu, M. Chen, F. R. Jones, P. F. James, *J. Eur. Ceram. Soc.* **1996,** 16, 619.

28. E. Medvedovski, *Ceram. Int.* **2006,** 32, 369.

29. H. Schneider, J. Schreuer, B. Hildmann, *J. Eur. Ceram. Soc.* **2008,** 28, 329.

30. J. Sun, L. Gao, W. Li, *Chem. Mater.* **2002,** 14, 5169.

31. X. Wang, N. P. Padture, H. Tanaka, *Nat. Mater.* **2004,** 3, 539.

32. P. D. Pria, *Eur. J. Ortho. Surgery Traumatology.* **2007,** 17, 253.

33. J. Pierri, E. B. Roslindo, R. Tomasi, E. M. J. A. Pallone, E. C. S. Rigo, *J. Non-Cryst. Solids.* **2006,** 352, 5279.

34. S. B. Colin, A. Mocellin, J. V. Stebut, K. Bordji, D. Mainard, *J. Mater. Sci.* **1998,** 33, 2837.

35. J. Leivo, V. Meretoja, M. Vippola, E. Levanen, P. Vallittu, T.A. Mantyla, *Acta Biomater.* **2006,** 2, 659.

36. X. Q. You, T. Z. Si, N. Liu, P. P. Ren, Y. D. Xu, J. P. Feng, *Ceram. Int.* **2005,** 31, 33.

37. P. Hvizdos, D. Jonsson, M. Anglada, G. Anne, O. V. Biet, *J. Eur.Ceram.Soc.* **2007,** 27, 1365.

38. M. I. Nieto, R. Martinez, L. Mazerolles, C. Baudin, *J. Eur.Ceram.Soc.* **2004,** 24, 2293.

39. L. Wang, J. L. Shi, J. H. Gao, D. S. Yan, *J. Eur.Ceram.Soc.* **2001,** 21, 1213.

40. S. Mezquita, R. Uribe, R. Moreno, C. Baudin, *Brit. Ceram. T.* **2001,** 100, 246.

41. W. R. Buessen, N. R. Thielke, R.V. Sarakaukas, *Ceramic Age,* **1952,** 60, 38.

42. M. M. A. Sekar, K. C. Patil, *Brit. Ceram.T.* **1994,** 93, 146.

43. J. J. Clevland, R. C. Bradt, J. Am. Ceram. Soc. **1978, 61**, 478.

44. F. J. Parker, R. W. Rice, *J. Am. Ceram. Soc.* **1989, 72**, 2364.

45. H. A. J. Thomas, R. Stevens, *Brit. Ceram. T.* **1989,** 88, 144.

46. K. Hamano, Z. Nakagawa, K. Sawano Y. Hasegawa, *J. Chem. Soc. Jp.* **1981,** 1981, 1647.

47. Y. Ohya, K. Hamano Z. Nakagawa, *Yogyo-kyokai-shi.* **1986,** 94, 665.

48. B. Freudenberg, A. Mocellin, *J. Am. Ceram. Soc.* **1987,** 70, 33.

49. I. Stamenkovic, *Ceram. Int.* **1989,** 15, 155.

50. H. Wohlfromm, P. Pena, J. S. Moya, J. Requena, *J. Am. Ceram. Soc.* **1992,** 75, 3473.

51. A. M. Segadaes, M. R. Morelli, R. G. A. Kiminami, *J. Eur. Ceram. Soc.* **1998,** 18, 771.

52. D. M. Ibrahim, A. A. Mostafa, T. Khalil, *Ceram. Int.* **1999,** 25, 697.

53. H. Morishima, Z. Kato, K. Uematsu, K. Saito, T. Yano, N. Ootsuka, *J. Mater. Sci. lett.* **1987,** 6, 389.

54. J. C. Russo, P. M. Harmer, M. H. Chan, *J. Am. Ceram. Soc.* **1992,** 75, 3396.

55. S. Pratapa, I. M. Low, *J. Mater. Sci.* **1998,** 33, 3047.

56. M. Takahashi, M. Fukuda, M. Fukuda, H. Fukuda, T. Yoko, *J. Am. Ceram. Soc.* **2002,** 85, 3025.

57. T. Korim, *Ceram. Int.* **2009,** 35, 1671.

58. H. Wohlfromm, T. Epicier, J. S. Moya, P. Pena, G. Thomas, *J. Eur. Ceram. Soc.* **1991,** 7, 385.

59. W. A. Zdaniewski, H. P. Kirchner, *Adv. Ceram. Mater.* **1986,** 1, 99.

60. N. P. Padture, S. J. Bermison, H. M. Chan, *J. Am. Ceram. Soc.* **1993,** 76, 2312.

61. D. P. H. Hasselman, K. Y. Donaldson, E. M. Anderson, T. A. Johnson, *J. Am. Ceram. Soc.* **1993,** 76, 2180.

62. J. Barolome, J. Requena, J. S. Moya, M. Li, F. Guiu, *Acta. Mater.* **1996,** 44, 1361.

63. J. Barolome, J. Requena, J. S. Moya, M. Li , F. Guiu, *Fatigue Fract. Eng. Mater. Struct.* **1997,** 20, 789.

64. S. Bueno, R. Moreno, C. Baudin, *J. Eur. Ceram. Soc.* **2003,** 21,71.

65. P. Manurung, I. M. Low, B. H. Connor, S. Kennedy, *Mater. Res. Bull.* **2005,** 40, 2047.

66. H. M. Okamura, E. A. Barringer, H. K. Bowen, *J. Mater. Sci.* **1989,** 24, 1867.

67. I. B. Arenas, O. Gil, *J. Mater. Process. Tech.* **2003,** 143–144, 838.

68. S. Y. Park, S. W. Jung, Y. B. Chung, *Ceram. Int.* **2003,** 29, 707.

69. B. Morosin, R. W. Lynch, *Acta Crystallographica.* **1972,** B28, 1040.

70. D. P. H. Hasselman, *J. Am. Ceram. Soc.* **1969,** 52 , 600.

71. D. C. Jia, Y. Zhou, T. C. Lei, *Ceram. Int.* **1996,** 22, 107.

72. M. I. Nieto, R. Martiez, L. Mazerolles, C. Baudin, *J. Eur. Ceram. Soc.* **2004,** 24, 2293.

73. D. P. H. Hasselman, *Am. Ceram. Soc. Bull.* **1970,** 49, 1033.

74. E. A. Bush, F. A. Hummel, *J. Am. Ceram. Soc.* **1959,** 42, 388.

75. Y. Ohya, Z. Nakagawa, K. Hamani, *J. Am. Ceram. Soc.* **1987,** 70, C184.

76. D. F. Mullica, W. O. Milligan, D. A. Grossie, G. W. Beall, L. A. Boatner, *Inorg. Chim. Actu.* **1984,** 95, 231.

77. Y. Hikichi, T. Nomura, Y. Tanimura, S. Suzuski, M. Miyami, *J. Am. Ceram. Soc.* **1990,** 73, 3594.

78. P. E. D. Morgan, D. B. Marshall, *J. Am. Ceram.Soc.* **1995,** 78, 1553.

79. J. B. Davis, D. B. Marshall, R. M. Housley, P. E. D. Morgan, *J. Am. Ceram. Soc.* **1998,** 81, 2169.

80. K. K. Chawla, H. Liu, J. J. Rusch, S. Sambasivan, *J. Eur. Ceram. Soc.* **2000,** 20, 551.

81. T. J. Hwang, M. R. Hendrick, *Mater. Sci. Eng. A.* **1998,** 244, 91.

82. W. Min, D. Miyahara, K. Yokoi, T. Yamaguchi, K. Daimon, Y. Hikichi, T. Matsubara, T. Ota, *Mater. Res. Bull.* **2001,** 36, 939.

83. R. Wang, W. Pan, J. Chen, M. Fang, M. Meng, *Mater. Lett* .**2002,** 57, 822.

84. Y. Konishi, T. Kusunose, P. E. D. Morgan, T. Sekino, K. Niihara, The Science of Engineering Ceramics II, Proc. 2nd Int. Symp. Sci. Eng. Ceram. **1998,** 161–3, 341.

85. D. G. Grossman, *J. Am. Ceram. Soc.* **1972,** 55, 446.

86. M. W. Barsoum, T. El-Raghy, *J. Am. Ceram. Soc.* **1996,** 79, 1953.

87. Introduction to Sol-Gel Processing, A. C. Pierre, Kluwer Academic Publishers, The Netherlands, **1998.**

88. Sol-Gel Science-The Physics and Chemistry of Sol-Gel Processing, Edited by C. J. Brinker, G. W. Sherrer, Academic Press, INC., New York, **1990.**

89. Principles of Colloidal and Surface Chemistry, P. C. Hiemenz, Marcel Dekker, New York, **1997.**

90. Purposive Design of Nano Composite, Entire Class of New Materials, R. Roy, Ceramic Microstructure 86, Role of Interface, 21, 25-32, **1987.**

91. S. Komarneni, Nanocomposites, *J. Mater. Chem.* **1992,** 2, 1219.

92. K. Nihara, *J. Am. Ceram. Soc.* **1991,** 99, 974-982.

93. R. E. Newnham, D. P. Skinner, L. E. Cross, *Mater. Res. Bull.* **1978,** 13, 525.

Chapter II

Alumina-Aluminium titanate Composites

2.1 Aluminium titanate- Introduction

Aluminium titanate (AT, Al_2TiO_5) is an excellent thermal shock resistant ceramic which has a pseudo brookite structure.[1] AT exists in two allotropic forms α and β and the low temperature phase is β-Al_2TiO_5. However, AT has two major problems limiting its wider application,[2] such as decomposition to alumina and titania in the range of 800 to 1280 °C [3] and spontaneous microcracking due to the thermal expansion anisotropy in the sintered ceramics which ultimately results in poor mechanical strength. Microcracks are found to develop predominately above the critical sintered grain size of 1.5 μm and therefore fine grained microstructure is necessary.[4] Additives such as Al_2O_3, MgO, SiO_2 and ZrO_2 are employed in the AT precursor to suppress decomposition of the phases.[5,6,7,8,9,10] Another approach is to control the sintered grain size to below 1.5 μm, for which nano size starting particle size is a possibility. Also in some cases sintering aids and grain growth inhibitors are used.[9] AT ceramic has many potential applications, such as thermal protection layers in internal combustion engines, kiln furniture and pouring spouts for foundry applications, due to its low thermal expansion coefficient (CTE: 0.2 x 10^{-6} to 1 x 10^{-6} K^{-1}), low thermal conductivity (0.9-1.5 $Wm^{-1}K^{-1}$) and high thermal shock resistance (about 500 Wm^{-1}).[11] AT is also recognized as a second phase

material for improving the thermo-mechanical properties like thermal shock resistance, toughness, and flaw tolerance behaviour of many ceramic matrix composites.[12] No detailed work has been reported in the synthesis and sintering features of aluminium titanate by aqueous sol-gel methods involving hydroxide precursors without any additives. Therefore we adopted a novel approach for the synthesis of nano size AT powders using $Ti(OH)_4$ and AlOOH nano precursors containing particle of size~100 nm. The hydroxide precursors have less volatiles and enhanced reactivity.

The usual synthetic methodologies for the synthesis of aluminium titanate, often requires heat treatment at high temperature which will result in considerable grain growth. Aqueous sol-gel approach for the synthesis of aluminium titanate associated with low tempearure formation of the phase and lower grain sizes are less reported. The role of precursors on the low temperature AT phase formation, sintering behaviour, grain growth effect, thermal expansion coefficient and microstructural features are studied and discussed in this chapter.

2.1.1 Experimental

Boehmite, (AlOOH) (99% purity, alumina content 70%, Condea Chemie, Germany) having BET surface area of 230 m^2/g and crystallite size 48-60 A° was used as precursor for alumina. Titanium hydroxide was prepared from titanium tetrachloride (99% Purity, M/s Kerala Minerals and Metals Ltd, Kollam India) using the following procedure. In a typical experiment, titanium tetrachloride was

dissolved in ice cold distilled water (0.2 M) and was hydrolysed by drop wise addition of 10 % ammonium hydroxide solution (S.D. Fine Chemicals, India) under constant stirring at room temperature. Once the reaction mixture attained pH=9.0, precipitate was formed, which was separated by filtration and repeatedly washed with distilled water for a minimum of six times to ensure the absence of free chloride which was further confirmed by $AgCl$ test.[13] The aluminium titanate precursor sol was obtained by dispersing boehmite (2.45 g) and titanium hydroxide precipitate (24.92 g) in 1000 mL of double distilled water under stirring for 3 h. Peptisation was carried out by the addition of 20% HNO_3 (Merck, India) and the pH was controlled at 2.5. The sol was aged for 24 h and then subjected to evaporation at 70 °C in hot air oven. The process flow sheet is presented in Fig.1. The dried precursor was powdered and was subjected to DTA (DTA - 50H, Shimadzu, Japan) and TGA (TGA-50H, Shimadzu, Japan) analysis at a heating rate of 5 °C min^{-1} up to 1400 °C. Cylindrical pellet of size 6 mm diameter and 8 mm height made by uniaxial compaction (200 MPa) was used for the dilatometric studies by thermo mechanical analyzer (TMA- 60H, Shimadzu, Japan) at a heating rate of 5 °C /min up to 1400 °C.

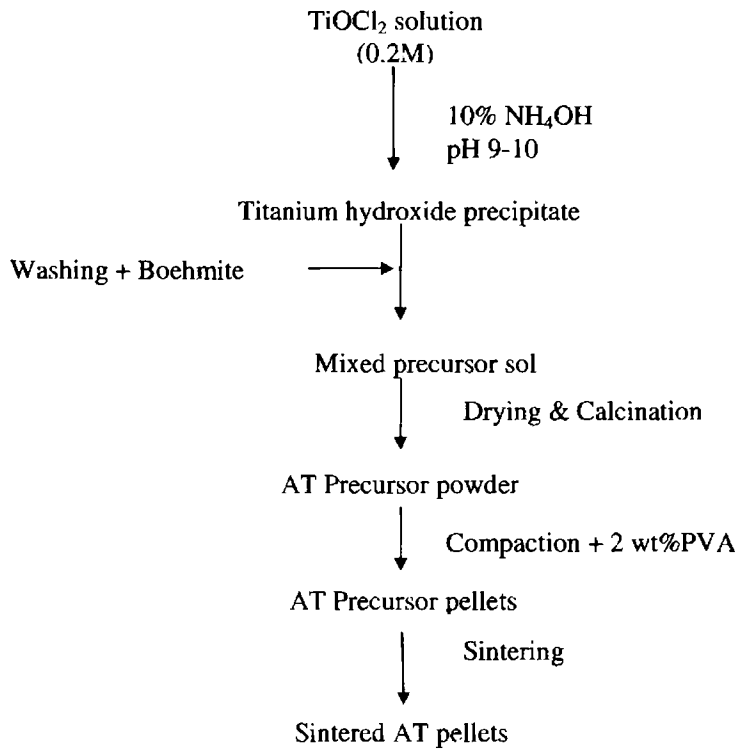

Figure 1. Flow diagram for the powder synthesis of aluminium titanate

The precursor was further heat treated at temperatures 400, 600, 800, 1000, 1320 °C respectively in muffle furnace at a heating rate of 3 °C/min and then subjected to X-ray analysis in the 2θ range of 20-60 CuKα (Philips PW 1170, The Netherlands). The particle size analysis was carried out using Laser Particle Size Analyzer on the powders calcined at 1000, 1200 and 1320 °C (Zeta Sizer, Malvern Instruments UK). The sample for the particle size analysis was made by ultrasonic dispersion of the respective powders (1 g) in aqueous medium (100 mL) at pH

<2.0. Average of three measurements with in a standard deviation of 3.0 % is reported.

The AT powder calcined at 1000 °C was compacted uni-axially at a pressure of 200 MPa using 2 wt% PVA as binder to form cylindrical pellets with dimensions 12 mm diameter and 2 mm height. The samples were sintered in the range 1350 to 1600 °C. The typical sintering schedule was as follows: RT to 800 °C at a rate of 3 °C/min and then up to the sintering temperatures at 10 °C/min. Density of the sintered samples was measured by Archimedes principle. Microstructure was observed on polished and thermally etched specimens using scanning electron microscopy (SEM, JEOL, JSM 5600 LV, Japan). The average grain size was calculated by the linear intercept method using the relation G = 1.5L/MN where 1.5 is a geometry dependent proportionality constant, L is the total test line length, M the magnification and N the total number of intercepts. For the grain size determination four representative micrographs with magnification of 5000X were analyzed. A test line of 9 cm length was marked on the micrograph and the number of intersections of the line with grain boundaries were counted.

The linear thermal expansion behavior of the sintered AT ceramics was observed using thermo mechanical analyzer (TMA 60H, Shimadzu, Japan). The sintered specimen having dimensions of 5 mm diameter and 7 mm height was used for the CTE measurement with a constant heating and cooling rate of 5 °C/min. Average value of CTE obtained from three measurements was reported.

2.1.2 Results and Discussion

2.1.2.1 Characterisation of Aluminium Titanate Precursor Powder

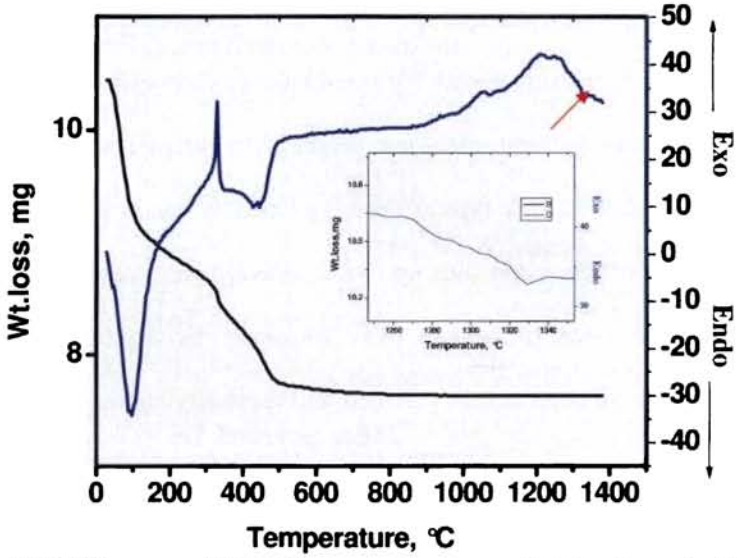

Figure 2. TG-DTA curve of the AT precursor measured at heating rate 5 °C/min in the flow of air

Figure 2. shows the TG/DTA analysis of the mixed gel precursor dried at 70 °C. The TG analysis shows that the decomposition of the AT precursor takes place in two steps below 500 °C. A total weight loss of 25 % is observed in this range. The first step below 200 °C is due to the dehydration of the mixed gel and above this range the weight loss is may be due to the dehydroxylation of the Ti $(OH)_4$-AlOOH inorganic moieties and decomposition of nitrates. From 600 to 1000 °C the weight loss is only 1.2%. The DTA pattern showed a sharp exothermic peak at 328 °C and one broad endothermic peak at 1200 °C followed by a small endothermic peak at 1320 °C. The first exothermic peak at 328 °C is

due to the decomposition of nitrates. [14] Rutilation occurs above 900 °C followed by the conversion of boehmite to alumina at 1000 °C.

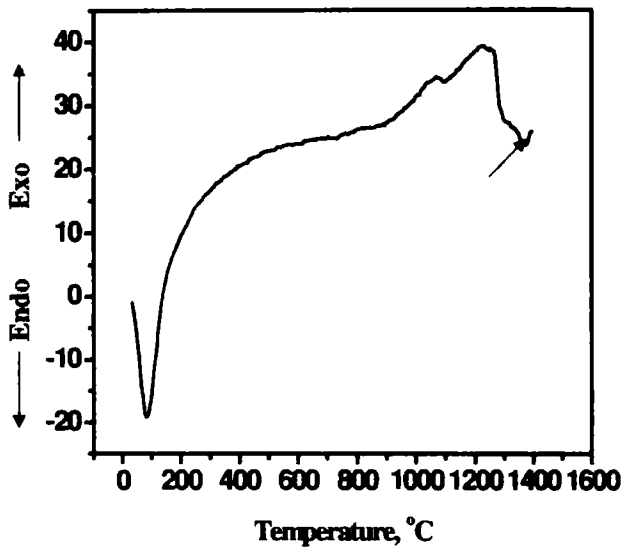

Figure 3. DTA of mixed gel precursor calcined at 600 °C

Figure 3 & 4 show the DTA curves of AT precursors calcined at 600 and 1000 °C. The AT phase formation is independent of the calcination conditions. In both the cases, the AT phase formation is observed only at 1320 °C. AT phase formation was examined by varying the heating rates **Figure 5**. It appears that at very slow heating rates (5 °C/min), the phase formation temperature is slightly shifted to lower range of temperature. The lowering of phase formation temperature is not very significant. Since the reaction between alumina and titania for resulting aluminium titanate is relatively a slow reaction, comparatively high temperature is essential for the completion of the AT phase.

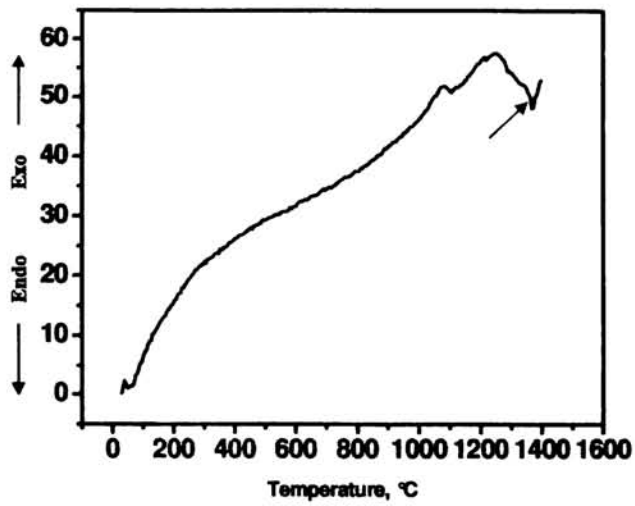

Figure 4. DTA of mixed gel precursor calcined at 1000 °C

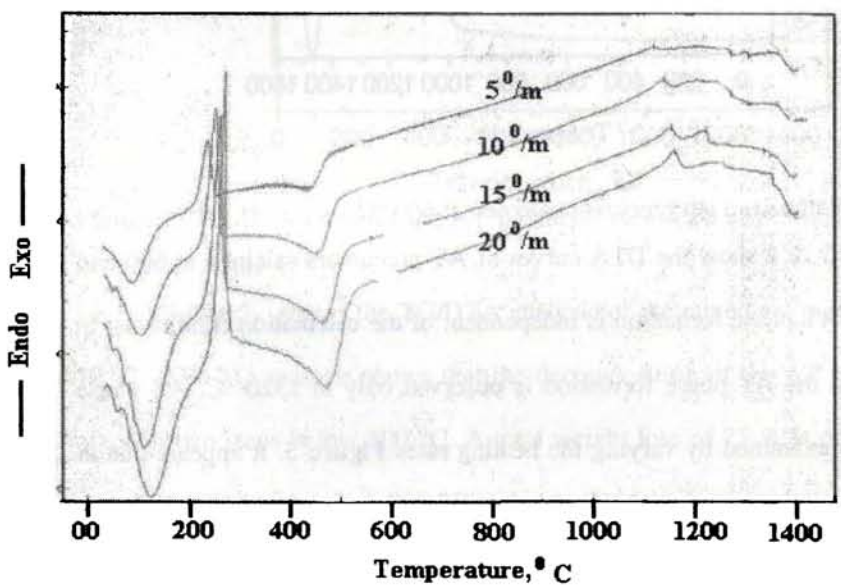

Figure 5. Effect of heating rate on AT phase formation

XRD pattern of mixed gel precursor was amorphous as seen from **Figure 6.** The anatase phase starts to crystallize at 800 °C. However, at 1000 °C major

phases are rutile, anatase and transition alumina. DTA indicates aluminium titanate formation by an endothermic peak at 1320 °C, which is lower than earlier reports, probably due to the smaller initial particle size in the precursor. The formation of β- AT at low temperature is attributed to nucleation and growth process. The XRD analysis of powder calcined at 1320 °C indicates the completion of formation of aluminium titanate phase. Vasudevan et al. reported AT formation at 1362 °C from aluminium nitrate derived boehmite and titanium isopropoxide.[14]

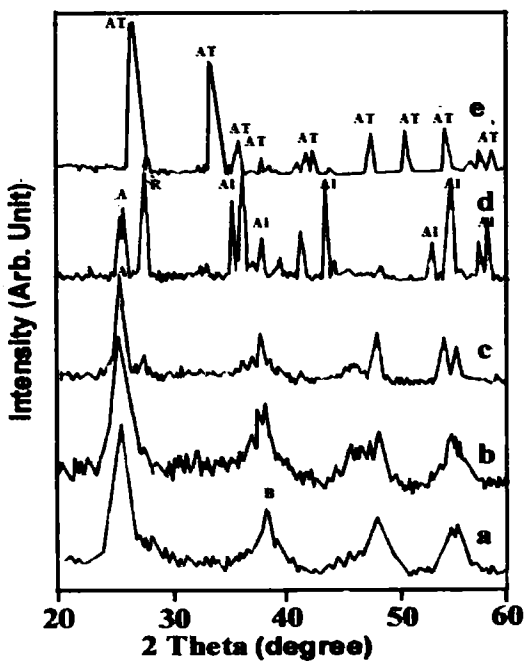

Figure 6. XRD patterns of AT precursor calcined at a) 400 °C b) 600 °C c) 800 °C d) 1000 °C e) 1320 °C, (**A**) anatase, (**R**) rutile, (**Al**) transition alumina, (**AT**) aluminium titanate, (**B**) Boehmite

The particle size distribution of a stable suspension of mixed gel precursor calcined at (1000, 1200, 1320 °C) is presented in **Figure 7.** The boehmite sol shows an average particle size of 90 nm (**Figure 7a**). The particle size of the aluminium titanate precursor powder calcined at 1000 °C has a fine particle size of 100 nm (**Figure 7b**).

The precursor calcined at 1200 °C shows (**Figure 7c**) an average particle size of 430 nm. The average particle size of sol-gel prepared aluminium titanate after calcination at 1320 °C was 700 nm (**Figure 7d**). XRD results show that the aluminium titanate formation was completed at 1320 °C. The presence of a bimodal distribution of aluminium titanate is due to the presence of aggregation in the nano range to form primary agglomerates (first peak).[16] The average particle size of aluminium titanate precursor synthesized through combustion was reported to be 930 nm.[17]

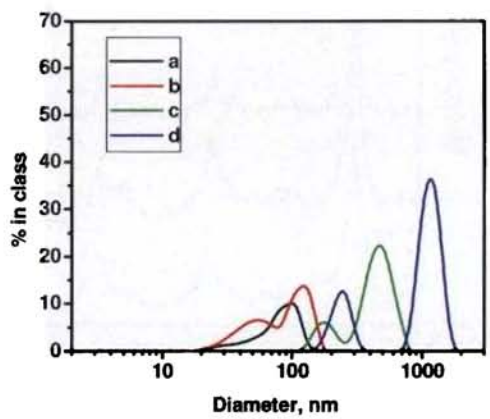

Figure 7. Particle size distribution of a) Boehmite sol, b) AT precursor calcined at 1000 °C, c) AT precursor calcined at 1200 °C d) AT precursor calcined at 1320 °C.

Figure 8. shows the dilatometric measurements of aluminium titanate precursor at different heating rate. The first peak represents the formation temperature of rutile titania and the second peak corresponds to the sintering starting temperature of aluminium titanate. The formation temperature of rutile titania (1000 °C) is similar for 5 and 10 °C/min heating rate but slightly higher for 15 °C/min. The sintering starting temperature for the 5 and 10 °C/min heating rate is similar (1300 °C) but higher for the heating rate of 15 °C/min because the formation of aluminium titanate is delayed at higher heating rate.

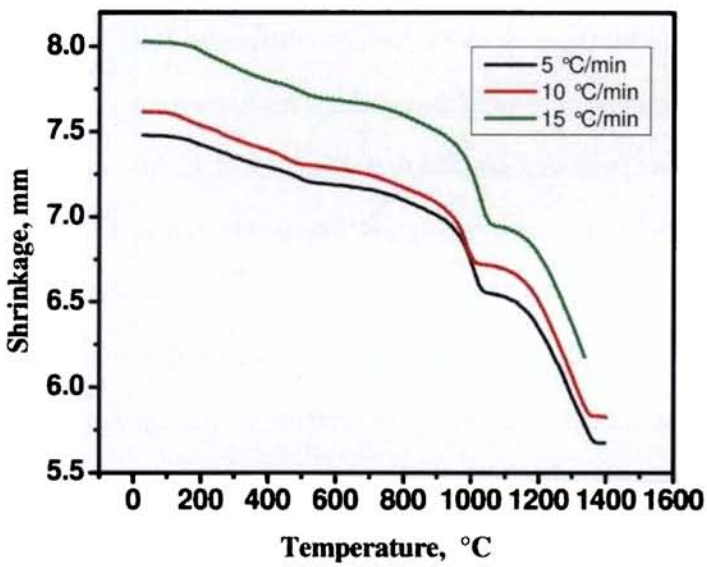

Figure 8. Dilatometric measurements curve of aluminium titanate precursor at different heating rates

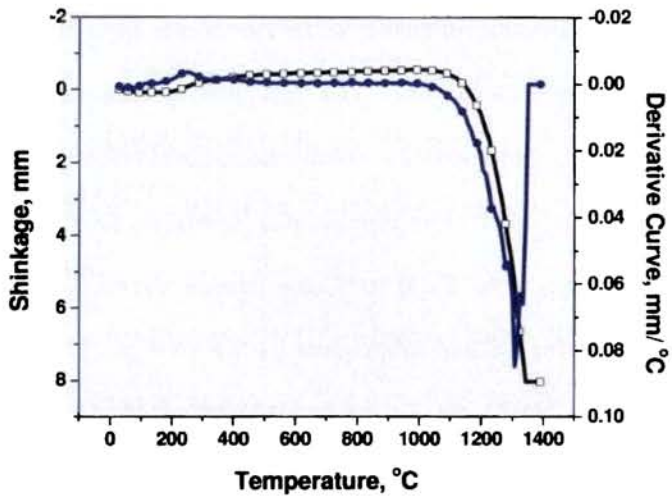

Figure 9. Dilatometric curves of AT precursor calcined at 1000 °C

The dilatometric curves of the compacts made from AT precursor calcined at 1000 °C shows three step densification (**Figure 9.**) .The first step occurs above 900 °C due to the formation of rutile phase followed by conversion of boehmite to alumina above 1000 °C (second step). The large shrinkage step is between 1200-1320 °C, where the aluminium titanate formation is also confirmed by XRD data. After the formation of aluminium titanate the further shrinkage was arrested.

2.1.2.2 Sintering Characteristics

The sintered density of aluminium titanate precursor calcined at 1000 °C with respect to temperature is presented in **Figure 10.** The pre-calcined AT precursor powder was compacted and sintered in the range of 1350-1600 °C, at a heating rate of 10 °C/min and soaking for 2 h. The samples sintered at 1350 °C attained 84% theoretical value, which is increased to 86% at 1450 °C. The high

sintered density is retained up to the sintering temperature of 1550 °C. At this temperature about 94% relative density was achieved. Above 1550 °C the density drop may be due to grain growth and microcracking. Hareesh et al. used suspension containing 2 wt% aluminium titanate as nucleating seed for the densification of AT at 1300 °C/30 min and retains fine grained distribution.[18]

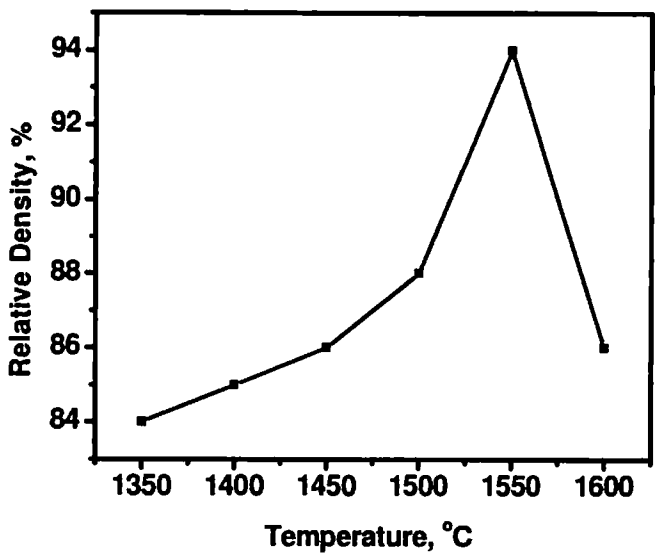

Figure 10. Effect of sintering temperature on densification

The thermal expansion curve of AT is presented in **Figure 11.** The α-Al_2O_3 (CTE: 8×10^{-6} K^{-1}) was used as reference material. The thermal expansion coefficient of aluminium titanate calculated from the measured data for the range 200-600 °C is 1.1×10^{-6} K^{-1}. This may be due to reduced final grain size of 2-3 μm of sintered AT which is further indicated by microstructural analysis.

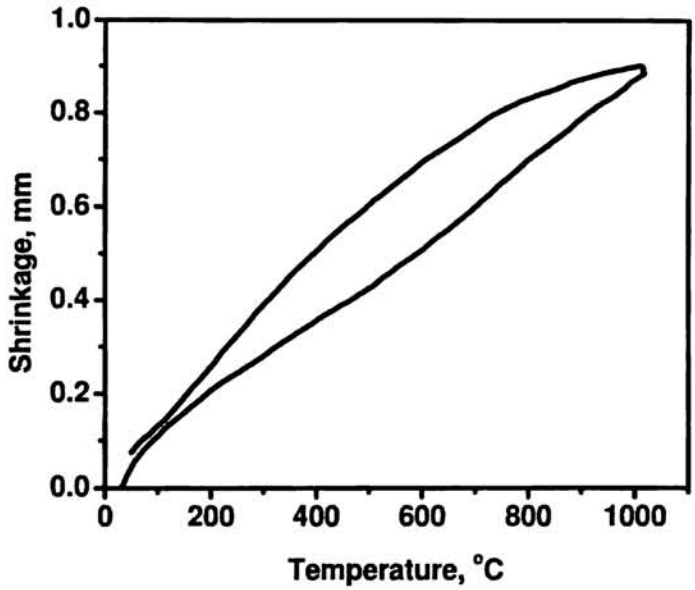

Figure 11. Thermal expansion curves of AT sintered at 1550 °C/2 h. Heating and cooling rate: 5 °C/min

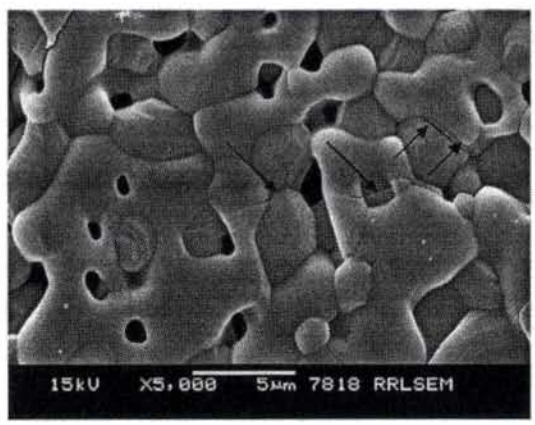

Figure 12. SEM of polished and thermally etched surface of AT sintered at 1550 °C/2 h.

The microcracks are formed in the aluminium titanate sample sintered at 1550 °C may be due to the thermal expansion anisotropy of aluminum titanate. These microcracks are responsible for the high thermal shock resistance of this material.[19] Parker et al. reported that aluminium titanate sintered at 1450 °C shows a sintered grain size of 13.3 μm and the corresponding thermal expansion coefficient $-1.5 \times 10^{-6} K^{-1}$. On further increase in the sintering temperature (at 1575 °C) the grain size increases to 13.7 μm and thermal expansion coefficient of $-1.2 \times 10^{-6} K^{-1}$, but at 1650 °C, the grain size further increases but the thermal expansion coefficient remains the same.[20] This shows that the thermal expansion coefficient depends on grain size and sintering temperature. In our method the grain size of aluminium titanate sintered at 1550 °C is controlled in the range of 2-3 μm, but due to presence of microcrack (for large grains), material shows low thermal expansion (**Figure 12.**). Kuszyc et al. have reported the existence of an abrupt grain size effect in relation to microcracking of polycrystalline ceramics composed of materials having high thermal expansion anisotropy.[21] Microcracking, therefore, must occur at a certain grain size, corresponding to a given firing period at a higher temperature, resulting in a thermal expansion hysteresis loop, as shown in **Figure 11.**

The AT synthesized by the co-precipitation of titanium tetrachloride and aluminium nitrate with 2 wt% MgO sintered at 1550 °C with soaking over a period of 4 h shows an average grain size of 3.6 μm.[22] Micrograph of AT sintered at 1350

°C over a period of 2 h shows that grain is in the range of 2-3 μm as in **Figure 13(a).** SEM of the sintered AT (1550 °C) is shown in **Figure 13 (b)-13(c).** The grain size is in the range of 2-3 μm and not associated with any cracks while larger grains show microcracks. Isolated closed pores are seen which may due to specific sintering schedule, since there is no presence of any liquid phase. In the process, direct sintering was adopted without any additives and the fine grain size should be due to the initial particle size as well as the enhanced reactivity of the hydroxide precursor. Stamenkovic reported that AT prepared by solid state reaction (mechanically mixed) with addition of 2 wt% MgO and sintered by hot press at 1450 °C and microstructure had a mean grain diameter of 3.8 μm.[23] In the present case the hydroxide precursors due to the fineness, high compaction efficiency and surface reactivity result in small grain size.

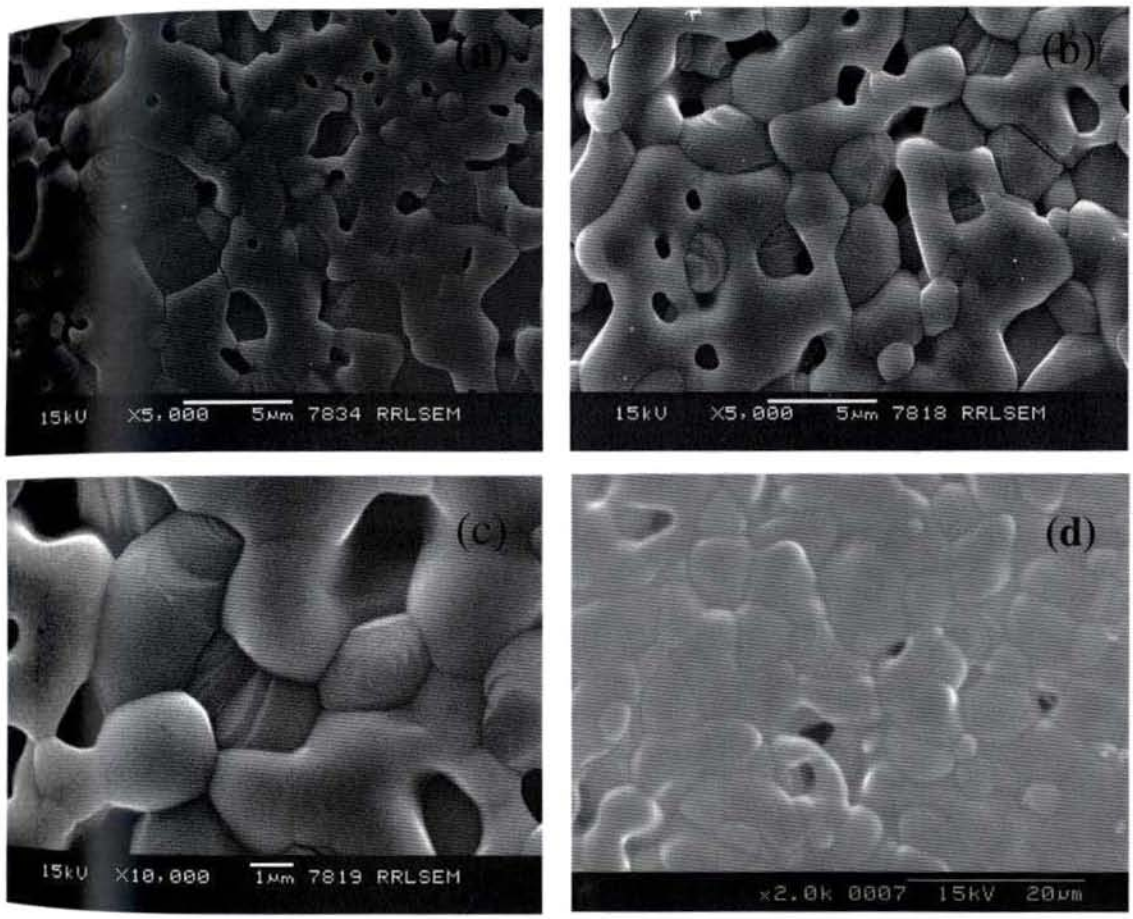

Figure 13. SEM of polished and thermally etched surface of sintered AT (a) at 1350 °C/2h (b, c, d) at 1550 °C/2 h.

2.2 Alumina- Aluminium titanate Composite- Introduction

Aluminium titanate has drawn much attention as a high temperature material due to the low thermal expansion coefficient[24]and high thermal shock resistance.[25] Aluminium titanate exhibits two allotropic forms such as α and β, where β aluminium titanate is the low temperature stable phase.[26] Aluminium titanate is usually formed by the solid state reaction between alumina and titania above the eutectoid temperature 1280 °C.[27] Aluminium titanate exhibits microcracking during cooling from the sintering temperature due to the thermal expansion anisotropy.[28] Microcracks are found to develop predominantly above a critical sintered grain size of 1.5 μm and therefore fine grained microstructure is necessary.[29] The excellent properties like thermal shock resistance and low thermal conductivity coupled with good chemical resistance to molten metals (particularly aluminium) enable aluminium titanate for fulfilling several metal contact applications in the foundry industry.[29]

However alumina lacks thermal shock resistance and has a relatively high thermal expansion coefficient of 8.7×10^{-6} °C^{-1}.[30] Earlier reports indicate that addition of higher quantity of aluminium titanate particles of uniform size would improve the thermo-mechanical response of the composite. The alumina-aluminium titanate composites exhibit functional as well as structural properties for applications such as thermal barrier coating, insulating components for diesel engines and high temperature substrate.

Usually alumina-aluminium titanate composite is synthesised by solid state reaction of alumina and titania.[31] However, the high processing temperatures (> 1600 °C) result in heterogeneous microstructure and abnormal grain growth in addition to the presence of unreacted residual titania phase. Alumina- aluminium titanate composites with controlled microstructure can be achieved starting from mixture of alumina and previously reacted aluminium titanate powders at high temperature. [32,33] Manurung et al. studied the effect of β- spodumene (maximum 15 wt%) addition on the thermo-chemical reaction of alumina-aluminium titanate composite and concluded that less than 5 wt% β -spodumene addition results in the formation of aluminium titanate which starts commencing at 1380 °C.[34] The green compact of alumina-20 vol.% of aluminium titanate composite which was prepared by covering titanium isopropoxide precursor on alumina powder and on subsequent heat treatment at 1300 °C resulted in high density. However, composites with larger second phase contents (20-40 vol.%) gave lower densities (95% of theoretical).[35] Padture et al. reported that alumina-aluminium titanate composite with a uniform distribution of alumina particles results in excellent flaw tolerance.[36] Different techniques are adopted for the fabrication of alumina-aluminium titanate composite. The aims of different techniques are to reduce the formation temperature of aluminium titanate as well as to avoid microcracking due to the thermal expansion anisotropy of aluminium titanate. Recently microcrack free alumina-aluminium titanate composite was prepared by colloidal filtration

method using alumina and titania as precursors and was finally sintered at 1450 °C but the average grain size reported here was above 5 μm for the 10% addition of aluminium titanate.[37] In many of the reports the sintered grain size of aluminium titanate is much higher than 1.5 μm which is the critical limit to initiate microcracking.[38] To the best of our knowledge no attempt has been made to synthesise aluminium titanate in alumina matrix through a simple sol-gel core-shell approach, which is shown to have advantage with respect to controlled fine grain size and homogeneity of distribution of phases.

Over the last decade there have been immense efforts to fabricate core shell materials with tailored structural, optical, and surface properties.[39] Earlier reports reveal that similar approach has been attempted in other composite systems such as AT-25% mullite composite[40] and $MgAl_2O_4$ – ZrO_2 nano composite.[41] Alumina was coated on silicon carbide particles to further process Al_2O_3- 5 vol% SiC nanocomposite at low temperature where silicon carbide particles could be dispersed preferentially at grain boundary of alumina very effectively.[42] The main application of nanocoated particles may either be seen in the formation of diffusion barriers to avoid grain growth or in the modification of physical properties of the core and the chemical properties of the surface.[43] Techniques similar to core-shell approach have been reported for preparing powder having a uniform coating of $BaTiO_3$ on Ni particles. The reduction in shrinkage rate is achieved by preventing Ni from oxidation during sintering, which make it useful as a multilayer ceramic capacitor.[44] Monodisperse silica spheres with magnetic

cores were formed by silica precipitation on to magnetite particles.[45] Titania coated silica spheres have received a lot of attention because of their potential use in catalytic, pigment, and photonic crystal application.[46] Micrometer sized iron particles were coated with silica by the hydrolysis of TEOS in order to improve the oxidation behaviour of iron particles.[47] Recently, boehmite coating on Si_3N_4 was found to improve the consolidation density as well as the green-state plasticity of Si_3N_4. Therefore, the ceramic coating not only can improve the distribution of sintering aids, but also modify the rheological and consolidation behaviour of a ceramic suspension.[48] Microcomposite particle consisting of alumina core and amorphous silica coating to form mullite phase are reported in which full densification is achieved at as low as 1300 °C. The problem of heterogeneity of the second constituent in the preparation of ceramics can be considerably solved by the core-shell approach.

In the present technique, nano titania coated alumina preferentially reacts to form aluminium titanate in the composite. This approach of in-situ reactive formation of aluminium titanate results in low temperature sintering of the composite. These results demonstrate that such powders can be sintered at 1350 °C and that a sintered grain size 1.5-2.0 μm can be achieved. This method is effective in controlling the grain size of alumina and aluminium titanate, low temperature formation of aluminium titanate and further low temperature sintering of the composite. The synthesis procedure, formation of high temperature phase,

densification and microstructural details of alumina-aluminium titanate are presented in this chapter.

2.2.1 Experimental

Titanium tetrachloride (99%purity M/S Kerala Minerals and Metals Ltd, Kollam, India) A16 SG alumina powder (99%purity ACC-ALCOA Chemicals, Kolkata, India, Av. Particle size 0.3 μm), HNO_3 (Merck, India) solution, and Ammonia solution 25% (S.D. Fine chemicals India) were used.

In a typical experiment, to prepare the titania sol, titanium tetra chloride was dissolved in ice cold distilled water (0.2 M) and was hydrolysed by slow addition of ammonium hydroxide (25% S.D. Fine Chemicals, India), solution under constant stirring at room temperature, until the reaction mixture attained pH=9.0. The precipitate was separated by filtration and was washed free of chloride ions (as was confirmed by the AgCl test) with hot distilled water. The precipitate (5 g) was further dispersed in 1000 mL water and was peptised by the addition of 20% HNO_3 (Merck, India) solution.[49]

The estimated titania sol was used to coat on alumina kept in suspension, which was prepared by dispersing alumina powder (depending on the respective compositions **Table 1.**) in 1000 mL of water. Stirring was continued for 30 min and the additional titania required for aluminium titanate was added in the form of titanium hydroxide precipitate (depending on the required compositions **Table.1**). The whole mixture was then peptised to a stable suspension by the addition of 20

% HNO_3 (Merck, India) which was flocculated by slow addition of ammonium hydroxide to bring to pH= 6.5 and was further dried in an oven at 80 °C.[50] The process flow sheet is provided in **Figure 14.**

Zeta potential was measured using Zetasizer Malvern Instrument UK. Small amounts of Al_2O_3, TiO_2, and Al_2O_3 @ TiO_2 powder were separately dispersed in water and the pH was adjusted using 0.1 M HNO_3 or NaOH for acidic and basic solution respectively. The final zeta potential was the mean value averaged from three measurements.

The particle size analysis was carried out using Laser Particle Size Analyzer on the powders calcined at 80 °C and 1000 °C (Zeta Sizer, Malvern Instruments UK).The sample for the particle size analysis was made by ultrasonic dispersion of the respective powders (1 g) in aqueous medium (100 mL) at pH <2.0. Average of three measurements with in a standard deviation of 3.0 % is reported.

The coating of titania on alumina particle was observed under Transmission Electron Microscope (FEI, TECNAI 30 S- Twin (Netherlands)) operated at 300 kV and equipped with an energy-dispersive X-ray analyzer (EDX)). The powder was dispersed in acetone and a drop of the suspension was deposited on a carbon-coated copper grid (TEM) and dried.

X-ray Photoelectron Spectroscopy (XPS) was performed using a Quantum 2000 device by Ulvac-Phi, Japan, on the composite precursor sample calcined at

1000 °C.

The dried precursor gels were subjected to DTA analysis (Shimadzu, DTA-50H) at a heating rate of 5 °C min^{-1} up to 1400 °C. The dried gels were individually heated at 1350 °C in electric muffle furnace and then cooled in air to room temperature. The phase identification was done using XRD (Philips PW 1170) in the 2θ range of 20-60 Cu Kα. The structure evolution was done by the FTIR analysis.

The precursor was calcined at 900 °C compacted uniaxially at 200 MPa using 2 wt% PVA as binder and sintered in the range 1350-1450 °C. Morphological characterization of the sintered pellet was performed using scanning electron micrograph (SEM, JEOL, JSM 560 LV, Japan) on samples after polishing and thermally etching at 1325 °C. The average grain size was calculated by the linear intercept method using the relation G = 1.5L/MN where 1.5 is a geometry dependent proportionality constant, L is the total test line length, M the magnification and N the total number of intercepts. For the grain size determination four representative micrographs with the magnification of 4000X were analyzed. A test line of 9 cm length was marked on the micrograph and the number of intersections of the line with grain boundaries was counted.

2.2.2 Preparation of a Reference Sample

In order to compare the reactivity of the titania coated alumina particles as well as the properties of final alumina-aluminium titanate powders with the

conventional solid-state process, a mixture of the same alumina powder used for the coating process and TiO_2 (anatase TiO_2 Sigma Aldrich) was prepared by ball milling in water. The powder was subjected to similar thermal treatment as that of the coated precursor.

Table 1. Alumina and titanium hydroxide in wt% used in 50 g batch of Al-AT composites

Composite	**A-5%AT**	**A-20%AT**	**A-40%AT**	**A-50%AT**
Alumina Al_2O_3	47.5 g	40.0 g	30.0 g	25.0 g
Titanium hydroxide $Ti(OH)_4$	1098 mL (Titania sol)	39.86 g	113.08 g	149.66 g

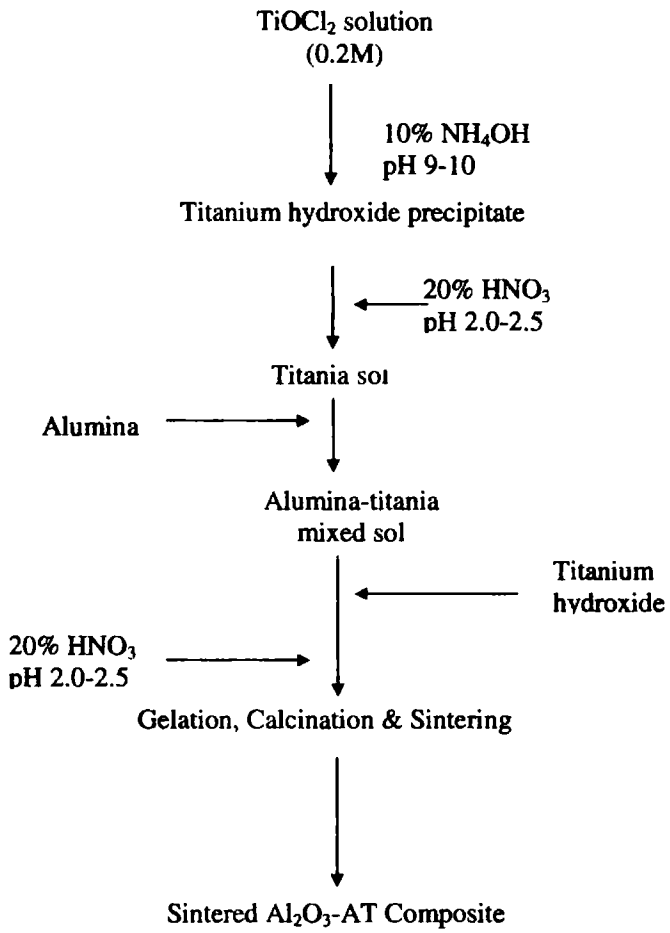

Figure 14. Flow sheet for the preparation of alumina-aluminium titanate composite

2.2.3 Results and Discussion

The synthesis of the precursors were done at controlled pH condition which create high zeta potential in aqueous suspension of alumina and nano size titania sol. When alumina particles are dispersed in water, protons or hydroxyls are adsorbed on the surface of the alumina particle. The addition of titanium hydroxide to this dispersion may result in a substitution reaction between the titanium hydroxide and the –OH groups on the surface of alumina. This may be the possible mechanism for titania coating over alumina particle.[51] Such a situation provides excellent distribution of titania species on individual alumina particles facilitating low temperature formation of aluminium titanate.

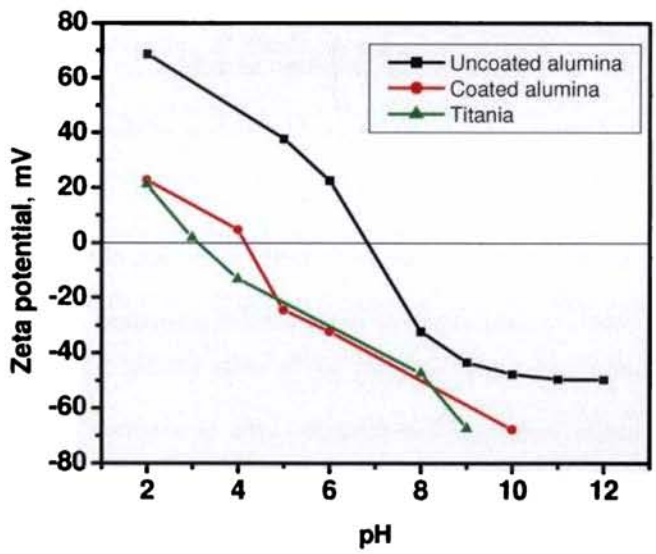

Figure 15. Zeta potential measurement of alumina, titania and titania coated alumina particle

Zeta potential of the alumina, titania, and the titania coated alumina were measured with Malven Zeta Sizer. The results are shown in **Figure 15.** The isoelectric point of alumina was located at the pH 7.8 which has shifted to 4.5 after coating with titania. Study reported on alumina coated SiC shows that the isoelectric point of SiC is shifted from pH 4 to pH 8 after coating with alumina.[52] The shift in the isoelectric point is explained on the basis of specific adsorption of alumina on SiC surfaces. In another study, the isoelectic point of α-Al_2O_3 was found to shift from pH 7.5 to pH 2.2 due to the specific adsorption of poly acrylic acid (PAA).[53] In the present work alumina suspension was prepared at pH=3.0 leading to a zeta potential value of +60 mV. Similarly titania sol prepared at pH=3.0 has a zeta potential value of +2.9 mV. Therefore the titania nanoparticles produced by the hydrolysis of the titanium tetrachloride solution will have a spontaneous tendency to self-assemble on the surface of the alumina particles by heterocoagulation. Since even a single layer of titania is sufficient to alter the electrokinetic behaviour of surface of alumina particles, this may indicate the uniformity of titania coating achieved in the present procedure.

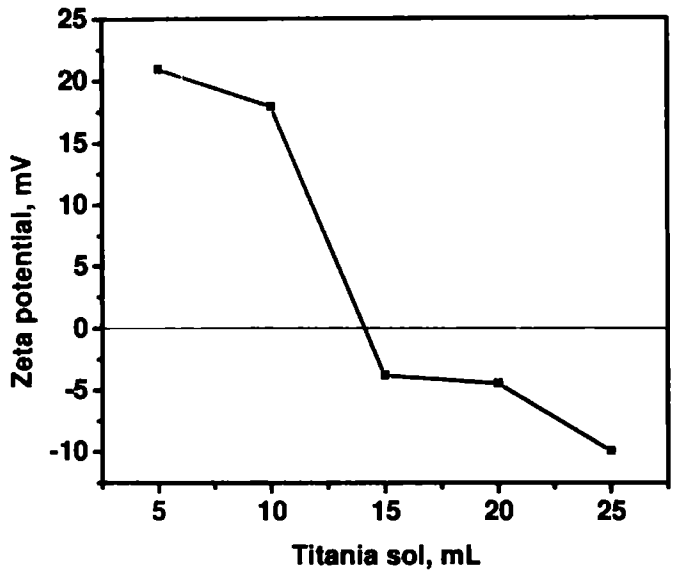

Figure 16. Variation in zeta potential of alumina suspension with respect to titania sol addition

The process of coating of titania on alumina was monitored by the addition of 5 mL to 25 mL titania sols to alumina suspension separately and measuring the zeta potential of the suspension. The corresponding results are shown in **Figure 16.** The initial pH was 2.0 and the zeta potential is 22.0 mV. The addition of titania sol from 5 mL to 25 mL causes a dramatic decrease of zeta potential values from 22.0 mV to -10 mV, while the pH value of the alumina suspension increased from 2.0 to 2.4. The sharp decrease in zeta potential indicated that titania particle had already got adsorbed on to the surface of alumina particle and is progressive with increasing titania concentration as shown in **Figure 16.**

Differential thermal analysis (DTA) of A-20%AT composite precursor, presented in **Figure 17** shows an endothermic peak at 80 °C which indicates the removal of physically adsorbed water. Rutile formation is observed at 1100 °C and an endothermic peak in the DTA at 1300 °C shows the presence of aluminium titanate in the composite. Earlier reports indicate that alumina-aluminium titanate composite synthesized by partial infiltration of a porous alumina preform with titanium ethoxide results in aluminium titanate formation at 1350 °C[54] and β-spodume addition in alumina–aluminium titanate composite results in the formation temperature of aluminium titanate at 1380 °C.[55] In the present method titania-alumina reaction is preferentially enhanced due to the high reactivity of the coated precursors.

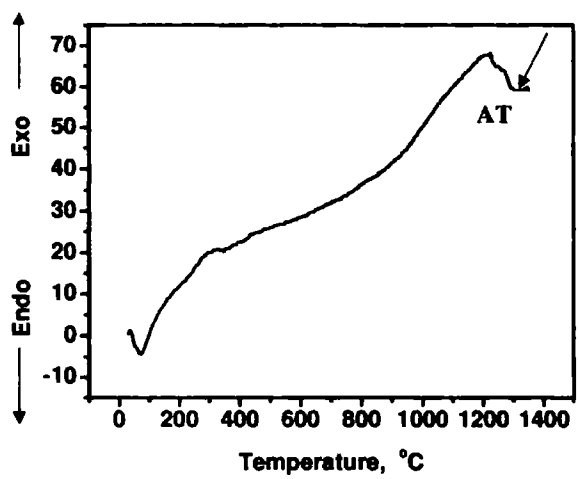

Figure 17. DTA analysis of A-20%AT composite.

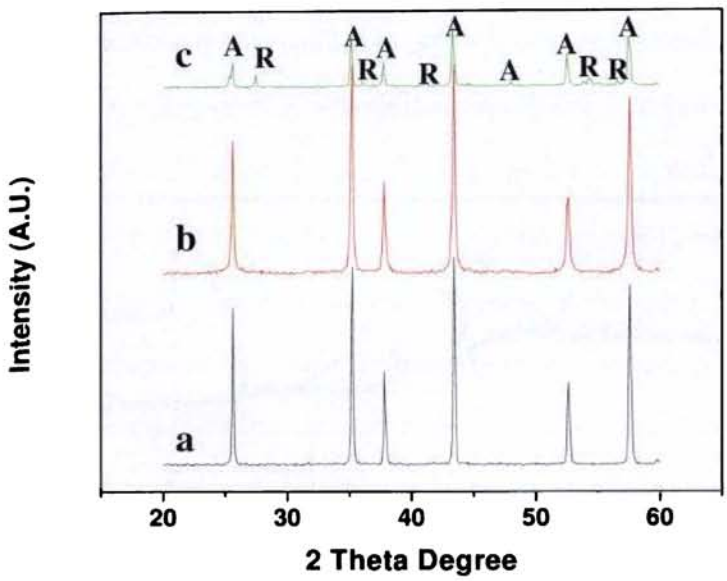

Figure 18. X-ray diffraction pattern of **a)** alumina **b)** alumina-aluminium titanate precursor dried at 80 °C **c)** alumina-aluminium titanate precursor calcined at 1000 °C, **A** alumina, **R** rulite titania

Figure 18. XRD patterns of the as–coated and dried powder show only the peaks of alumina, meaning that the TiO_2 coating is mainly amorphous. The intensity of the titania diffraction pattern was much lower than that of Al_2O_3 hence it was very hard to detect such pattern from normal XRD pattern. The 1000 °C calcined powder shows highly crystalline peaks for titania. The coating is confirmed by the results of the X-ray photoelectron spectroscopy (XPS) studies. According to literature the highest intensity peaks of Al (2S) & Al (2P) are observed at 74.0 eV and 74.2 eV respectively.[56] The results of XPS (powder

calcined at 1000 °C) show that the highest intensity peaks of alumina are attenuated and hence it is confirmed that a uniform coating of titania exits over alumina (**Figure 19 a**). The XPS spectrum also shows the presence of major peaks of Ti (2P) 458.5 eV.[57]

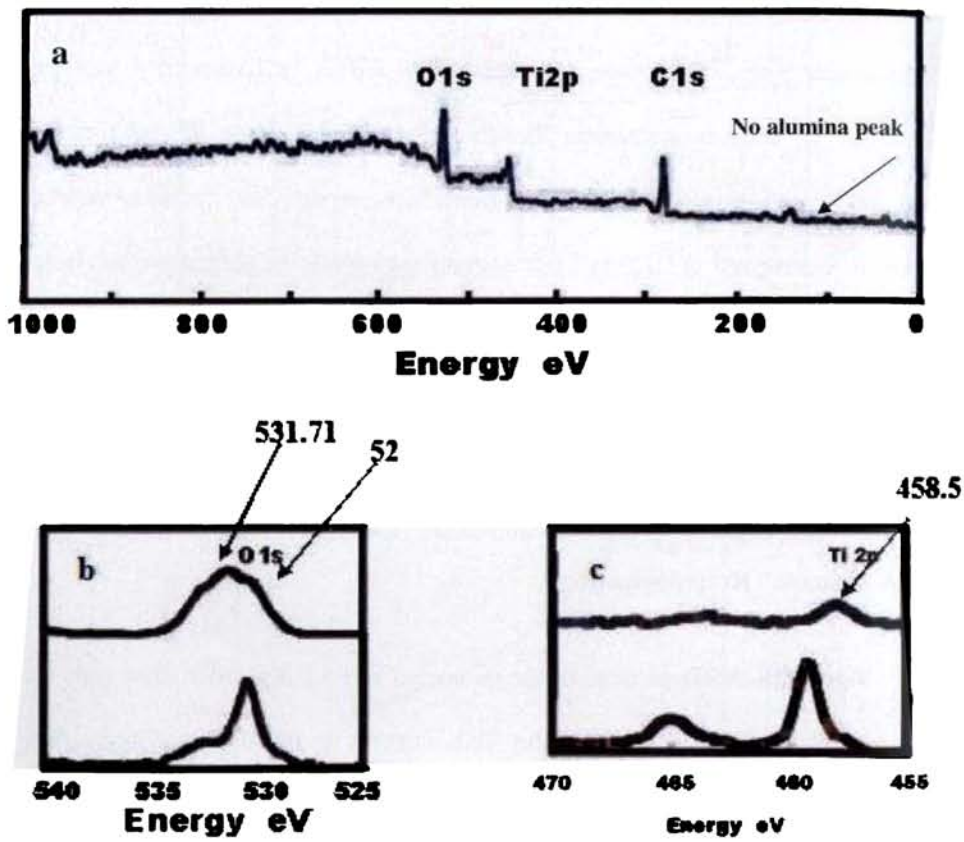

Figure 19 a. XPS survey of Al- 20%AT precursor calcined at 1000 °C

Figure 19 b. High resolution XPS spectra of the O1s of the Al-20%AT precursor calcined at 1000 °C

Figure 19 c. High resolution XPS spectra of the Ti 2P of the Al- 20%AT precursor calcined at 1000 °C

The high resolution XPS spectra of the O1s and Ti 2p are shown in **Figure 19b & 19c** respectively. The peak of Ti 2P at 458.5 eV is shifted compared to pure titania. The O1s peak of TiO_2 coated alumina particle was shown in **Figure 19b** which indicates that the main peak of O1s consists of a main peak and a shoulder.[58] According to literature one peak can be assigned to bulk O^{2-} and the other peak to –OH. The –OH and bulk O^{2-} peaks of the coated Al_2O_3 particle surface are assigned to Ti $(OH)_4$. The intensity of –OH is large compared to the bulk O^{2-} and this is due to the adsorbed coating film of hydrous $Ti(OH)_4$ rich in –OH.[59] The absence of alumina peak in the titania coated alumina particle suggested that a thick coating of titania is formed on the alumina particle.[60] Therefore only the peaks of titanium, oxygen and carbon are observed in the spectra of titania coated alumina particle.[61]

The microstructure of titania coating on alumina was observed by TEM and details are presented in **Figure 20a.** Alumina particles are fully covered by titania with an average thickness of almost 24 nm. The TiO_2 coated alumina powder calcined at 1000 °C shows the presence of a smooth layer of titania coating. In some case a cluster of alumina particles is uniformly coated with nano titania layers with an average coating thickness of 24 nm or sometimes titania coated alumina particles are stacked together as is shown in **Figure 20b.** Particles even larger than 200-400 nm could be easily coated by the present approach.

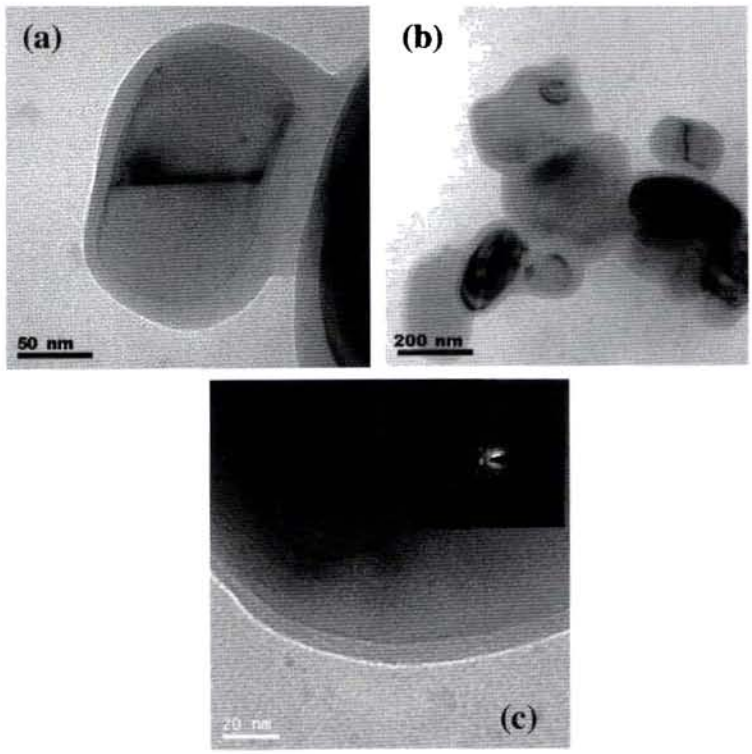

Figure 20a. Typical TEM image of TiO_2 coated Al_2O_3 single particle

Figure 20b. Typical TEM image of TiO_2 coated Al_2O_3 a cluster of particles

Figure 20c. Morphology of TiO_2 coated Al_2O_3, and insert the corresponding SAED pattern

The coating was crystalline as shown by the SAED pattern presented in **Figure 20c.** The macroscopic driving forces responsible for the spontaneous assembly of the nanocrystals in the shell are related to the replacement of solid-liquid interfaces by solid-solid interface of lower energy. Also the entropy is increased because water and absorbed ions are removed.[61] The centre of the

alumina particle is darker than their outer regions because the centre of a spherical particle is thicker.[62]

Many researchers refer to electrostatic attraction in order to explain the coating of the shell-particles on a core in an aqueous medium because of opposite surface charges. Other suggested mechanisms are the heterogeneous nucleation on the core particle or ion adsorption on the core. Furthermore Wu et al. suggested the collision of the shell-particle and core particle substrate followed by a condensation between them.[63]

The particle size distribution of TiO_2 coated Al_2O_3 dried at 80 °C and 1000 °C is presented in the **Figure 21.** The powder dried at 80 °C shows an average particle size of 340 nm with a PDI value (poly dispersity index) of 0.4, where as 1000 °C calcined sample shows 486 nm average particle size with a PDI value of 0.6. Al_2O_3 mechanically mixed (solid state mixing) with TiO_2 shows higher particle size distribution. The sample at 1000 °C shows a higher particle size due to aggregation of the particle in aqueous medium compared to as dried powder.

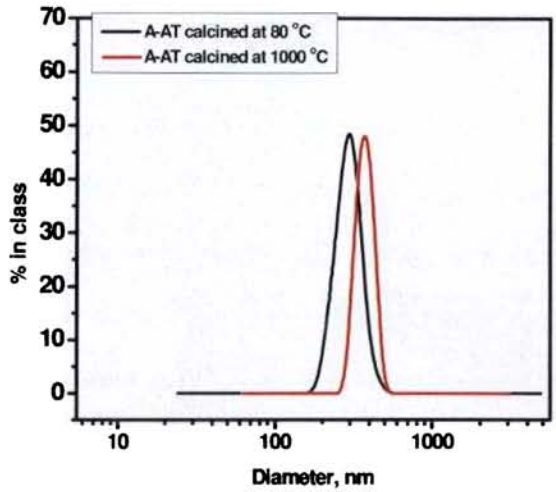

Figure 21. Particle size of sol-gel coated A-20%AT at 80 °C and 1000 °C

The XRD analysis of the reference sample calcined at 1300 °C presented in Figure **22.** shows the presence of alumina and rutile titania phase where as the core-shell approach shows the presence of alumina and aluminium titanate phases. This shows that the present core-shell approach was effective in the low temperature formation of aluminium titanate compared to the conventional solid state mixing route because of the faster diffusion rate due to proximity of alumina and titania.

The formation of aluminium titanate occurs above the eutectoid temperature 1280 °C. The solid state reaction between Al_2O_3 and TiO_2 involves the vapour phase transport or bulk diffusion of one or both of the reactants. Aluminium titanate formation is a nucleation growth process. A slow first stage

which involves nucleation is followed by a rapid second stage associated with an appreciable increase in the reaction rate and grain growth. The activation energy for the reaction of 229 ± 45 kJ.[65] This value corresponds closely to that for the diffusion of Ti in presence of small amounts of alumina.

$$Al_2O_3 + TiO_2 \longrightarrow Al_2TiO_5$$

Heating above 1280°C was accompanied by rapid grain growth resulting in formation of microcracks. It was reported that titanium has limited solubility in alumina (0.5% per Al_2O_3 unit) and the diffusion of the titanium is also slow. An initial rapid period characterised by the nucleation and growth of the aluminium titanate cells, followed by subsequent removal of the remaining unreacted oxides governed by diffusion which occurs slowly. The faster diffusion rate of titania into the alumina matrix can be achieved through the core-shell approach, compared to the solid state mixing where the contact area of the reactant is minimum. This is similar to mechanism of formation of $BaTiO_3$ by a core-shell approach. The formation of $BaTiO_3$ layer is explained to occur at the $BaCO_3/TiO_2$ interface, and further the growth proceeds by diffusion of the barium ion across the perovskite layer toward the $BaCO_3/TiO_2$.[66]

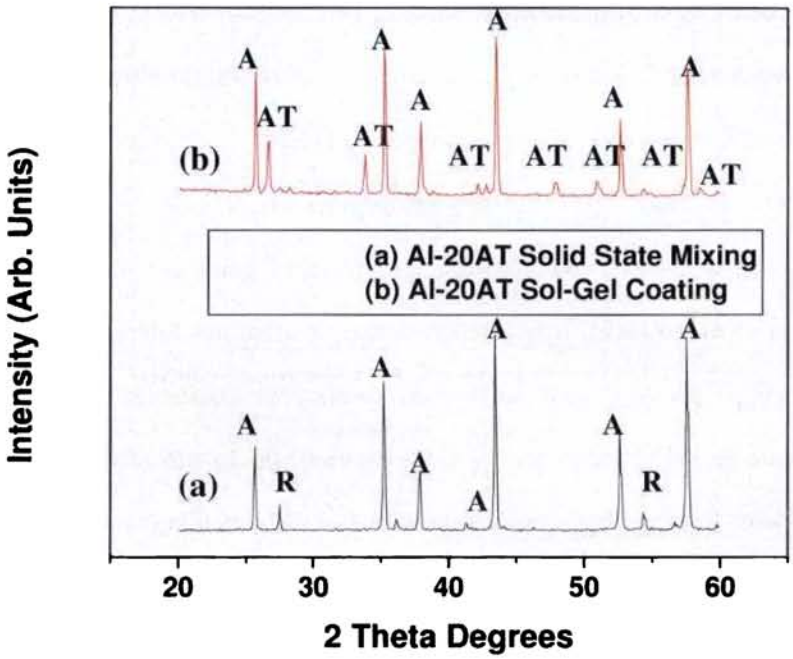

Figure 22. XRD of Al-20%AT (a) solid state mixing and (b) sol-gel coating at 1300 °C, **R** rulite titania, **A** alumina, **AT** aluminium titanate

The XRD analysis (**Figure 23.**) of composite precursor calcined at 1350 °C shows the presence of α- alumina, aluminium titanate and the absence of rutile phase. The XRD peak intensity of aluminium titanate increases with the amount of aluminium titanate. The diffraction intensities of the (110) & (023) planes of Al-5%AT, Al-20%AT, Al-40%AT, Al-50%AT, are larger compared with those of alumina indicating the presence of anisotropic grains oriented along the (110) &

(023) planes.[64] XRD analysis shows that 50% addition of aluminium titanate in the composite dominates in aluminium titanate phase.

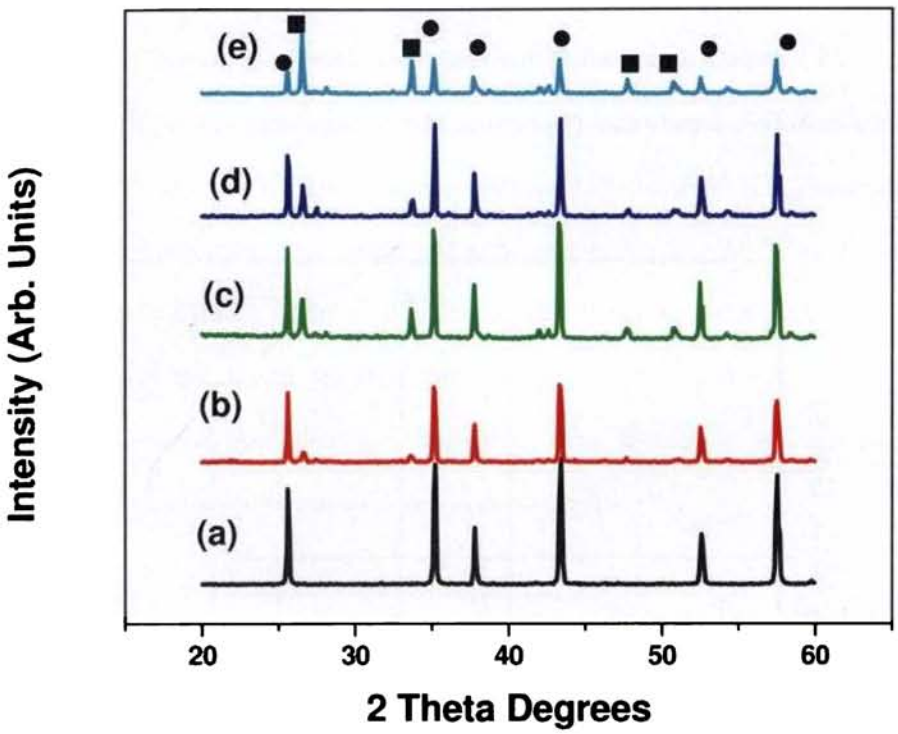

Figure 23. XRD of alumina-aluminium titanate composite calcined at 1350 °C/3h, (a) Alumina, (b) Al-5%AT (c) Al-20%AT (d) Al-40%AT (e) Al-50%AT.
• Alumina, ■ Aluminium titanate

The densification behaviour of the composite precursor (Al-20%AT) and alumina calcined at 900 °C was monitored by dilatometry as shown in **Figure 25.** The densification takes place in one step up to 1350 °C. Differential of shrinkage

curve of composite shows that the shrinkage rate is higher compared to pure alumina. In the composite, the shrinkage starts at 1100 °C and continues up to 1350 °C. The former is due to the formation of rutile phase (confirmed by XRD **Figure 24.**) and the latter is due the formation aluminium titanate phase. The major shrinkage is seen to take place in the temperature range 1100-1350 °C.

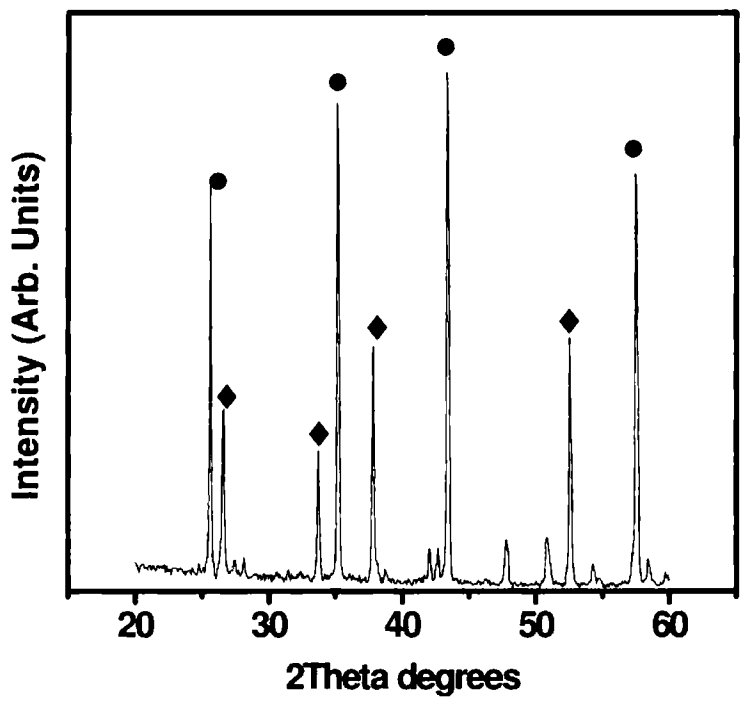

Figure 24. XRD of alumina-aluminium titanate composite precursor (Al-20%AT) calcined at 1100 °C/3 h, Alumina ●, Rutile ◆.

The sintering of alumina-aluminium titanate precursor compact was carried out at temperature range of 1350-1450 °C with 3 h soaking time. The typical

sintering schedule was as follows: RT to 800 °C at a rate of 3 °C/min, 800 to 1200 °C at a rate of 5 °C/min and then up to maximum sintering temperatures at 10 °C/min. The relative density of the sintered specimen was calculated by rule of mixtures. The theoretical density of alumina and aluminium titanate was taken as 3.97 g/cm^3 and 3.70 g/cm^3 respectively. Alumina without any additives sintered to 85% density at 1350 °C (green density 66.4%) and 95% at 1450 °C. The sintering temperature of alumina was further reduced considerably (by 100 °C) in presence of aluminium titanate. Addition of as low as 5 %(weight) aluminium titanate was able to raise the density by about 98% at 1350 °C (green density 66%). The tendency of enhanced sintering is shown up to an addition of 40% aluminium titanate after which higher temperature is necessary.

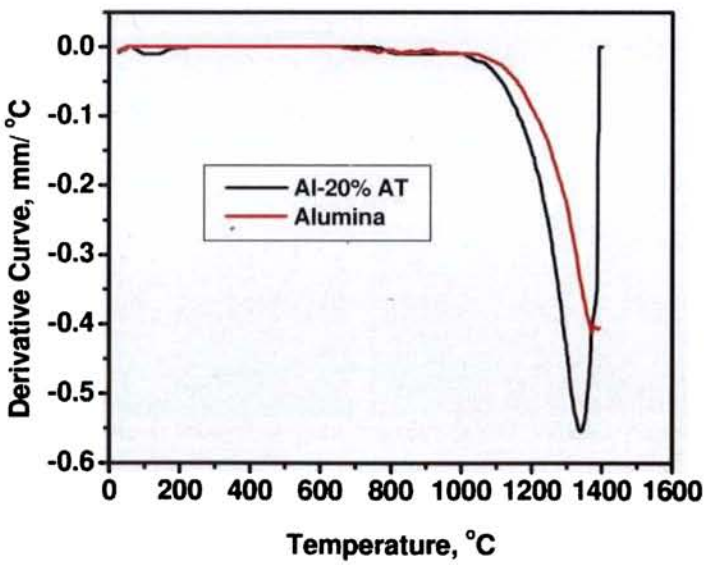

Figure 25. Differential shrinkage behaviour of alumina and Al-20% AT composites

The low temperature sintering is due to the faster diffusion rate in core-shell particle compared to the conventional solid state sintering route. The average grain size of aluminium titanate and alumina is 1.5 μm, 2.0 μm respectively. **Figure 26 (a) & 26 (b)** show SEM micrograph of sintered Al-5%AT and Al-20%AT composites at 1350 °C respectively. The addition of AT to Al_2O_3 is expected to control the grain growth of both alumina and aluminium titanate. On the other hand, **Figure 26(c)** indicates further grain growth observed and this sample was sintered at 1450 °C. No microcracks are observed in any of the samples sintered at lower temperature indicating the absence of abnormal grain growth of AT grains. Under the present conditions of preparation the aluminium titanate particles were preferentially distributed at the grain boundaries and this could be due to the novel approach of the pre-coated precursor. The homogeneous distribution of aluminium titanate grains in the alumina matrix was confirmed by SEM-EDX analysis as shown in **Figure 27.** The microstructure analysis of the composite shows that the grain size of aluminium titanate is lower than the initial particle size of alumina. The titania in the precoated alumina particles get converted to rutile at 1200 °C and get distributed at the grain boundaries of alumina which could initiate the sintering process. Further, the aluminium titanate formed in-situ may act as centre for controlling the grain growth of alumina. Hence the grain growth in alumina is prevented and the composite gets sintered at a low temperature.

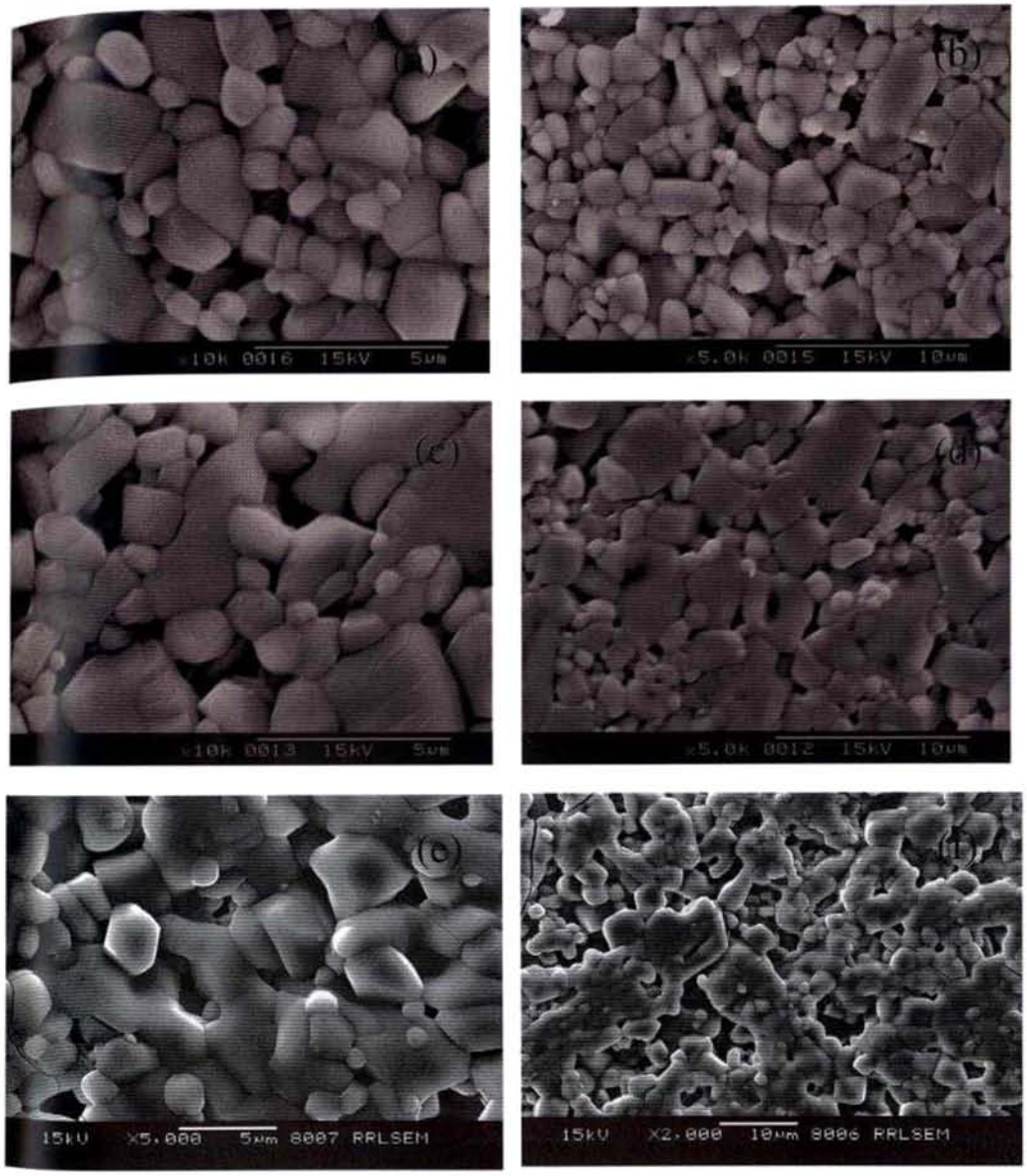

Figure 26. Al-AT composite sintered at 1350 °C/3 h. (a,b) Al-10%AT, (c,d) Al-20%AT, (e,f) Al-40%AT

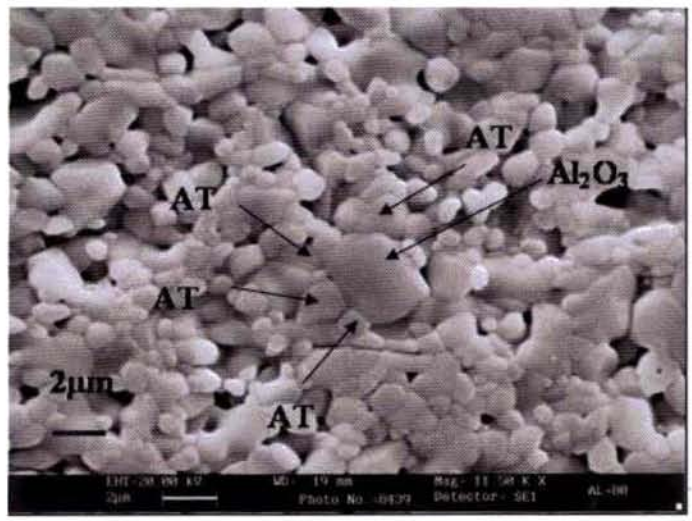

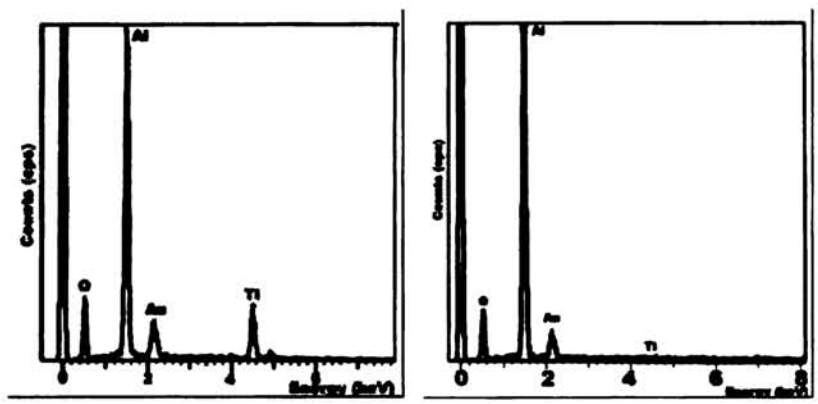

Figure 27. Al-20%AT composite sintered at 1350 °C (marked area is the spot were the EDX analysis was performed)

FTIR spectrum (**Figure 28.**) has been used to follow the in-situ formation of the high temperature aluminium titanate phase. The spectral ranges (1) 3000-

3500 cm^{-1}, where the OH vibrations of water and OH groups appear and (ii) 200-850 cm^{-1} where the Al-O and Ti-O stretching and bending vibration are followed. The Al-20%AT gel dried at 80 °C, shows a very board band above 3000 cm^{-1} with a peak at 3436 cm^{-1}, which is assigned to the stretching mode of absorbed water. The intensity of these bands decreases gradually with increase in temperature. The IR band of the gel calcined at 250 °C shows a shoulder at 850 cm^{-1} which is due to the metal-oxygen bond (Al-O tetrahedral). It was reported that during the aluminium titanate formation all the Al-O tetrahedral vibration changes to octahedral Al-O vibration. The sample (Al-20%AT **Figure 29.** calcined at 1300 °C shows complete absence of an intense band at 441 cm^{-1} which clearly indicates the absence of tetrahedral vibration but the sample shows the presence of an intense band at 465 cm^{-1} which is due to the presence of octahedral vibration. The reference sample shows an intense band at 436 cm^{-1} which clearly indicates the presence of tetrahedral vibration.[68] The FTIR studies show that the core shell approach is effective in the low temperature formation of aluminium titanate compared to the solid-state mixing.

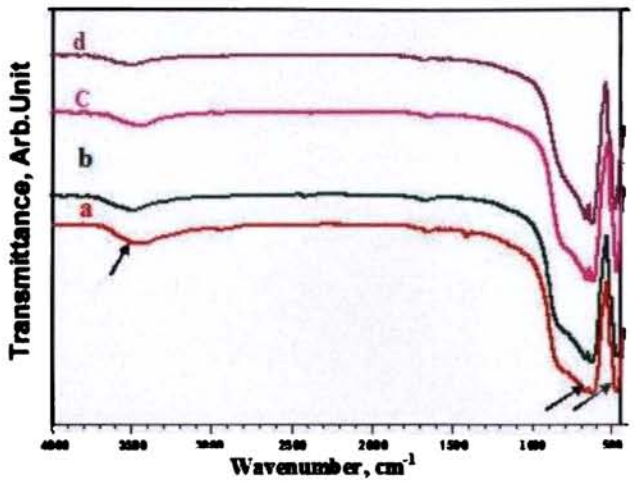

Figure 28. FTIR Spectrum of Al-20%AT calcined at (a) 80 °C (b) 250 °C (c) 1000 °C and (d) 1300 °C

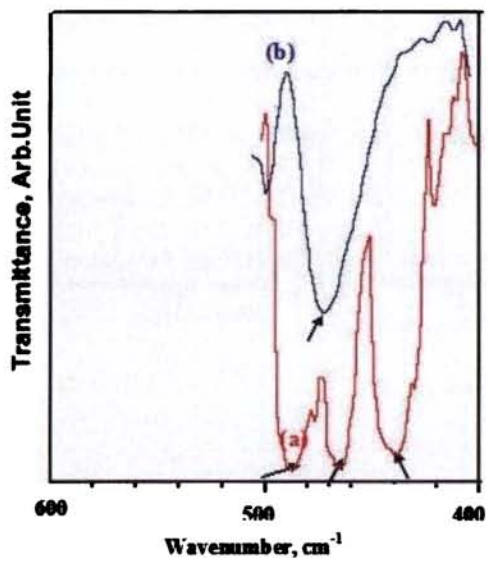

Figure 29. FTIR Spectrum of Al-20%AT calcined at 1300 °C (a) reference sample (b) core-shell sample

2.2.4 Coefficient of Thermal Expansion

The linear thermal expansion coefficient of Al-20% AT composite compared with alumina are presented in **Figure 30&31.** The average linear thermal expansion of alumina is 8.62×10^{-6} °C^{-1} and aluminium titanate is -9.7×10^{-6} °C^{-1}. The alumina-20% aluminium titanate sintered at 1350 °C shows a thermal expansion coefficient value of (5.77×10^{-6} °C^{-1}) which is about 44% less of that of alumina. The aluminium titanate shows an average thermal expansion value of 1.1×10^{-6} °C^{-1}.[49]

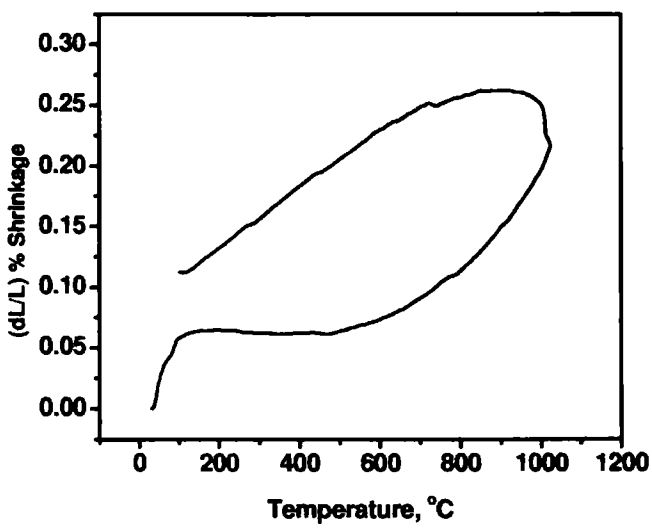

Figure 30. Coefficient thermal expansion plot of Al-20% AT sintered at 1350 °C

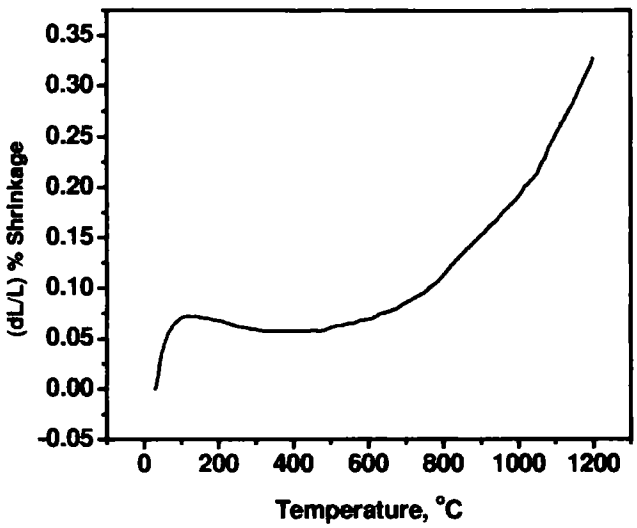

Figure 31. Coefficient of thermal expansion plot of alumina sintered at 1600 °C

2.2.5 Thermal Shock Resistance

Alumina is regarded as one of the most promising ceramic materials because of its attractive properties such as wear, deformation resistance and chemical inertness but lacks thermal shock resistance which limits its high temperature application. The maximum temperature drop, ΔT_c that the material can sustain without cracking is a measure of its thermal shock resistance. The classic equation that describes the thermal shock resistance of brittle materials under mild thermal shock condition was established by Hasselman in 1969.[69] The

maximum temperature increment that the material can stand without fracture, T_c is given by,

$R = k \sigma_f / E\alpha$

where k= conductivity, σ_f = strength, E= Young's modulus, α= thermal expansion coefficient. It was difficult to vary the strength, thermal conductivity and thermal expansion coefficient of monolith but we can control these parameters by the addition of second phase. A second phase with lower young's modulus and thermal expansion coefficient than alumina matrix would improve its resistance to thermal shock. The main factors affecting the thermal shock damage of ceramic material are surface finish, strength, thermal expansion coefficient, thermal conductivity, elastic modulus, dimension of the sample and Poisson's ratio.[70]

The beneficial effect of mullite, neodymium titanate, aluminium titanate, aluminium nitride as second phase on the thermal shock resistance of alumina was reported by other authors. In a previous work Budian et al. reported that 10 vol% mullite as a second phase in alumina matrix shows good thermal shock resistance (≈12%) was due solely to the decrease of the product $E \cdot \alpha$.[71] It was also reported that for a composition Al–10%AT ΔT_c was further increased (≈30–40%) due to the toughening effect of the second phase.[72] Aluminium nitride (AlN) is also used as second phase material to improve the thermal shock resistance of alumina. AlN might have some toughening effect on the composite due to its thermal expansion

mismatch with alumina, as observed for alumina-aluminium titanate composites.[73] The alumina–aluminium metal composites with improved thermal shock resistance under severe thermal shock conditions have been reported by Aghajanian et al.[74] Wang et al. reported that alumina shows 120 °C higher thermal shock than the monolith with the addition of piezoelectric secondary phase like neodymium titanate.[75]

Water quenching technique was used for thermal shock tests. The sintered specimens were heated at a rate of 5 °C/min to a pre-set temperature and held at this temperature for 3 h. Then the heated specimens were dropped into a water bath which was maintained at 20 °C. At least three specimens were tested to obtain the average compressive strength. The compressive strength is measured using a Universal Testing Machine (INSTRON 1195), using sample size where the height of the sample is 2 times higher than the diameter.

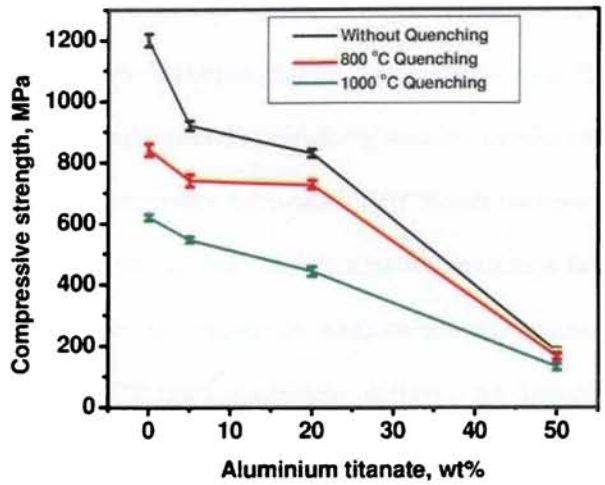

Figure 32. Compressive strength of alumina-aluminium titanate composite with varying aluminium titanate addition before and after quenching

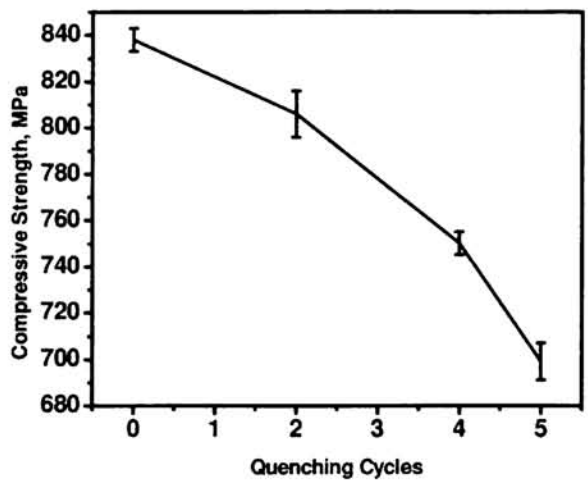

Figure 33. Compressive strength of Al-20%AT after different quenching cycles at 800 °C

The thermal shock behaviour of the composite was measured based on the strength degradation in the composite with respect to the temperature increment (**Figure 32**). The strength of a range of alumina-aluminium titanate composite was measured after thermal shock. The Al-20% AT shows comparable strength before and after thermal shock resistance at 800 °C, but the strength degradation start at 1000 °C. This shows that the Al-20% AT composite show better thermal shock resistance compared to monolith alumina at 800 °C. The quenching cycle experiment on Al-20% AT was also performed which shows that the strength gradually degrades after each thermal cycling (**Figure 33**).

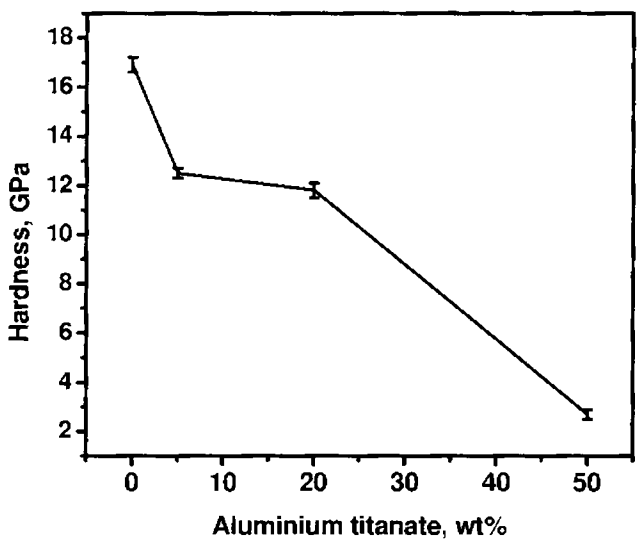

Figure 34. Vickers hardness of different aluminium titanate content in the alumina matrix

Hardness is an important parameter as an indication for machinability of ceramics. For sintered ceramics having comparable grain sizes, and lower hardness values indicate better machinability. Vickers hardness (HMV 200, Shimadzu) was measured under a load of 4.9 N and at a dwell time of 14 s on the polished surface of the composite sintered at 1350 °C and pure alumina sintered at 1650 °C. **Figure 34.** shows the experimental relationship between Vickers hardness and different aluminium titanate content in the alumina matrix. Along the addition of aluminium titanate, a sharp decrease in the hardness of the Al_2O_3/AT composites due to the soft interface formation. The hardness of alumina-aluminium titanate composite containing varying aluminium titanate addition was measured. The results show that the hardness of alumina decreases with increase in addition of aluminium titanate.

2.3 Conclusions

The effect of hydroxide precursors on the sol-gel synthesis of aluminium titanate was studied. The in-situ peptisation of the hydroxide precursors resulted in nano scale starting particles which facilitate the formation of aluminium titanate phase at considerably low temperatures. The average particle size of 100 nm was achieved for the aluminium titanate precursor calcined at 1000 °C. The aluminium titanate phase formation was observed at lower temperature of 1320 °C. This may be due to close proximity of hydroxide of both alumina and titania. The aluminium titanate sintered at 1550 °C showed 94% relative density. The microstructure indicates crack free dense aluminium titanate grains of size 2-3 μm. The thermal expansion coefficient was as low as 1.1×10^{-6} K^{-1} over a temperature range of 200-600 °C.

Further, a novel synthesis route based on core-shell approach for alumina-aluminium titanate composites as well as the low temperature sintering resulting in a fine grained microstructure was reported. Formation of amorphous titania shell on alumina particles which are kept in suspension without segregation was achieved at high zeta potential value of +20 mV. The formation temperature of aluminium titanate from the precursor containing Al_2O_3 and TiO_2 can be drastically reduced by the TiO_2 coated Al_2O_3 precursor particles instead of using a mechanical mixture of alumina and titania. The low temperature formation of aluminium titanate in the alumina matrix can be attributed to maximum contact area between the reactants in the core-shell approach when compared to the solid

state mixing route. The present approach results in good densification without significant grain growth. The composite sintered at 1350 °C shows a sintered density of 98% with an average grain size of 2 μm and 1.5 μm for alumina and aluminium titanate respectively.

The thermal shock resistance of in situ-formed alumina –AT composites was evaluated by water-quenching technique. Alumina with 20wt% addition of aluminium titanate shows excellent thermal shock resistance as indicated by critical temperature differential without fracture. Thermal stress developed in the material during quenching can be reduced by the high toughness value alumina-aluminium titanate composite by its bridging mechanism. The retained strength of the composite compared to alumina also is indicative of good thermal shock resistance. The results demonstrate that the addition of 20wt% aluminium titanate can improve the thermal and mechanical properties and hence improve the thermal shock resistance.

References

1. H. A. J. Thomas, R. Stevens, *Brit. Ceram. T.* **1989**, 88, 144 .
2. A. V. Prasadarao, U. Selvaraj, S. Komarneni, A. S. Bhalla, R. Roy, *J. Am. Ceram. Soc.* **1992,** 75, 1529.
3. E. Kato, K. Daimon, J. Takahashi, *J. Am. Ceram. Soc.* **1980,** 63, 355.
4. Y. Ohya, Y. Takahashi, Z. Nakagawa, *J. Mater.Sci.* **1996,** 31, 1361.
5. F. J. Parker, R. W. Rice, *J. Am. Ceram. Soc.* **1989,** 72, 2364.
6. K. Hamano, Z. Nakagawa, K. Sawano, Y. Hasegawa, *J. Chem. Soc. Jpn.* **1981,** 1981, 1647.
7. D. S. Perera, *J. Mater. Sci. Lett.* **1989,** 8, 1057.
8. M. Kaijiwara, *Brit. Ceram. T.* **1987,** 86, 77.
9. H. Wholfromm, J. S. Moya, P. Pena, *J. Mater. Sci.* **1990,** 25, 3753.
10. V. Buscaglia, P. Nanni, G. Battilana, G. Aliprandi, C. Carry, *J. Eur. Ceram. Soc.* **1994,** 13, 411.
11. V. Buscaglia, P. Nanni, *J. Am. Ceram. Soc.* **1998,** 81, 2645.
12. J. F. Bartolome, J. Requena, J. S. Moya, M. Li, F. Guiu, *Acta Mater.* **1996,** 44, 1361.
13. K. V. Baiju, C. P. Sibu, K. Rajesh, P. Krishna Pillai, P. Mukundan, K. G. K. Warrier, W.Wunderlich, *Mater. Chem. Phys.* **2005,** 90, 123.
14. A. K. Vasudevan, T. V. Mani, A. D. Damodaran, K. G. K.Warrier, *J. Mater. Sci.* **1995,** 14, 1317.
15. I. Stambolova, A. Toneva, V. Blaskov, D. Radev, Y. Tsvetanova, S. Vassilev, P. Peshev, *J. Alloy. Compd.* **2005,** L1, 391.
16. Y. M. Naseer, *Mater. Chem. Phys.* **2005,** 94, 3331.
17. A. M. Segadaes, M. M. Moreli, R. G. Akimininami, 5th ECERs Part I, Trans. Tech. Publication, **1997,** 209.
18. U. S. Hareesh, A. K. Vasudevan, P. Mukundan, A. D. Damodaran, K. G. K. Warrier, *Mater. Lett.* **1997,** 32, 203.

19. D. P. H. Hasselman, *J. Am. Ceram. Soc.* **1969,** 52, 600.

20. F. J. Parker, R. W. Rice, *J. Am. Ceram. Soc.* **1989,** 72, 2364.

21. J. A. Kuszyc, R. C. Bradt, *J. Am. Ceram. Soc.* **1973,** 56, 420.

22. Y. X. Huang, A. M. R. Senos, J. L. Baptista, Fourth Euro Ceramic –Vol-1 187.

23. I. Stamenkovic, *Ceram. Int.* **1989,** 15, 155.

24. K. Hamano, Taikabutu. **1975,** 27, 520.

25. J. J. Clevland, R. C. Bradt, *J. Am. Ceram. Soc.* **1978,** 61, 478.

26. P. Innocenzi, A. Martucci, L. Armelao, S. Licoccia, M. L. D. Vona, E. Traversa, *Chem. Mater.* **2000,** 12, 517.

27. B. Freudenberg, A. Mocellin, *J. Am. Ceram. Soc.* **1987,** 70, 33.

28. Y. Ohya, Z. Nakagawa, *J. Am. Ceram. Soc.* **1987,** 70, C184.

29. T. Matsudaira, Y. Kuzushima, S. Kitaoka, H. Awaji, D. Yokoe, *J. Ceram. Soc. Jpn.* **2004,** Suppl. 112–1, Pacrim 5 Special Issue, S327.

30. J. Barolome, J. Requena, J. S. Moya, M. Li, F. Guiu, *Acta. Mater.* **1996,** 44, 1361.

31. J. Barolome, J. Requena, J. S. Moya, Li M, F. Guiu, *Fatigue Fract. Eng. Mater. Struct.* **1997,** 20, 789.

32. J. L. Ruryan, S. J. Bennison, *J. Eur. Ceram. Soc.* **1991,** 7, 93.

33. R. Uribe, C. Baudin, *J. Am. Ceram. Soc.* **2003,** 86, 846.

34. P. Manurung, I. M. Low, B. H. Connor, S. Kennedy, *Mater. Res. Bull.* **2005,** 40 2047.

35. H. M. Okamura, E. A. Barringer, H. K. Bowen, *J. Mater. Sci.* **1989,** 24, 1867.

36. N. P. Padture, S. J. Bermison, H. M. Chan, *J. Am. Ceram. Soc.* **1993,** 76, 2312.

37. S. Bueno, R. Moreno, C. Baudin, *J. Eur. Ceram. Soc.* **2003,** 21, 71.

38. Y. Ohya, Y. Takahashi, Z .Nakagawa, *J. Mater. Sci.* **1996,** 31, 1361.

39. Y. Yang, O. Chen, A. Angerhofer, Y.C. Cao, *J. Am. Chem. Soc.* **2006,** 128, 12428.

40. Y. X. Huang, A. M. R. Senos, J. L. Baptista, *J. Eur. Ceram. Soc.* **1997,** 17, 1239.

41. A. Boulle, Z. Oudjedi, R. Guinebretiere, B. Soulestin, A. Dauger, *Acta. Mater.* **2001,** 49, 811.

42. C. H. Yang, W.Y. Shih, W. H. Shih, *J. Am. Ceram. Soc.* **2000,** 83, 1879.

43. Y. F. Tang, L. Feng, Y Chen, A. Li , *Adv. Eng. Mater.* **2004,** 6, 69.

44. J. Y. Lee, J. H. Lee, S. H. Hong, Y. K. Lee, J. Y. Choi, *Adv. Mater.* **2003,** 15, 1655.

45. Q. Liu, Z. Xu, J. A. Finch, R. Egerton, *Chem. Mater.* **1998,** 10, 3936.

46. W. P. Hsu, R. Yu, E. Matijevic, *J. Colloid. Interface. Sci.* **1993**, 156, 56.

47. D. Ma, T. Veres, L. Clime, F. Normandin, J. Guan, D. Kingston, B. Simard, *J. Phys. Chem. C.* **2007,** 111, 1999.

48. C. Y. Yang, W. Y. Shih, W. H. Shih, *J. Am. Ceram. Soc.* **2001,** 84, 2834.

49. M. Jayasankar, S. Ananthakumar, P. Mukundan, K. G. K. Warrier, *Mater. Lett.* **2007,** 61, 790.

50. M. Jayasankar, S. Ananthakumar, P. Mukundan, K. G. K. Warrier, *J. Am. Ceram. Soc.* **2007,** 90, 3091.

51. M. Schehl, L. A. Diaz, R. Torrecillas, *Acta Mater.* **2002,** 50, 25.

52. U. S. Hareesh, M. Sternitzke, R. Janssen, N. Claussen, K. G. K. Warrier, *J. Am. Ceram. Soc.* **2004,** 84, 1024.

53. J. S. L. Gao, W. Li, *Chem. Mater.* **2002,** 14, 5169.

54. I. M. Low, *Mater. Res. Bull.* **1998,** 33, 1475.

55. P. Manurung, Ph.D Thesis, Curtin University of Technology, August, **2001.**

56. M. Casarin, D. Falcomer, A. Glisenti, A. Vittadini, *Inorg. Chem.* **2003,** 42, 436.

57. Handbook of X-ray Photoelectron spectroscopy, Edited by C. D. Wagner, W. M. Riggs, L. E. Davis, J. F. Moulder, G. E. Muilenberg, Perkin-Elmer Corporation, Eden Prairie, MN, **1979**.

58. X. C. Guo, P. Dong, *Langmuir.* **1999,** 15, 5535.

59. R. Sanjnes, H. Tang, H. Berger, F. Gozzo, G. Margaritnondo, F. Levy, *J. Appl. Phys.* **1994,** 75, 2945.

60. G. Wang, A. Harrison, *J. Colloid. Interface. Sci.* **1999,** 217, 203.

61. C. J. Chisholm-Brause, G. A. O'Day, G. E. Brown, G. A. Parks, *Nature.* **1990**, *348*, 528.

62. L. F. Hakim, J. A. McCormick, G. D. Zhan, A. W. Weimer, P. Li, S. M. Geroge, *J. Am. Ceram. Soc.* **2006,** 89, 3070.

63. H. X. Wu, T. J. Wang, Y. Jin, *Ind. Eng. Chem. Res.* **2006,** 45, 1337.

64. E. Kato, K. Daimon, J. Takahashi, *J. Am. Ceram. Soc.* **1980,** 63, 355.

65. G. Bayer, *Proc. Brit. Ceram. Soc.* **1972,** 22, 39

66. M. T. Baucaglia, V. Bauscaglia, R. Alessuo, *Chem. Mater.* **2007,** 19, 711.

67. I. H. Joe, A. K. Vasudevan, G. Aruldhas, A. D. Damodaran, K. G. K.Warrier, *J. Solid. State. Chem.* **1997,** 131, 181.

68. P. Padmaja, K. G. K. Warrier, M. Padmanabhan, W. Wunderlich, F. J. Berry, M. Mortimer, N. J. Creamer, *Mater. Chem. Phys.* **2005,** 94, 3331.

69. D. P. H. Hasselman, *J. Am. Ceram. Soc.* **1969,** 52, 600.

69. H. Morishima, Z. Kato, K. Uematsu, K. Saito, T. Yano, N. Ootsuka, *J. Am. Ceram. Soc.* **1986,** 69, C-226.

70. T. Yano, M. Kiyohana, N. Otusuka, *J. Ceram. Soc. Jpn. Int. Ed.* **1992,** 100, 487.

71. R. Moreno, S. Mezquita, C. Baudin, *Brit. Ceram. T.* **2001,** 100, 241.

72. X. Q. You , T. Z. Si, N. Liu, P. P. Ren, Y. D. Xu, J. P. Feng, *Ceram. Int.* 2005, 31, 33.

73. M. I. Nieto, R. Martinez, L. Mazeroiles, C. Baudin, *J. Euro. Ceram. Soc.* **2004,** 24, 2293.

74. M. K. Aghajanian, N. H. Macmillan, C. R. Kennedy, S. J. Luszez, R. Ray, *J. Mater. Sci.* **1989,** 24, 658.

75. L. Wang, J. L. Shi, J. H. Gao, D. S. Yan, *J. Am. Ceram. Soc.* **2002,** 85, 718.

Chapter III

Alumina-Lanthanum Phosphate Composites

3.1 Introduction

Ceramics are increasingly being used in engineering components such as bearings, rotors, nozzles, valves, and heat exchangers. Most of these components have complex shapes and require a good tolerance and surface finish. Such characteristics are usually achieved by machining, which is both costly and potentially damaging to the strength of the component. Machining is emerging as an inevitable requirement for flexible use of advanced ceramics, especially for structural ceramics. However, the extremely high hardness and brittleness of ceramics makes conventional machining very difficult or even impossible. In some cases (especially optical and electronic applications), machining damage may be so intrusive as to necessitate additional polishing operations.[1] In this context the machining may be seen as a major limiting step in ceramics manufacturing.

In the past years, much research has been focused on the improvement of ceramic machinability.[2,3,4] Generally, two methods were used for improving the machinability of ceramic materials. One method is to introduce a weak interface or layered structured material in the matrix to facilitate crack deflection or healing during machining, such as mica containing glass-ceramic.[5] The other method is the structure-design method, where the machinability of ceramics is optimized by adjusting the distribution of phase and porosity.[6]

The most popular machinable glass-ceramics, consisting of finely dispersed mica platelets in a glass matrix, can be cut and drilled using conventional metal-working tools. The ease of cutting derives from the cleavage of the mica crystals beneath the cutting tool, and material removal by linking of the microcrack. These materials are used in a variety of applications requiring their high-temperature properties, high hardness, electrical or thermal insulation, or dielectric properties, combined with the convenience of machining. However, their high temperature use is limited by softening of the glass phase or coarsening of the crystallites, usually at temperatures above 800 °C.[7,8] Attempts have been made to develop analogous, more refractory systems. Barsoum et al. showed that Ti_3SiC_2, consisting of large, plate-shaped, easily cleaved grains, could be drilled and tapped using high-speed steel tools.[9] Padture et al. showed that material removal rates during diamond grinding and drilling of silicon carbide could be substantially increased by incorporating elongated grains, weak interphase boundaries, and high internal stresses into the microstructure.[10] The microstructure was consisted of plate-shaped SiC grains with a second phase of yttrium-aluminium garnet with relatively weak interphase bonding. Machinability has also been reported in very fine-grained silicon carbide containing porosity and free carbon.[11] Another important high temperature ceramics which can be used as a machinable ceramic is lanthanum phosphate.[12]

Interest in monazite ceramics during the eighties was due to its high temperature stability, high melting point (> 1900 °C) higher than that of

alumina (Al_2O_3) and low thermal conductivity and diffusivity.[13] Later, in mid nineties search for high temperature, oxidation resistant and weakly bonded interface materials for ceramic composites had also ended up in monazite ceramics, especially lanthanum phosphate ($LaPO_4$).[14] Due to the identical thermal expansion coefficients of Al_2O_3 and $LaPO_4$ their composites were widely investigated and were found to be chemically inert.

Morgan et al. reported that monazite-type $LaPO_4$ was stable and its phases were compatible with Al_2O_3 at temperatures at least as high as 1750 °C in air and two-phase composites consisting of $LaPO_4$ or $CePO_4$ and Al_2O_3, mullite or zirconia were first found to be machinable.[15,16,17] Chawla et al. reported that the incorporation of $LaPO_4$ interphase coating by the sol-gel dip coating method is an effective way of creating weak interfacial bonds between $LaPO_4$ and Al_2O_3.[18]

Moreover the Al_2O_3 - $LaPO_4$ composites has a layered structure suitable for inhibiting crack growth and along with their better toughness qualifies well for use as interface material.[19] Usual procedures for synthesis of these composites utilise solid state and wet mixing methods and also reactive hot pressing has been attempted.[20,21,22] Even when nano sized precursors are used for the synthesis of the composite, sintered grain sizes approach micron range in most cases. Also, the more efficient and flexible sol-gel method has not been investigated in detail for the preparation of these nanocomposites. Mechanical properties of these nanocomposites are also not reported.

3.2 Experimental

The starting materials were lanthanum nitrate (purity 99% Chempur, Karlsruhe, Germany) and orthophosphoric acid (Purity 85% Chem Solute, Renningen, Germany). For the synthesis of 20 g lanthanum phosphate, 0.05 M solution of La $(NO_3)_3.6H_2O$ in distilled water was first prepared. Orthophosphoric acid solution was added slowly to the lanthanum nitrate solution while keeping the solution under stirring. White precipitate of lanthanum phosphate formed was completely flocculated using 25% ammonia solution at pH=6 and then filtered. The precipitate was then washed with hot water, acetone and finally with hot water again to remove the nitrate and excess phosphates. Then the precipitate was peptized in distilled water by adding 20% nitric acid and maintaining the pH between 1.8 and 2.2.[23] The suspension was kept under stirring for about 4 h until a stable sol was obtained. To prepare the composite, Al_2O_3 (mean particle size of 0.2 μm, purity of 99.99%, Taimei Chemical Co., Ltd., Japan) required for the nanocomposite composition was added to the stabilized $LaPO_4$ sol and stirred well for 2 h. This composite precursor suspension was flocculated with ammonia (purity 25%, Chem solute, Renningen, Germany) at pH=5. The compositions synthesised were 10, 20, and 30 wt%, of lanthanum phosphate added alumina. The precursors were calcined at 400 °C and were ground, attrition milled in water and dried. The process flow sheet is presented in **Figure 1.**

The typical sintering schedule was as follows: RT to 800 °C at a rate of 3 °C min^{-1} and then up to the sintering temperatures at 5 °C min^{-1}. The densities

of the sintered materials were measured on ground specimens by the Archimedes principle using distilled water as the reference medium. The theoretical densities were calculated using the values of $3.97 g/cm^3$ for alumina and 5.07 g/cm^3 for $LaPO_4$.

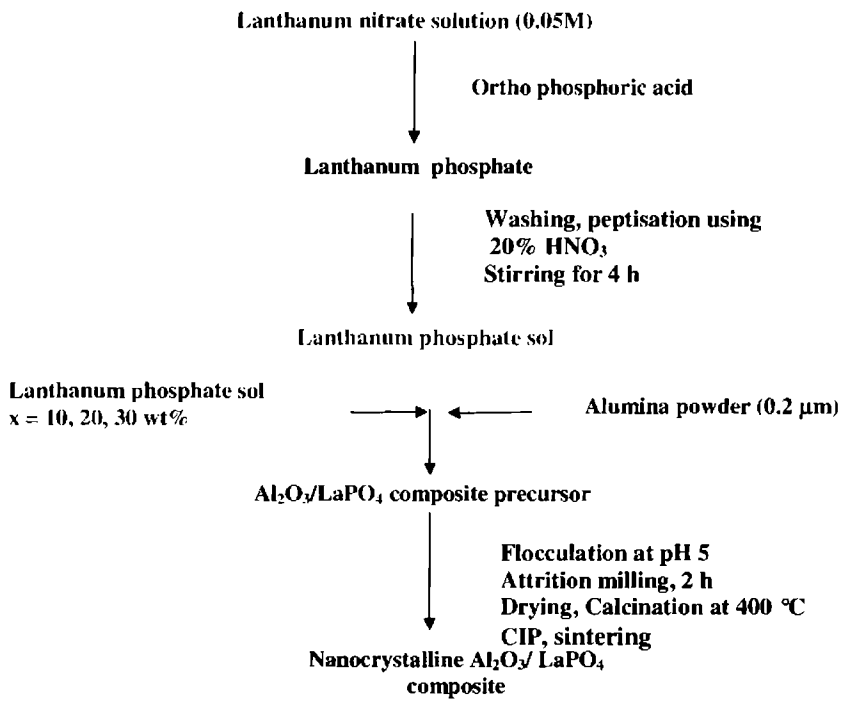

Figure 1. Flow diagram for the sol-gel synthesis of alumina-lanthanum phosphate

Bars of dimensions 4.5 mm × 6 mm × 40 mm were compacted by uni-axial pressing at 20 kN, followed by cold isostatic pressing at 200 MPa. The sintering was conducted in a chamber furnace at temperatures ranging from 1450 to 1500 °C, with a soaking period of 3 h under air atmosphere.

The phase content of the nanocomposite powder precursors was examined by X-ray diffraction with Cu Kα radiation (D8 Discover, Bruker AXS, Karlsruhe, Germany). The microstructures of the sintered materials were investigated by scanning electron microscopy (LEO 1530 FESEM, Gemini/Zeiss, Oberkochen, Germany). SEM specimens were polished and thermally etched at 1420 °C for 20 min in air atmosphere. The grain size analysis was done by the linear intercept method using a correction factor of $\pi/2$.

The flexural strength of composite samples was measured by four point bend testing. A schematic representation of a typical four point fixture is represented in **Figure 2.** The samples were ground to bars of dimensions 3 mm × 4mm × 40 mm and the tensile face and adjoining sides were polished down to 1 μm surface finish. The edges were uniformly chamfered at 45°. The strength testing was performed on a universal testing machine (Series 1600, ATS, Butler, PA) with a crosshead speed of 0.5 mm/min. The inner and outer spans of the loading rig were 15 and 25 mm, respectively. The breaking loads for the samples give the flexural strength using the standard formula for the strength of a beam in four point flexure, as

$$\sigma_B = M_B / W$$

$$M_B = P_B . (l_1 - l_2 / 4)$$

$$W = bh^2/6$$

Here 'M_B' represents the bending moment at fracture and 'W' is the section modulus. 'P_B' is the fracture force, 'b' is the width and 'h' the height of the

sample. For every test series, ten values were to be determined. The values and their mean value as well as the standard deviation are also determined.[24]

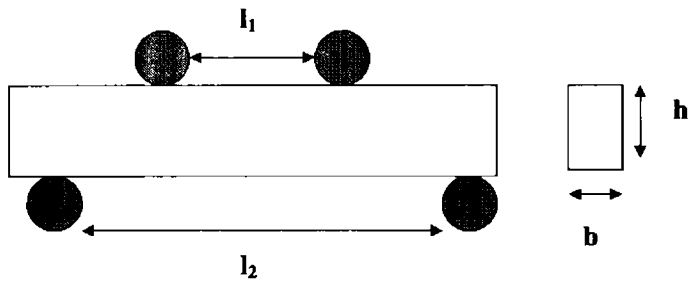

Figure 2. Schematic illustration of a four point bending fixture

Fracture toughness (KI_c) was measured by the Single Edge V-notch Beam (SEVNB) method. A schematic representation of a typical SEVNB's V-notch is represented in **Figure 3.** For that purpose the notch was cut with a diamond saw blade of 120 μm thickness and sharpened with a razor blade in a special mechanical appliance (SEVNB). Using diamond paste of 6, 2.5 and 1 μm grain size, the curvature radius of the notch tip was reduced to less than 10 μm.[25]

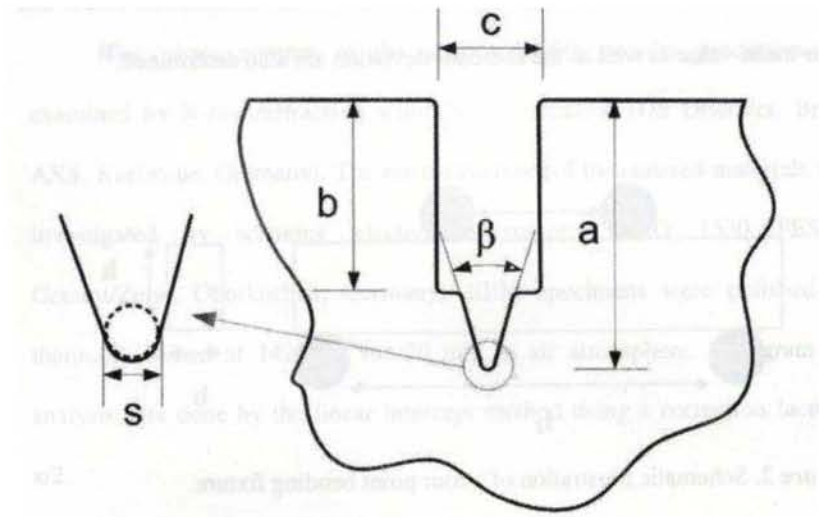

Figure 3. Schematic illustration of a V-notch of a SEVNB

The fracture toughness can be computed from the maximum load F_{max}

$K_{Ic} = F_{max}/ B\sqrt{w} \times S_1\text{-}S_2/W \times 3\Gamma_M\sqrt{\alpha}/2(1-\alpha)^{1/2}$

$\Gamma_M = 1.1215\sqrt{\Pi}\ [5/8 - 5/12\alpha + 1/8\ \alpha^2 + 5\ \alpha^2\beta^6 + 3/8 \exp(-6.1342\ \alpha/\beta)$

Where $\beta = 1-\alpha$

S_x - Span
a – Notch depth
B – Specimen width
W – Specimen height
$\alpha = a / W$

Hardness (*H*) measurements were conducted at room temperature using a Vickers diamond indentor (CLEMEX JS 2000) under a load of 2 Kg with a loading time of 10 s. An average hardness was then calculated from the results of 5 indentations using the following equation:

$H = F / 2a^2$ (2)

Where *a* is the half length of the indent and *F* is the load.[26]

3.3 Results and Discussion

The XRD diffraction patterns of $LaPO_4$, Al_2O_3-30$LaPO_4$ nanocomposite heated at 400 °C were analysed and presented in **Figure 4 & 5.** The XRD analysis of the composite shows the presence of $LaPO_4$, α-Al_2O_3 phases but $LaPO_4$ sample shows the presence of amorphous $LaPO_4$ phase. The XRD diffraction patterns of Al_2O_3-30$LaPO_4$ nanocomposite heated at various temperatures were analyzed. All the peaks were well assigned and we do not find any reactive phase at 1450 °C.[27] Diffractograms of compositions of the various composites heated at 1450 °C are presented in **Figure 6.** At this temperature $LaPO_4$ is in monazite monoclinic phase (JCPDS file no. 35-0731) and Al_2O_3 is in the alpha phase (JCPDS file no. 10-173) is presented.

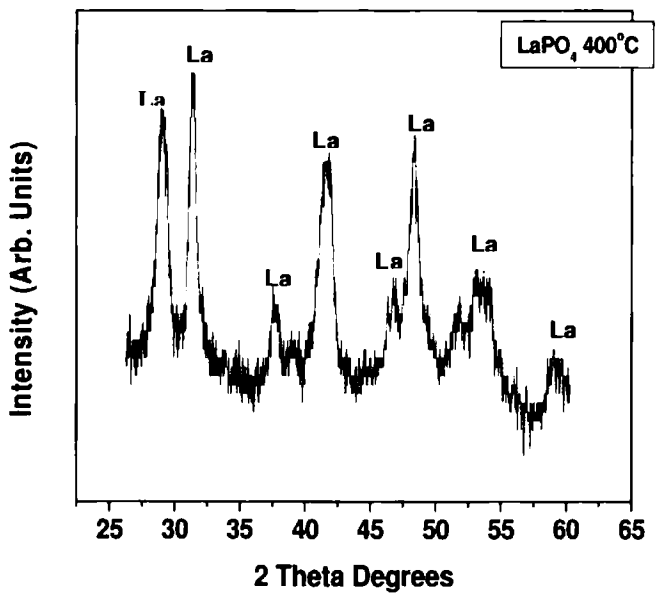

Figure 4. XRD of $LaPO_4$ calcined at 400 °C

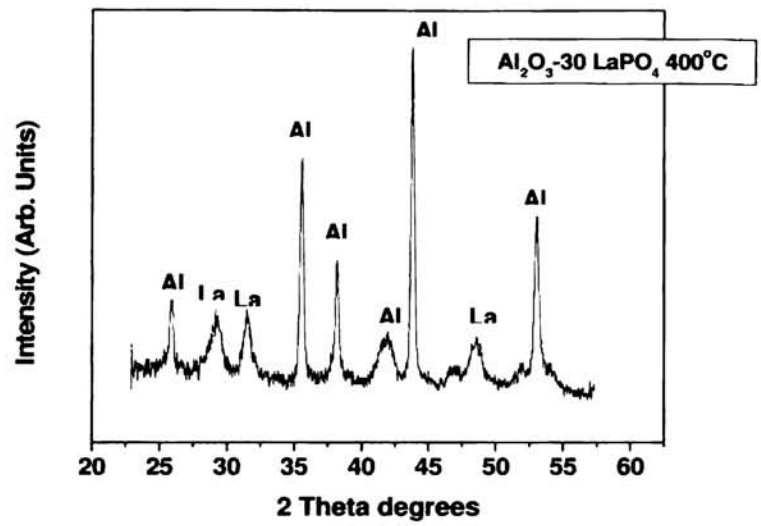

Figure 5. XRD of Al_2O_3-30$LaPO_4$ calcined at 400 °C

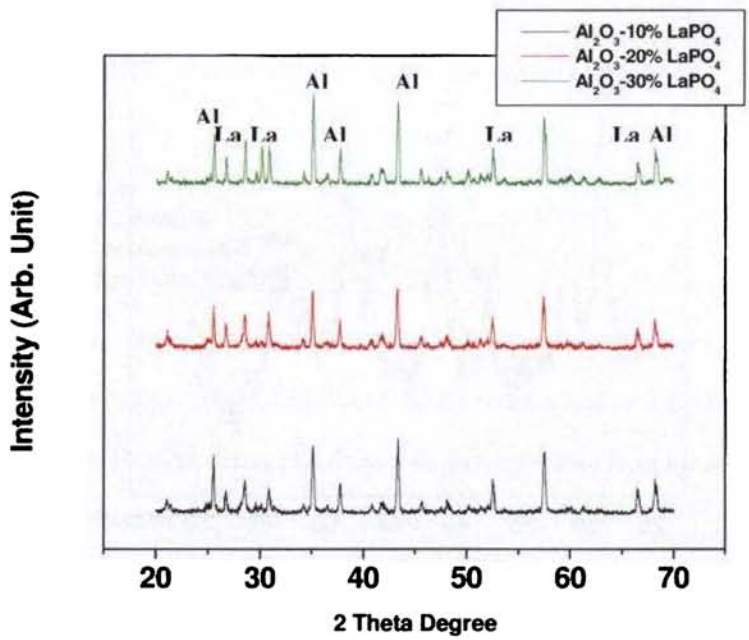

Figure 6. XRD of Al_2O_3-10$LaPO_4$, Al_2O_3-20$LaPO_4$, Al_2O_3-30$LaPO_4$, composite calcined at 1450 °C

The sintered densities of the composites were measured using the Archimedes method. A density of 98-99% was obtained for the composite when sintered at 1450 °C and presented in **Table 1.** To the best of our knowledge, this is the lowest temperature reported for achieving such densities for Al_2O_3-$LaPO_4$ composite. The superior densification obtained in the present method could be due to the nano size of the particles and the high surface area. Recently Gong et al. reported relative density of 91-95% was reported for pressure less sintered Al_2O_3- $LaPO_4$ composite.[28] Wang et al. has shown that Al_2O_3- $LaPO_4$ composites can be sintered at a lower temperature of 1450 °C by hot pressing.[29] Min et al. reported the synthesis of Al_2O_3-$LaPO_4$ composite where the $LaPO_4$ was synthesized from La_2O_3 and H_3PO_4 as starting precursor and the composite can be sintered at 1600 °C.[30]

Table 1. Density results of Al_2O_3-$LaPO_4$ composites

Content of $LaPO_4$	**Calculated density (g/cm^3)**	**Sintered density(g/cm^3)**	**Relative density %**
0	3.99	3.96± 0.01	99.2
10	4.01	4.00± 0.01	99.7
20	4.13	4.08± 0.01	98.7
30	4.25	4.20± 0.01	98.8

Theoretical density: Al_2O_3 3.97 g/cm^3, $LaPO_4$= 5.07 g/cm^3

According to **Table 1.** although due to high density of $LaPO_4$ (=5.07 g/cm^3), the bulk density of composites increased with increasing $LaPO_4$ addition, at the same time the relative density of composites decreased compared with pure Al_2O_3 and $LaPO_4$ ceramics. $LaPO_4$ addition is found to have reduced the sinterability of $Al_2O_3/LaPO_4$ composites, leading to a decrease of mechanical properties of composites.[31]

3.3.1 Mechanical Properties

Figure 7. showed the influence of $LaPO_4$ content on the bending strength of Al_2O_3-$LaPO_4$ composites. Incorporating $LaPO_4$ particles remarkably reduced the fracture strength of Al_2O_3. The monolithic Al_2O_3 sintered at 1500 °C exhibited a maximum strength of 424±24 MPa, while the strength of 30 wt% Al_2O_3-$LaPO_4$ composite and $LaPO_4$ ceramic are 174±11 and 68±11 MPa respectively. Due to the weak bonding between Al_2O_3 and $LaPO_4$ and layered soft $LaPO_4$ phase, the microstructure greatly affected the mechanical properties such as fracture strength, elastic modulus and hardness. Generally, the refinement of the matrix grain size and homogeneity in the matrix grain size distribution will result in improvement of mechanical properties.[32] It is well known that the strength is proportional to (maximum grain size) $^{-1/2}$. However, due to the weak bonding of Al_2O_3 and $LaPO_4$ and layered soft $LaPO_4$ phase, the fine and homogeneous microstructure by $LaPO_4$ addition resulted in the reduction of mechanical properties of the composites.

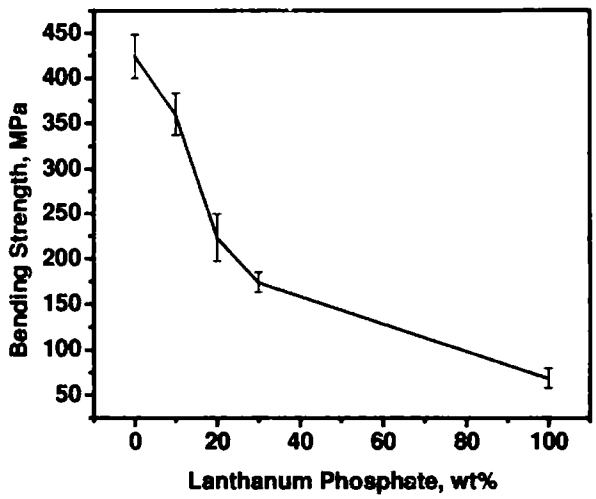

Figure 7. Effect of $LaPO_4$ content on the bending strength of Al_2O_3-$LaPO_4$ composites

The fracture toughness value of Al_2O_3 remains the same with increasing $LaPO_4$ addition showed in **Table 2**, the facture toughness remains 2.16 ± 0.22 even after 30 wt% addition of $LaPO_4$.

Table 2. Fracture toughness results of Al_2O_3-$LaPO_4$ composites

Sample details	Fracture toughness (K_{Ic}) MPa $m^{1/2}$
Al_2O_3	2.60±0.20
Al_2O_3-10$LaPO_4$	2.49±0.15
Al_2O_3-30$LaPO_4$	2.16±0.22

Hardness is an important parameter as an indication of ceramic machinability. Generally, lower the hardness, more excellent machinability.

Vickers's hardness was measured on the polished surface of the composites. **Figure 8.** showed the effects of $LaPO_4$content on the hardness change of Al_2O_3- $LaPO_4$ composites. The decrease of hardness can be attributed to the crack weakening at crack tip, and bridging at process zone wake by second phase. In this system, the crack propagated along weak bonding of Al_2O_3 and $LaPO_4$ and layered $LaPO_4$ phase. Therefore the improved crack deflection ability may contribute to the machinability improvement in the composites. The Vickers hardness of 30 wt% Al_2O_3- $LaPO_4$ composite and $LaPO_4$ was 8.6±0.5 and 4.6±0.5 GPa, respectively. Those values are close to that of machinable mica glass-ceramic (3 GPa)[33] and layered ternary compounds Ti_3SiC_2 (4–5 GPa).[34] This indicated that $LaPO_4$ ceramic and 30 wt% Al_2O_3-$LaPO_4$ composite could possess excellent machinability. **Figure 9.** shows the optical images of the Vickers indent made of various composite samples.

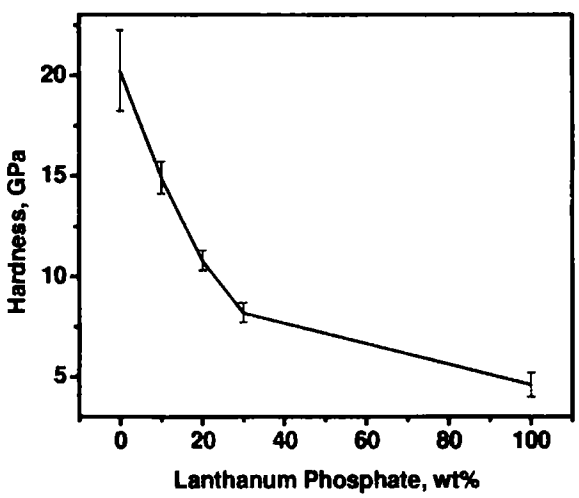

Figure 8. Effect of $LaPO_4$ content on the hardness of Al_2O_3-$LaPO_4$ composites

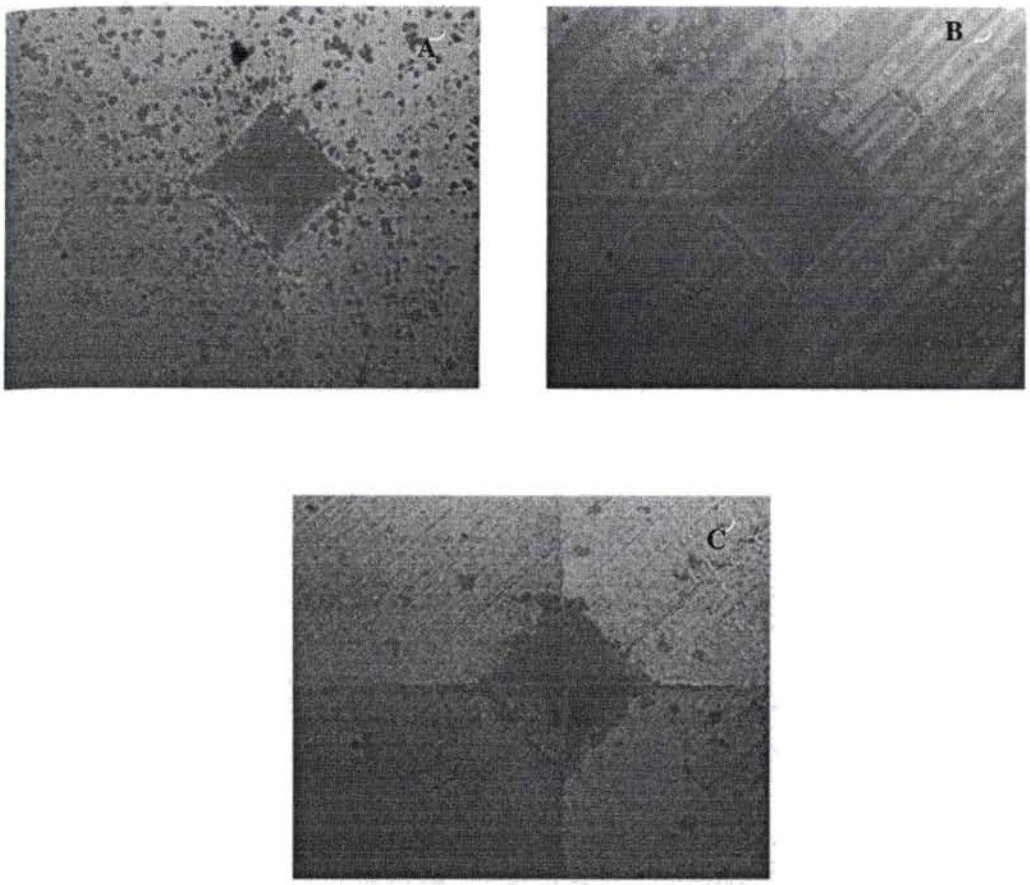

Figure 9. Optical images of the indentation made on the composite (1000 X) (A) Al_2O_3-10$LaPO_4$ (B) Al_2O_3-20$LaPO_4$ (C) Al_2O_3-30$LaPO_4$

3.3.2 Microstructure

Scanning electron micrographs illustrating the microstructures of Al_2O_3/$LaPO_4$ composites with different $LaPO_4$ addition are shown in **Figure 10.** The SEM of Al_2O_3: $LaPO_4$ (90:10 wt%, 80:20 wt % and 70:30 wt%)

composites are provided in **Figure 10(a), (c) & (e).** respectively. The micrographs show that $LaPO_4$ grain growth was restricted to around 1-2 μm whereas that of Al_2O_3 was restricted to 2–3 μm for all compositions. Increasing $LaPO_4$ content in the composite increased the restriction of Al_2O_3 grain growth. This synergistic effect of restriction of mutual grain growth is however contradictory to that observed by other researchers. Researches have observed the restriction of grain growth of Al_2O_3 by $LaPO_4$ in their composites but simultaneous growth of $LaPO_4$ grains was also observed.[20,29]

The dependence of the grain size on the second phase content can be explained by using Zener's equation, which suggests a relationship between grain size of matrix and volume fraction and particle size of the second phase

$$G = K (r/f)$$

where G, k, r and f are mean grain size of matrix, constant, mean grain size of second phase and volume fraction of second phase, respectively. The equation shows that the grain size of matrix depends on particle size and volume fraction of second phase. The Zener's equation also suggests that mean grain size (G) decrease with increasing volume fraction (f) of $LaPO_4$.[35] From the microstructure of composites, it was also obvious that the addition of $LaPO_4$ prohibited the abnormal growth of alumina grains. In the present sol-gel derived composites, mutual restriction of grain growth could be achieved. Such fine-grained, sintered microstructure should result in better mechanical and structural properties.[36]

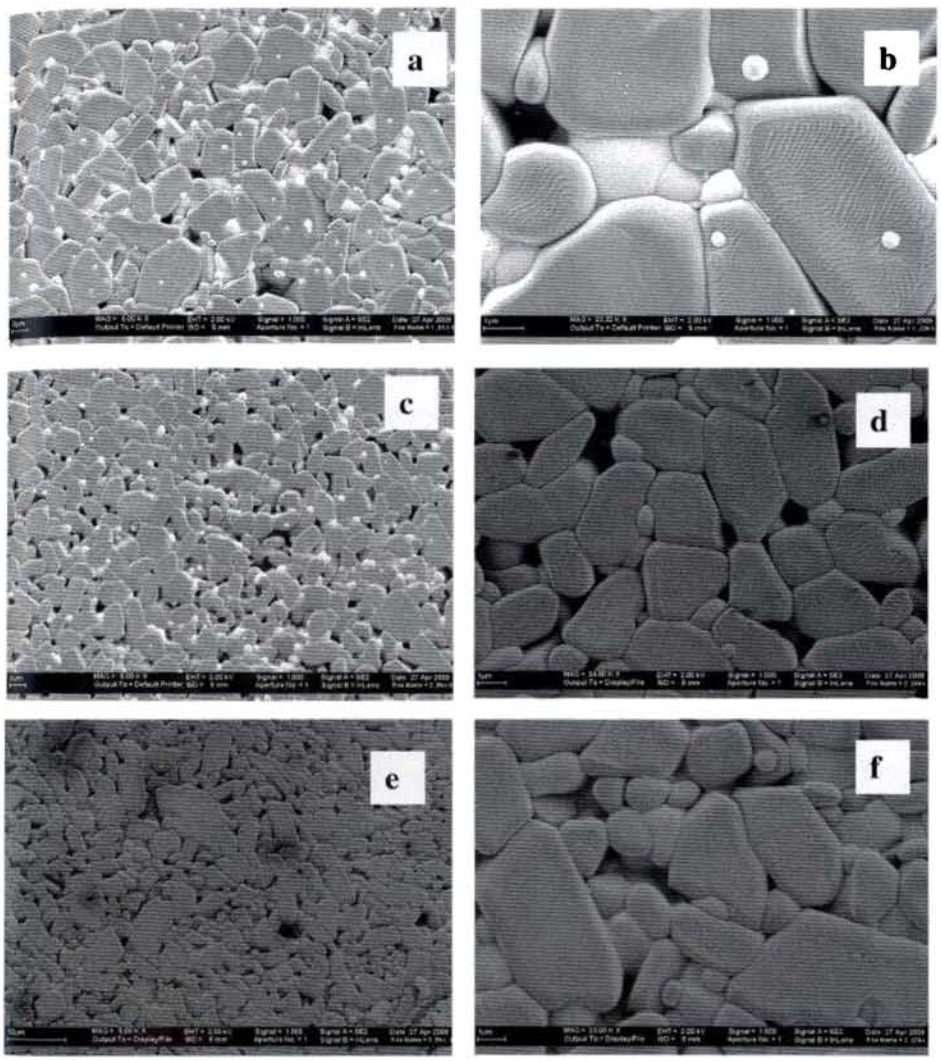

Figure 10. SEM of polished and thermally etched surface of sintered Al_2O_3-10 $LaPO_4$ (a, b), Al_2O_3-20 $LaPO_4$ (c, d), and Al_2O_3-30 $LaPO_4$ (e, f) at 1450 °C/3h.

3.3.3 Grinding Studies

Machining test was conducted on the four samples from each batch alumina- lanthanum phosphate composites, having dimension rectangular bars 3 mm × 4 mm × 35 mm. The prospective test surfaces were diamond polished to 1 μm surface finish. Grinding tests were performed on an automatic grinding machine. Four samples from alumina, lanthanum phosphate, alumina-lanthanum phosphate composite were glued symmetrically about the centre of a circular metal plate, which was then attached to the grinding machine. The specimens were ground on a 220 particle (SiC) per inch grit for 60 min (normal pressure 2 bar or 30 psi). The thickness of material removed from each of the specimens was measured at 15 min intervals using a precision micrometer (accuracy ± 0.1) and the removal rates (depth removed per unit time) thereby evaluated.[37]

In the grinding tests on the Al_2O_3, Al_2O_3-30$LaPO_4$, $LaPO_4$, the mean surface removal rate for the $LaPO_4$ is the highest and presented in **Table 3.** The mean surface removal rate for Al_2O_3-30$LaPO_4$ is higher compared to Al_2O_3 by a factor of 2. This was a good indication of better machinability of alumina-lanthanum phosphate compared to alumina.[38] The values obtained for various materials given below.

Table 3. Surface removal rate results

Time	30min (μm/s)	60 min (μm/s)
Al_2O_3-30$LaPO_4$	Not determined	9.5 ±0.3
$LaPO_4$	40±2.0	Not determined
Al_2O_3	Not determined	4.5±0.2

The layered structure of $LaPO_4$ and the weak interface at the Al_2O_3/$LaPO_4$ grain boundaries are the main reasons for the improvement of the machinability.[39] Both of them enhance the crack deflection and avoid the catastrophic failure of the material during drilling. According to study of An et al. weak grain/interphase boundaries can promote the formation of bridging sites and coarse grains and residual thermal stresses enhance the bridging intensity.[40] Thus ceramic materials can be toughened by grain bridging in the wake of propagating cracks. The very weak-interface characteristic that promotes easy grain detachment suppresses macrocrack formation.

To characterize the machinability of the composites, we calculated the brittleness index B ($B=H_v/K_{IC}$) of the composites and the results are presented in **Table 4.** shows the brittleness index B of the composites as a function of $LaPO_4$ content.[41] It can be observed that the brittleness index of composites decreases with increasing $LaPO_4$ content. Especially, when the $LaPO_4$ content

was higher than 30 wt%, the brittleness index of the composites exhibited a dramatic decrease, 3.79 $\mu m^{-1/2}$ and it was much lower than that of glasses and ceramics, whose values are generally in the range from 3 to 7 $\mu m^{-1/2}$, which suggests that the composites have excellent machinability.[42]

Table 4. Brittleness index results of Al_2O_3-$LaPO_4$ composites

Sample Details	Brittleness index B ($\mu m^{-1/2}$)
Al_2O_3	7.78
Al_2O_3-10$LaPO_4$	5.20
Al_2O_3-30$LaPO_4$	3.79

Table 5. Bending Strength results of Al_2O_3-$LaPO_4$ composites after grinding

Samples Details	Bending Strength before grinding (MPa)	Bending Strength after grinding (MPa)
Al_2O_3	424±20	229±10
Al_2O_3-30$LaPO_4$	174±11	160±12
$LaPO_4$	69±5	39±5

To characterize the ability of machinability of the composites sample we conducted a bending strength measurement on the sintered sample after grinding for 1 h. We have selected Al_2O_3, $LaPO_4$ and Al_2O_3-30 $LaPO_4$ as testing sample. Four samples from alumina, lanthanum phosphate, alumina-lanthanum phosphate composite are ground for 1 h and the sample used for bending strength measurement. **Table 5.** shows the bending strength values of the samples before and after machining. The bending strength value of Al_2O_3 reduces from 424±20 to 229±10 where as in the case of the Al_2O_3-30 $LaPO_4$ the reduction in the bending strength is smaller compared with the alumina (174±11 to 160±12). This was an indication of better machinable substrate for various engineering applications.[43]

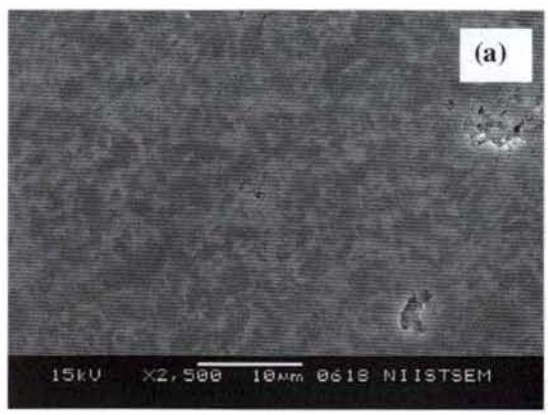

Microstructure of the ground portion were taken and presented in **Figure11.** The ground surface micrograph of Al_2O_3-30$LaPO_4$ composite

indicate relatively plain morphology with less surface defects after 1h of grinding.

Figure 11. Micrographs of ground samples (a) Al_2O_3-30$LaPO_4$ (b) Al_2O_3

The ground micrograph of Al_2O_3 after grinding test indicate more surface damage. The lanthanum phosphate forms weak interface with alumina. Thus lanthanum phosphate addition can cause crack deflection, branching and blunting which help to prevent microscopic fractures from propagating in the composite compare to alumina.[44]

3.4 Conclusions

Alumina-lanthanum phosphate composite was synthesised by sol-gel method. A lower sintering temperature for the composite was achieved as low temperature as 1450 °C due to the nano size particles. The XRD analysis of the sintered alumina-lanthanum phosphate showed no reactive additional phase formation at the sintering temperature. The grinding studies indicated that the mean surface removal rate for the $LaPO_4$ is the highest. The mean surface removal rate for Al_2O_3-30$LaPO_4$ is higher compared to Al_2O_3 by a factor of 2. This was a good indication of better machinability of alumina-lanthanum phosphate compared to alumina. The bending strength and hardness of the composite decreases with increasing the $LaPO_4$ content. The monolithic Al_2O_3 sintered at 1500 °C exhibited a maximum strength of 424±24 MPa, while the strength of 30 wt% Al_2O_3-$LaPO_4$ composite and $LaPO_4$ ceramic are 174±11 and 68±11 MPa respectively. The Vickers hardness of 30 wt% Al_2O_3- $LaPO_4$ composite and $LaPO_4$ was 8.6±0.5 and 4.6±0.5 GPa, respectively. The sintered micrographs of the Al_2O_3-$LaPO_4$ composite show that $LaPO_4$ grain growth was restricted to around 1-2 μm whereas that of Al_2O_3 was restricted to 2–3 μm for all compositions. Increasing $LaPO_4$ content in the composite increased the restriction of Al_2O_3 grain growth. After the grinding studies of the composite the bending strength value of Al_2O_3 reduces from 424±20 to 229±10 where as in the case of the Al_2O_3-30 $LaPO_4$ the reduction in the bending strength smaller compared the alumina (174±11 to 160±12). This means that the strength of the composite is maintained even after 1 h of grinding.

References

1. L. M. Sheppard, *Am. Ceram. Soc. Bull.* **1992,** 71, 1590.
2. D. G. Grossman, *J. Am. Ceram. Soc.* **1972,** 55, 446.
3. T. Kusunose, T. Sekino, Y. H. Choa, K. Niihara, *J. Am. Ceram. Soc.* **2002,** 85, 2689.
4. C. Kawai, A. Yamakawa, *J. Ceram. Soc. Jpn.* **1998,** 106, 1135.
5. H. H. K. Xu, S. Jahanmir, *J. Am. Ceram. Soc.* **1995,** 78, 497.
6. W. Pan, R. G. Wang, *Rare Metal. Mat. Eng.* **2000,** 29, 84.
7. Electron Microscopy and Structure of Materials. C. K. Chyung, G. H. Beall, D. G. Grossman, Edited by G. Thomas, R. M. Fulrath, R. M.Fisher. University of California, Berkeley, CA, **1972.**
8. Fluorophlogopite Mica Glass-Ceramics, K. Chyung, G. H. Beall, D. G. Grossman, *10th Proc. Int. Glass Congr.* **1974.**
9. M. W. Barsoum, T. El-Raghy, *J. Am. Ceram. Soc.* **1996,** 79, 1953.
10. N. P. Padture, C. J. Evans, H. H. K. Xu, *J. Am. Ceram. Soc.* **1995,** 78, 215.
11. T. Tanimoto, T. Morii, M. Okumura, A. Nakazawa, G. Suganuma, G. Sasaki, K. Niihara, Mechanical Properties and Nanostructure of Machinable SiC, pp. 419–24 in Proceedings of 1st International Symposium on Science of Engineering Ceramics. Edited by S. Kimura, K. Niihara. The Ceramic Society of Japan, Tokyo, Japan, **1991.**
12. P. E. D. Morgan, D. B. Marshall, *J. Mater. Sci. Eng.* **1993,** A162, 15.
13. Y. Hikichi, T. Nomura, *J. Am. Ceram. Soc.* **1987**, 70, C-252.
14. P. E. D. Morgan, D. B. Marshall, *J. Am. Ceram. Soc.* **1995**, 78, 1553.
15. P. E. D. Morgan, D. B. Marshall. U. S. Patent No. 424767, **1996.**
16. J. B. Davis, D. B. Marshall, R. M. Housley, P. E. D. Morgan, *J. Am. Ceram. Soc.* **1998,** 81, 2169.
17. J. B. Davis, D. B. Marshall, P. E. D. Morgan, *J. Eur. Ceram. Soc.* **2000**, 20, 583.
18. K. K. Chawla, H. Liu, J. Janczak-Rusch, S. Sambasivan, *J. Eur. Ceram. Soc.* **2000,** 20, 551.

19. P. E. D. Morgan, D. B. R. Marshall, M. Housley, *Mater. Sci. Eng. A.* **1995**, 195, 215.

20. R. Wang, W. Pan, J. Chen, M. Fang, J. Meng, *Mater. Lett.* **2002**, 57, 822.

21. R. Wang, W. Pan, J. Chen, M. Fang, Z. Cao, L. Yongming, *Mater. Chem. Phys.* **2003**, 79, 30.

22. R. Wang, W. Pan, J. Chen, M. Fang, M. Jiang, Z. Cao, *Ceram. Int.* **2003**, 29, 83.

23. K. Rajesh, P. Shajesh, O. Seidel, P. Mukundan, K. G. K. Warrier, *Adv. Funct. Mater.* **2007**, 17, 1682.

24. Modern Ceramic Engineering: Properties, Processing and Use in Design, D. W. Richerson, Marcel Dekker, Inc, **1992** pp 180-181.

25. J. Kubler, Fracture toughness of ceramics using the SEVNB method: from a preliminary study to a standard test method. In Fracture Resistance Testing of Monolithic and Composite Brittle Materials, *ASTM STP 1409*, ed. J. A. Salem, M. G. Jenkins and G. D. Quinn. American Society for Testing and Materials, West Conshohocken, PA, **2001.**

26. U. S. Hareesh, M. Sternitzke, R. Janssen, N. Claussen, K. G. K. Warrier, *J. Am. Ceram. Soc.* **2004**, 84, 1024.

27. K. Rajesh, K. V. Baiju, M. Jayasankar, K. G. K. Warrier, *J. Am. Ceram. Soc.* **2008**, 91, 2415.

28. G. Gong, B. Zhang, H. Zhang, W. Li, *Ceram. Int.* **2006**, 32, 349.

29. R. Wang, W. Pan, J. Chen, M. Fang, M. Jiang, Z. Cao *Ceram. Int.* **2003**, 29, 83.

30. W. Min, D. Miyahara, K. Yokoi, T. Yamaguchi, K. Daimon, Y. Hikichi, T. Matsubara, T. Ota, *Mater. Res. Bull.* **2001**, 36, 939.

31. R. Wang, W. Pan, J. Chen, M. Jiang, Y. Luo, M. Fang, *Ceram. Int.* **2003**, 29 19.

32. M. Sternitzke, *J. Eur. Ceram. Soc.* **1997,** 17, 1061.

33. M. W. Barsoum, Tamer El-Raghy, *J. Am. Ceram. Soc.* **1996,** 79, 1953.

34. M. W. Barsoum, W. Michel, *Scripta Mater.* **1997,** 36, 535.

35. N. A. Haroun, D. W. Budworth, *J. Mater. Sci.* **1968,** 3, 326.

36. H. P. Kirchner, R. M. Gruver, *J. Am. Ceram. Soc.* **1970,** 53, 232.

37. W. Kou, M. Molin, G. Sjogren, *J. Oral. Rehabil.* **2006,** 33, 117.

38. A. Kubota, Y. Shinbayashi, H. Mimura, Y. Sano, K. Inagaki, Y. Mori, K. Yamauchi, *J. Electron. Mater.* **2007,** 36, 92.

39. D. H. Kuo , W. M. Kriven, *J. Am. Ceram. Soc.* **1997,** 80, 2987.

40. L. An, *J. Am. Ceram. Soc.* **1999,** 82, 78.

41. E. A. Tsitrou, , S. E. Northeast, R. V. Noort, *J. Dent.* **2007,** 35, 897.

42. A. R. Boccaccini, *J. Mater. Process. Tech.* **1997,** 65, 302.

43. H. Wu, C. Lawrence, S. Roberts, B. Derby, *Acta Mater.***1998,** 46, 3839.

44. R. Wang, W. Pan, J. Chen, M. Fang, M. Jiang, Y. Luo, *Mater. Design.* **2002,** 23, 565.

Chapter IV

Mullite -SiC Composites

4.1 Introduction

Ceramic filters are widely used in locations where hot gas cleaning is crucial particularly in application such as coal combustion and gasification in the power generation industry.[1,2,3] The "dirty" gases emitted require adequate filtration to minimise particulate waste to a gas stream and also the atmosphere and surrounding environment. Leading ceramic filter candidates for high temperature use are cordierite, mullite, alumina and silicon carbide. The design requirements for these ceramic filters, whose main function is removal of fine particles at elevated temperature, are high porosity (≈50 to 80%), adequate strength (generally exceeding 5 MPa at the operating temperature based purely on the gas pressure used), oxidation resistance, erosion resistance, thermal shock resistance and decent flow or permeability characteristics.[4]

Films and coatings represent the earliest commercial use of sol-gel processing. Sol-gel films can be deposited by spraying, dip coating, and spin coating. Sol-gel techniques offer the following advantage in coating, control of microstructure, pore size and surface area. By controlling these parameters, the film properties can be tailored. Irregularly shaped surface can also be coated. Porous film can be prepared by changing the reaction conditions and the amount of porosity in a sol-gel derived film can be controlled by the pH. A higher porosity can be achieved when base catalysed sols are used. The sol-gel

film formed strong bonds to both oxide powders and substrate by interaction with functionalised surface hydroxyl groups on the oxide powders and the oxide layer of substrates which reduces cracking. Also to avoid cracking caused by large capillary stress during evaporation of the solvent in the drying process, either slow evaporation (slow process) or supercritical drying (fast process) is used. Thick coating through sol-gel process are also reported. The problems of shrinkage and cracking and the limitation of coating thickness can be addressed by increasing the particle loading in the sol-gel process.[5] This approach involved dispersing large size ceramic powder in sol-gel solution and applying the mixture on the substrate by various methods such as dipping and spraying. Coating with a thickness up to 200 μm was also possible. The shrinkage problem associated with the conventional sol-gel approach was minimized due to the high loading of ceramic powders.

Silicon carbide is a commonly used filter material because of its high temperature strength and thermal shock resistance. One potential barrier to such applications is their environmental durability.[6,7,8,9] The oxidation behaviour of SiC can be divided into two oxidation modes, passive and active. Passive oxidation forms a coherent, dense SiO_2 layer on the surface, which suppresses further oxidation.[10] On the contrary, active oxidation forms gaseous SiO, which dissipates away from the surface, promoting further oxidation and hence, the oxidation becomes severe.[11,12,13] The temperature, at which the oxidation mode changes, from passive to active, decreases with decreasing oxygen partial pressure. For most applications, the oxidation of SiC should be

constrained within the passive oxidation regime.[14] He et al. observed that the onset-temperature for significant oxidation of the SiC powder of smaller particle size is much lower than that for the SiC powder of larger particle size.[15]

One strategy to protect SiC ceramic is to use refractory oxide coatings with little or no silica activity. Several researchers have also explored possibility of providing aluminosilicate coating with a coefficient of thermal expansion (CTE) that is reasonably close to the CTE of the underlying ceramic. For example, being the simplest aluminosilicate, mullite has an average CTE of 5.1×10^{-6} °C that is only slightly higher than the average CTE of 4.7×10^{-6} °C for SiC.[16] Also, experiments show that mullite coating can extend the life of Si-based ceramic components under some conditions.

Mullite ($3Al_2O_3$ $2SiO_2$) is one of the important ceramic materials for high temperature application because of its special properties like low thermal expansion coefficient, high creep resistance and low dielectric constant. The crystal structure of mullite can be described as a modified defect structure of sillimanite (Al_2O_3 SiO_2). Sillimanite consists of edge-sharing aluminium-oxygen octahedral chains cross-linked by double chains of ordered SiO_4 and AlO_4 tetrahedra.[17] The low coefficient of thermal expansion (CTE), low density and low thermal conductivity of mullite make it useful for optical applications as mid-infrared windows.[18] Its low dielectric constant and dielectric loss, coupled with a smaller CTE mismatch to silicon than Al_2O_3 also make it a valuable material for use in microelectronics packaging and substrates.[19]

Different approaches are adopted to synthesize phase-pure mullite, such as solid-state mixing of fine oxides of alumina and silica, co-precipitation from mixed salt solutions and sol-gel methods involving both particulate sols and alkoxides.[20,21,22,23,24] The sol-gel method is found to be one of the best especially in view of the excellent homogeneity of the precursor phases.[25] The formation characteristics of mullite depend largely on the nature of precursors. Molecular level mixing of the aluminum and silicon species and low-temperature crystallization of mullite at around 980°C by an exothermic reaction are reported in precursors involving an aluminium salt and TEOS.[26] On the other hand, in diphasic colloidal gels obtained by mixing sols of boehmite and silica, the crystallization takes place in the range 1250-1350 °C.[27]

Possibility of providing a coating of mullite as a barrier for oxygen diffusion which can improve the oxidation resistance of silicon carbide ceramic has been reported.[28] Mullite coated SiC exhibits excellent oxidation resistance by forming a slowly growing SiO scale at the mullite-SiC interface.[29] Mullite coating was reported for protecting carbon, SiC, and Si_3N_4 ceramic from oxidation by pulsed- laser deposition, chemical vapour deposition and plasma spraying techniques. Chemically vapour deposited (CVD) mullite coating is reported to improve the resistance of silicon–based ceramic to corrosive or oxidative attack by molten salt. However, the microstructure and composition of CVD mullite can vary depending on deposition conditions, which may substantially influence coating oxidation resistance. The coating thickness also varies with temperature.[30] Mullite was coated on SiC by plasma spray

techniques and contains metastable phases because of rapid cooling from high temperature. One key issue with plasma-sprayed mullite coating is phase instability.[31] The mullite processed with conventional plasma spraying contains a significant amount of metastable amorphous phase because of the rapid cooling of molten mullite during the solidification on a cold substrate. A subsequent exposure of the mullite to a temperature above 1000 °C causes the crystallization of the amorphous phase. Shrinkage accompanies the crystallization, leading to cracking and delamination of the mullite. Dipcoating processes are mostly used to produce mullite layers from mixed oxide or mullite suspensions or from sol-gel systems respectively. Damjanovic et al. reported that electrophoretic deposition (EPD) is a suitable technique to produce mullite layers for acceptable oxidation protection of C/C–SiC composites. Combining sol–gel synthesis of $3Al_2O_3$ $2SiO_2$ mullite through hydrolysis and condensation of tetraethoxysilane (TEOS) and aluminum-tri-sec-butylate (Al-$(OBu)_3$) with EPD yields sufficiently thick and homogeneous layers, which transform into mullite at 1300 °C.[32]

This chapter presents a procedure for sol-gel mullite coating on SiC substrate, where the mullite preferentially forms in-situ from the precursors at a low temperature of 1300 °C. The formation of needle shaped mullite grains at low temperature of 1300 °C is also presented for the first time which will enhance the mechanical properties of the coating. The mullite coated SiC substrates have been tested for gas filtration.

4.2 Experimental

Boehmite sol was synthesized from $Al(NO_3)_3 \cdot 9H_2O$ by controlled precipitation followed by peptisation with dilute nitric acid at pH 3–3.5 as reported earlier.[33] Boehmite sol and TEOS were used as the precursors for alumina and silica respectively. Mullite precursor sol was prepared by reacting boehmite sol and TEOS in a stoichiometric ratio 3:2 at a pH of the sol 3.5. The detailed flow chart is presented in **Figure 1.**

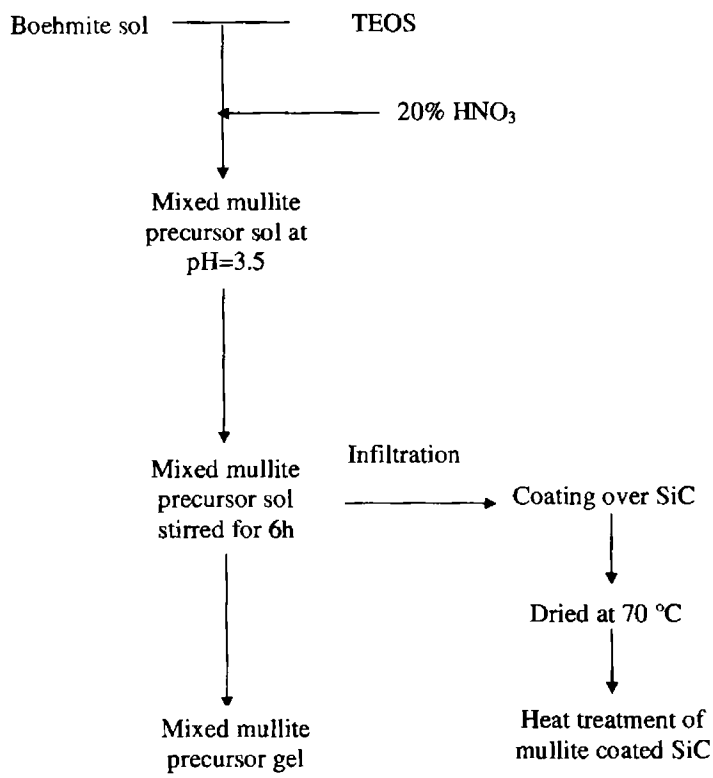

Figure 1. Flow chart for the synthesis of mullite precursor sol and coating over SiC

In a typical experiment 5.21 mL of TEOS was added drop wise to 262.11 mL of boehmite sol (5 g basis of mullite) during vigorous stirring, keeping the pH of the mixture at 3.5. The mixture was stirred for 6 h to achieve maximum homogeneity and then aged for 10 h at 30 °C.[34]

The particle size analysis was carried out using Laser Particle Size Analyzer keeping refractive index as 1 on the boehmite sol and mullite precursor sol (Zeta Sizer, Malvern Instruments UK). Five measurements were done and the average value was taken. The dried precursor was powdered and was subjected to DTA (DTA - 50H, Shimadzu, Japan) and TGA (TGA-50H, Shimadzu, Japan) analysis at a heating rate of 5 °C min^{-1} up to 1200 °C. Cylindrical pellet of size 6 mm diameter and 8 mm height made by uniaxial compaction (200 MPa) was used for the dilatometric studies by Thermo Mechanical Analyzer (TMA- 60H, Shimadzu, Japan) at a heating rate of 5 °C min^{-1} up to 1200 °C.

The viscosity of mixed sol was measured using RheoLab MC1 Reho viscometer, (Anton Paar (Physica) Germany).

The portion of precursor were further heat treated at temperatures 1200, 1250, 1300 °C respectively in muffle furnace at a heating rate of 3 °C min^{-1} and then subjected to X-ray analysis in the 2θ range of 20-60 Cu Kα (Philips PW 1170, The Netherlands).

The morphology of boehmite and mullite precursor powder calcined at 800 °C was observed under Transmission Electron Microscope (FEI, TECNAI 30 S- Twin (Netherlands)) operated at 300 kV and equipped with an energy-

dispersive X-ray analyzer (EDX). The powder was dispersed in acetone and a drop of the suspension was deposited on a carbon-coated copper grid (TEM) and dried. The substrate (SiC) was coated with mullite sol by infiltration method based on the gravitational flow of the sol. The coated substrate was further first slow dried at room temperature and then the substrate was sintered at 1300 °C for 2 h. The typical sintering schedule was as follows: RT to 800 °C at a rate of 3 °C min^{-1} and then up to the sintering temperatures at 10 °C min^{-1}. Microstructure was observed on fracture of sintered mullite coated SiC specimens using scanning electron microscopy (SEM, JEOL, JSM 5600 LV, Japan).

Gas permeation analysis of mullite coated SiC was also conducted. Gas permeability of the materials was studied using a permeability apparatus based on the ASTM standard and the flow chart is presented in **Figure 2.**[35] Air was passed through the chamber in which the sample is tightly held in a central hole of a thick polyurethane holder and two sensors measured the pressure in the inlet and outlet gas line at ambient temperature. A flow meter was used to determine the gas flow, Q, in litres per minute. The permeability of a porous material is governed by Darcy's law.[36,37]

Specific permeability = (Flow rate × Viscosity of air × Thickness) / (Pr.drop × Area) m^2

Where

Viscosity of Air = 1.84×10^{-5} P sec

Viscosity of nitrogen=1.75×10^{-5} P sec

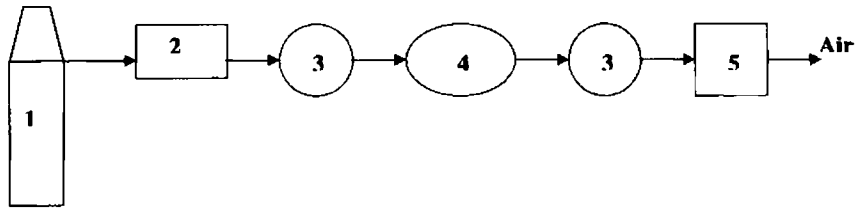

Figure 2. Schematic diagram of permeability apparatus used in this work

1- Air Supply, 2- Pressure valve, 3- Gas manometer, 4- Sample holder, 5- Gas flow meter

4.3 Result and Discussion

The particle size analysis of boehmite sol and the mixed sol (boehmite and TEOS) were measured by using Malvern zeta sizer (Zeta Sizer, Malvern Instruments UK). The average particle size of boehmite sol was 205 nm and the mixed sol shows an average particle size of 250 nm. Both the boehmite sol and mixed sol give mono modal particle size distribution (**Figure 3&4**). The mono modal distribution is due to the homogeneous mixing of boehmite and TEOS and also near identical particle size distribution.

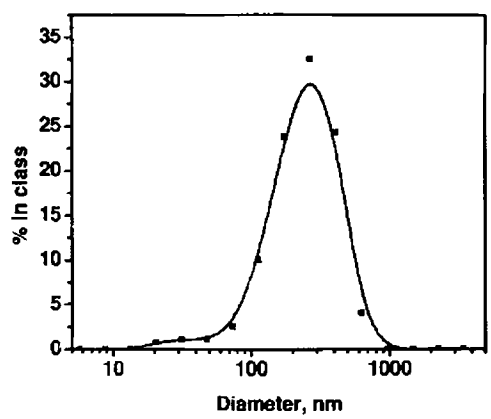

Figure 3. Particle size distribution of boehmite sol

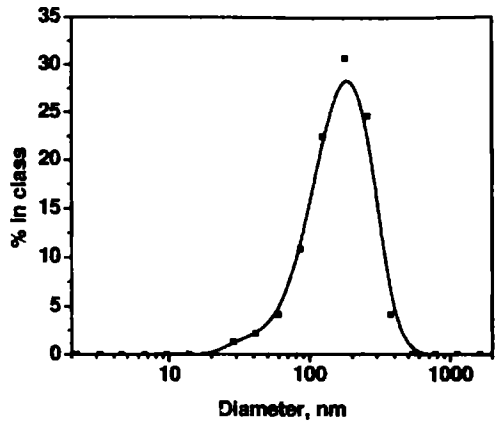

Figure 4. Particle size distribution of mixed sol

The viscosity of mixed sol was measured using Anton paar (Physica) Germany. The viscosity of the mixed sol was measured at a pH of 3.5. The viscosity was 0.35 cP at a shear rate of 800 s^{-1} (**Figure 5.**). The viscosity of the sol increases with increase in shear rate which is due to the shear thickening behaviour.[38]

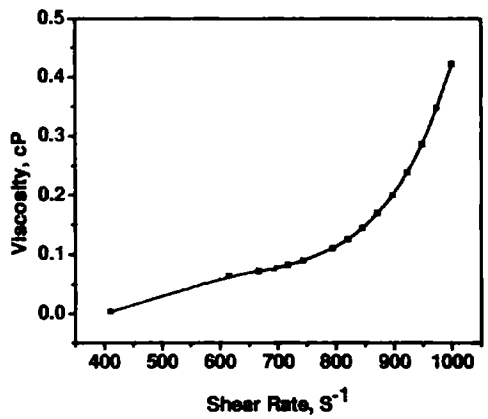

Figure 5. Viscosity measurement of mixed sol

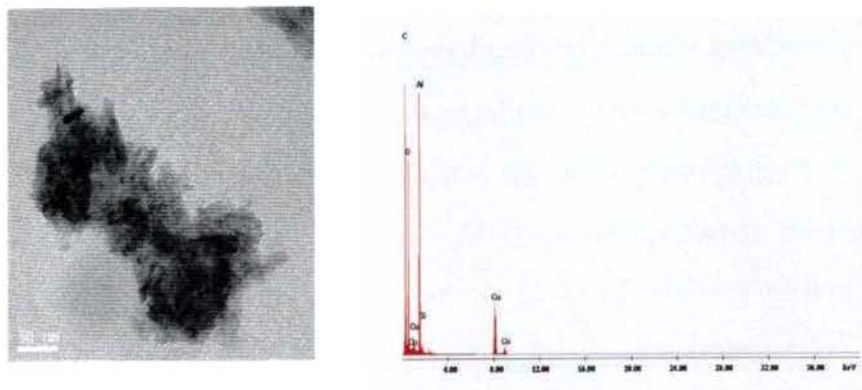

Figure 6. TEM image of aggregated boehmite sol particles calcined at 600 °C

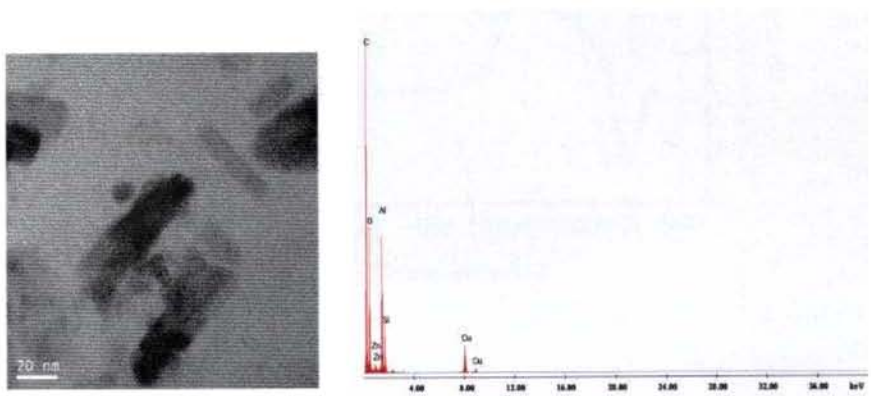

Figure 7. TEM image of mullite precursor sol particle calcined at 600 °C

The TEM observation indicates that boehmite particle has rod shaped morphology and mostly aggregated in the powder form when calcined at 600 °C (**Figure 6.**). The aggregation was due to formation of hydrogen bonding between the particles.[39] Lee et al. reported that acidic condition favoured the formation of nano rods of boehmite nano particle and basic condition favoured

the formation of nano flakes under hydrothermal condition. In other words, the acidic conditions are favourable for the formation of the 1D nanostructure, and the basic conditions favour the formation of the 2D nanostructures.[39] The mullite precursor calcined at 600 °C also shows rod shaped particle morphology (**Figure 7.**).

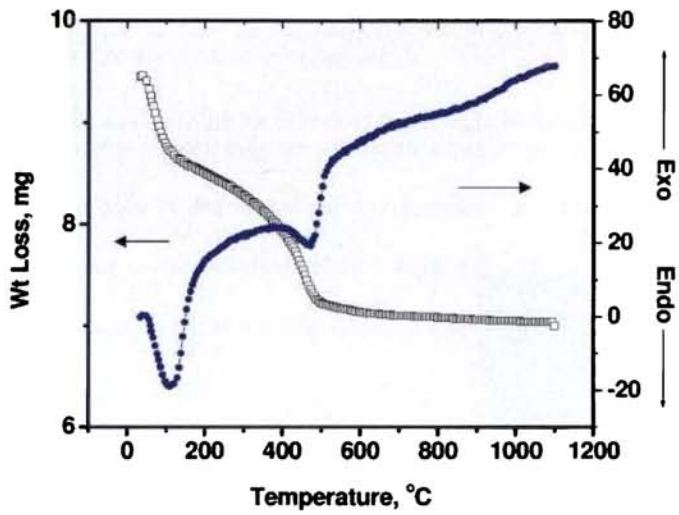

Figure 8. TG-DTA curve of the mullite precursor measured at heating rate 5 °C min^{-1} in the flow of air

To gain the insight into the formation behaviour of mullite from the diphasic mullite precursor, DTA was carried out and presented in the Fig.8. One exothermic peak is presented above the temperature 1100 °C, based on XRD results which were due to the formation of mullite. The thermogravimetric curve of the mullite precursor indicates a three step decomposition involving weight losses both due to absorbed water, the organics and the chemically bound gel water.[40] The major decomposition peak is supported by an endothermic transition at above 150 °C. The endotherm

above 400 °C could be due to the formation of precursor oxide phases along with the elimination of bonded water. The small exothermic peaks at higher temperature (above 1100 °C) are due to the formation of mullite from particulate precursor, based on XRD results the mullite formation start at 1200 °C and completed at 1300 °C.

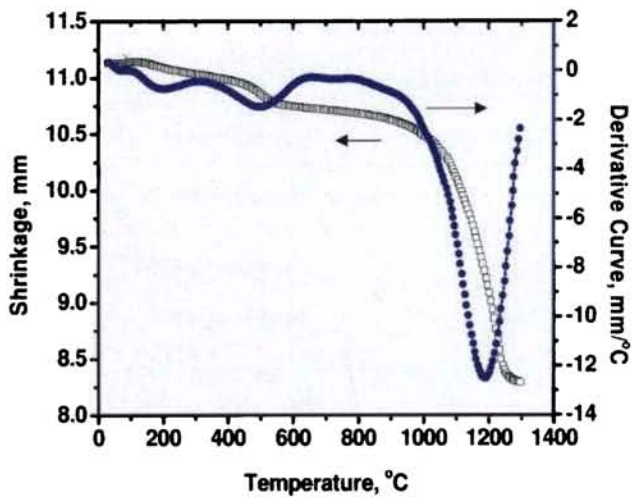

Figure 9. Differential shrinkage behaviour of mullite precursor.

The shrinkage and differential shrinkage behaviour of mullite precursor is shown in **Figure 9.** The gel shows very little shrinkage around 700 °C. Another shrinkage around 1200 °C indicates the formation of mullite.

The XRD patterns of the mullite precursor powder calcined at 1200, 1250, and 1300 °C are presented in the **Figure 10.** This indicates that the mullite formation starts at 1250 °C and highly crystalline phase of mullite is formed at 1300 °C (JCPDS- 15-0776). The low temperature formation of mullite is attributed to the homogeneous mixing of nano size boehmite and silica through the sol-gel process. As in a diphasic mullite gel, mullite

formation in the sample was likely through a nucleation and growth mechanism.[41]

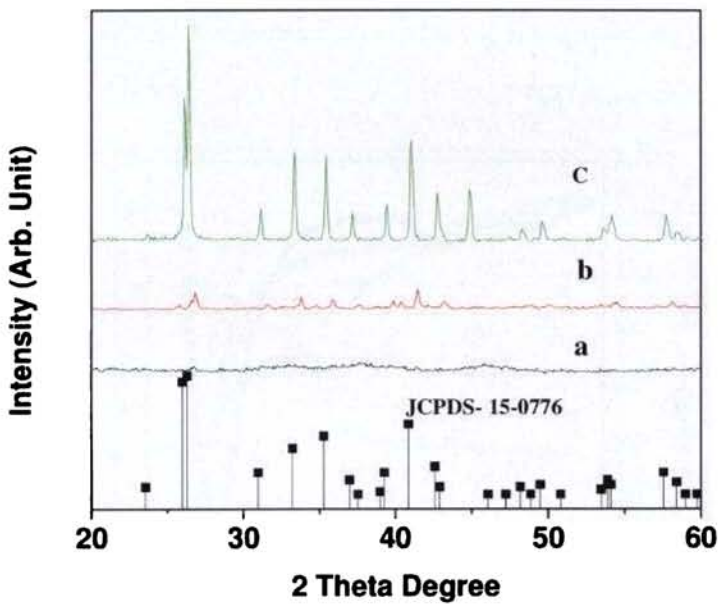

Figure 10. XRD analysis of mullite precursor calcined at (a) 1200 °C (b) 1250 °C and (c) 1300 °C

Enhanced phase formation was earlier reported for the samples prepared from γ-Al_2O_3-TEOS mixture compared to the precursor gel prepared from boehmite sol and TEOS.[42] However, the former one results in the formation of traces of α-Al_2O_3 phase also along with mullite, while the latter one directly transforms to phase-pure mullite. In diphasic precursors, the mullitization occurs mainly by the reaction between transitional alumina and silica or some times by transformation from Al-rich spinel to mullite. Another study has reported the possibility of transitional alumina β-crystobalite reaction.[43]

However, in the present study no β-crystobalite is observed, even at a high temperature, and the reaction to form mullite is observed to be between transitional alumina and amorphous silica.

4.3.1 Different Coating Methods Attempted

Different types of coating methods are attempted to understand the variation in the microstructure (**Figure 11**). 1) Vacuum infiltration 2) Infiltration method 3) Dip coating method. The vacuum infiltration and infiltration methods are more effective because these two methods cover most of the pores. Here we adopted the infiltration method for coating SiC disc.

1. Vacuum infiltration

   The substrate was kept in a beaker containing mullite precursor sol and place in a vacuum desicator and the vacuum was applied using a vacuum pump (pressure at 0.001 Torr, RPM= 600).

2. Infiltration method

   In infiltration method the sol was infiltrated through the substrate by gravitational flow of the mullite precursor sol.

3. Dip coating method

   In dip coating method the substrate was dipped in the precursor sol, held for 3min after which it was drawn and kept for drying.

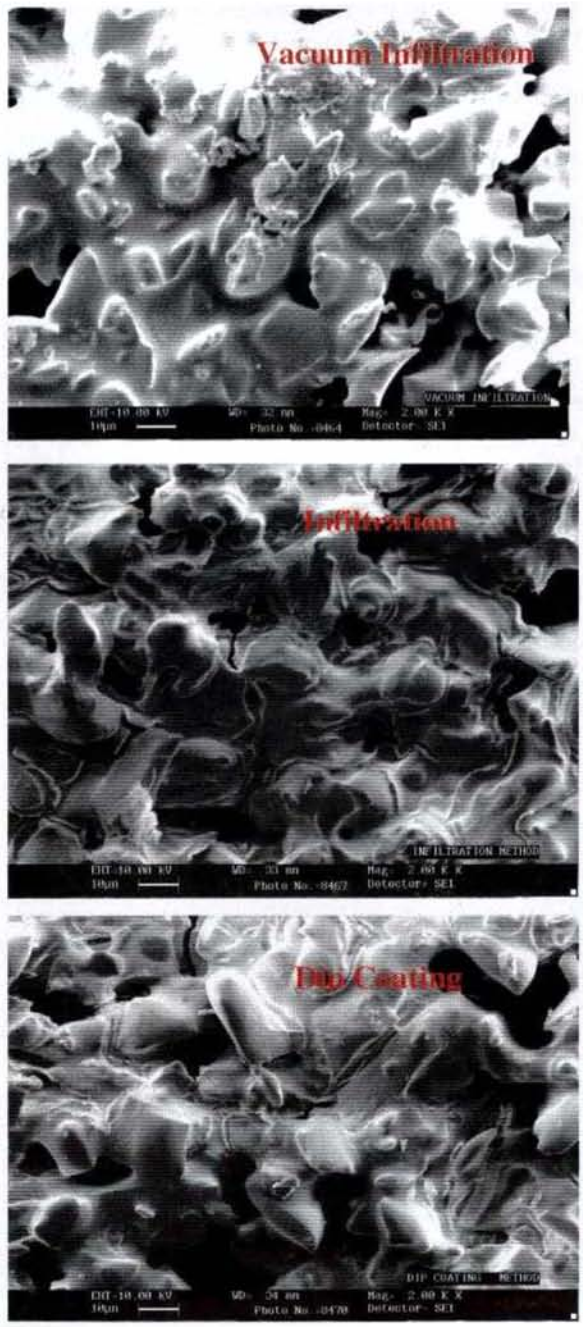

Figure 11. SEM of mullite coated SiC disc by different coating methods (the coating method is indicated in the SEM)

The SEM of SiC disc before coating indicated that the pore size distribution is in the range of 20-50 μm and presented in **Figure 12.** , the samples also show large amount of closed pores. **Figure 13.** shows the mullite precursor sol coated SiC disc calcined at 1300 °C in an inert atmosphere. The mullite grains have evenly covered the surface of SiC and the grain morphology is nearly spherical (**Figure 14.**). The mullite is coated in the pore channels without any crack.

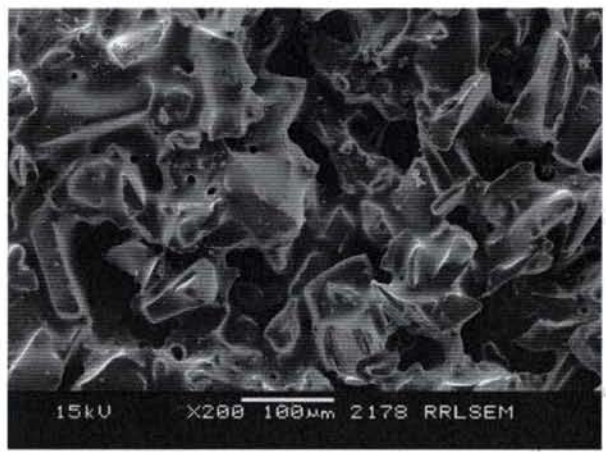

Figure 12. SEM of SiC disc

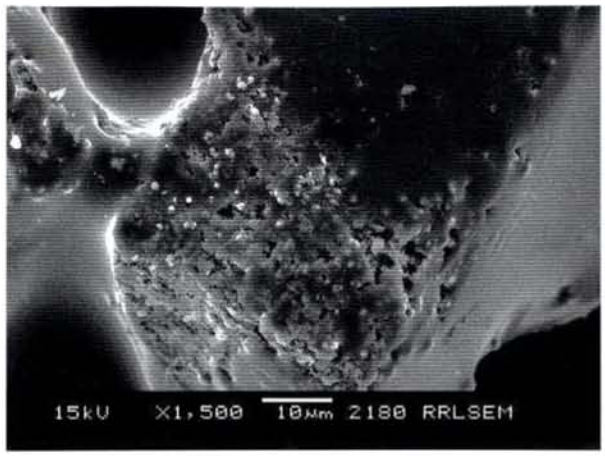

Figure 13. SEM of SiC disc coated with mullite precursor sol and fired at 1300 °C

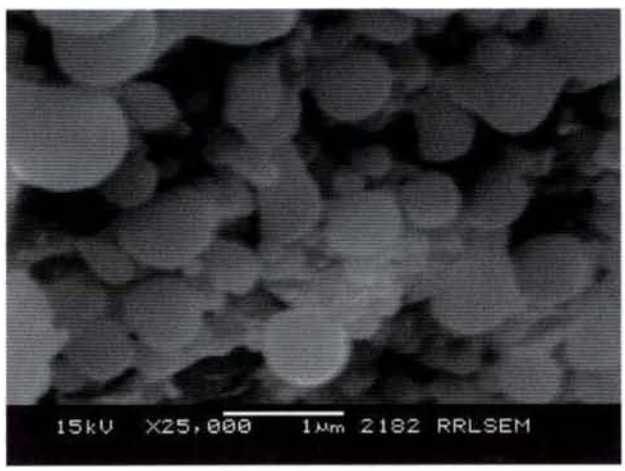

Figure 14. SEM of SiC disc coated with mullite precursor sol –size of coated particles < 500 nm and fired at 1300 °C

4.3.2 Boehmite Sol- High Solid Content

Boehmite sol having high solid content (by increasing the molar concentration of aluminium nitrate 0.9 M) was prepared through sol-gel route. The high solid content boehmite sol was achieved by varying the molar concentration of aluminium nitrate solution and the solid content was increased from 0.37 g/100 mL to 2.5 g/100 mL. The particle size analysis of boehmite sol and the mixed sol (boehmite and TEOS) were measured using Malvern zeta sizer (Zeta Sizer, Malvern Instruments UK). The average particle size of boehmite sol was 165 nm and the mixed sol shows an average particle size of 170 nm. Both the boehmite sol and mixed sol give mono model particle size distribution (**Figure 15 & 16.**).

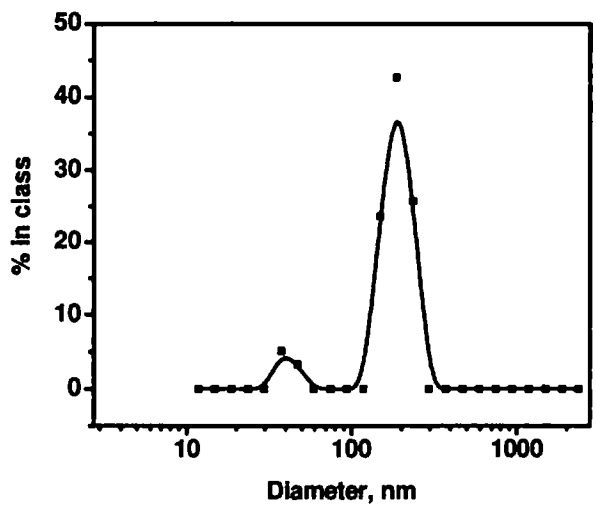

Figure 15. High solid content boehmite particle size

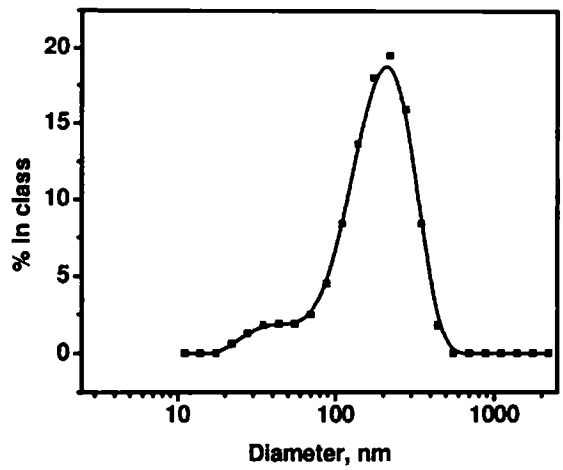

Figure 16. Particles size analysis of mullite precursor having high alumina content

The viscosity of the mixed sol was measured at a pH of 3.5. The viscosity of mullite precursor sol having high boehmite content shows a viscosity of 6 cP at a shear rate 800 s^{-1} as presented in **Figure 17.** which is higher than the low content boehmite mullite precursor sol.

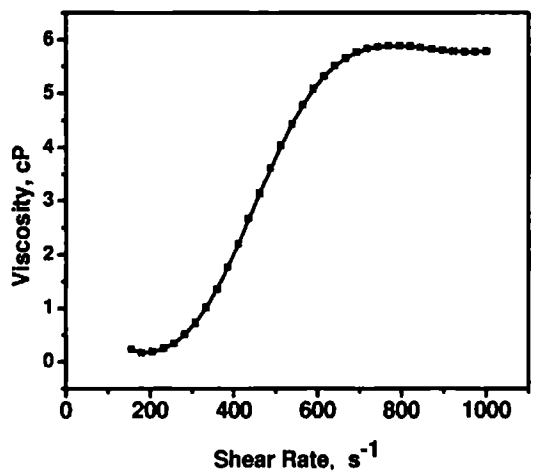

Figure 17. Viscosity of Mullite precursor having high solid content

The viscosity of the sol increases with increase in shear rate which is due to the shear thickening behaviour. The modified mullite precursor sol was used to obtain a thicker coating over SiC disc. The stereo microscope image indicated that the particles are much more packed in the coated sample compared to the uncoated SiC disc (**Figure 18.**).

Figure 18. Stereo microscope image (1000 X) of SiC disc coated with thicker mullite precursor sol

Figure 19. show the high boehmite content mullite precursor sol coated SiC disc calcined at 1300 °C under an inert atmosphere. The mullite is coated at pore channel of SiC were the mullite coating appears to be much thicker than the coating of mullite using low boehmite content.

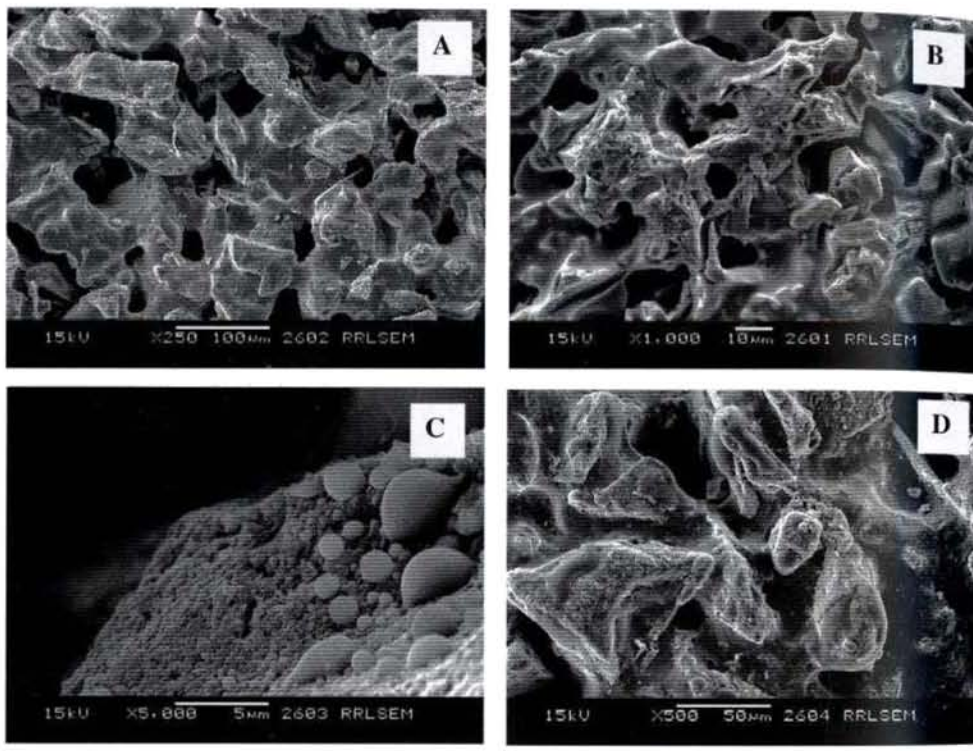

Figure 19. SEM of SiC (A,B, C, D) coated with high alumina content- mullite precursor sol fired at 1300 °C

4.3.3 Gas Permeation Study on Mullite Coated SiC Disc

The gas permeation analysis of mullite coated SiC disc was conducted at BHEL Bangalore. The SiC disc was coated with mullite precursor sol for 3 to 4 times. The gas permeation analysis indicates that mullite is found to be coated on the SiC surface hence a pressure drop was found in the gas permeation analysis for 3 and 4 times mullite coated SiC samples (**Figure 20.**).

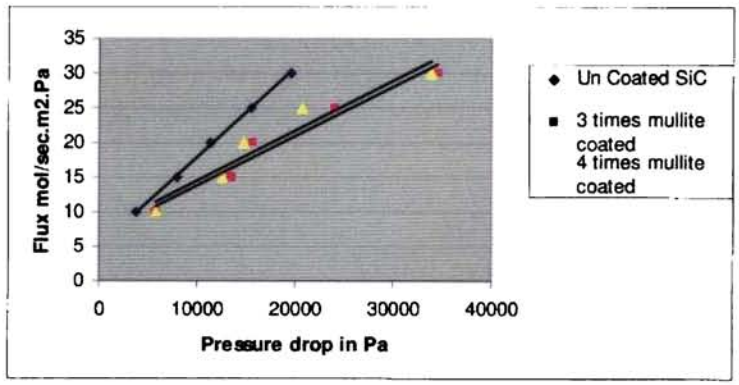

Figure 20. Gas permeation analysis of mullite coated SiC disc

4.3.4 Sol- Particle Size Variation

In order to increase the particle size of the coating precursors and also the thickness of the coatings, the particle size of mullite precursor sol was varied by the addition of mullite precursor powder and further stabilising the sol using glycerine as a dispersant (2 wt%). The powder addition varied from 2 wt% to 20 wt% and the sol was stabilised at a pH of 3.5. This method is effective in varying the particle size from 217- 1021 nm. Particle size of modified mullite precursor sol was measured using Malvern Zeta Sizer (**Figure 21.**). The sample with powder addition of 10 wt% and 20 wt% shows a bi-model particle size distribution because the sol was not completely stabilised. This shows that above 10wt% addition of mullite precursor powder needed more amount of dispersant to the stabilise the sol. Higher the solid content in the sol greater is the chance to peel off the coating after drying.

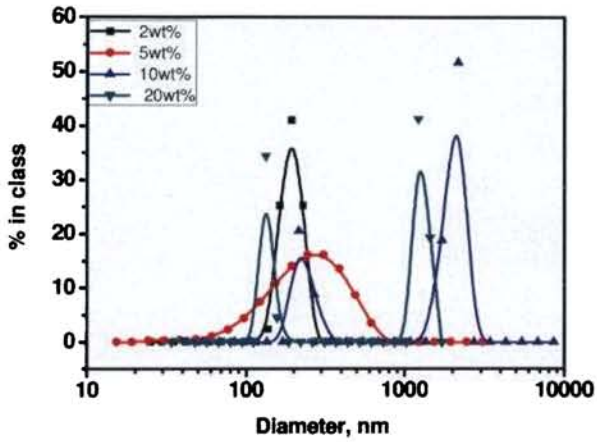

Figure 21. Particle size distribution of mullite precursor sol containing different weight percentage addition mullite precursor powder.

Table 1. Particle size results of mullite precursor powder added mullite precursor sol

No	Mullite added in wt%	Average particle size (nm)
1	2	217
2	5	346
3	10	643
4	20	1021

The surface of mullite coated SiC after heat treatment at 1300 °C inert atmosphere was analysed using X-ray diffraction (**Figure 22 & 23.**). This clearly coincided with the XRD analysis mullite precursor powder calcined at

1300 °C, which was also indicating the presence of mullite formation at low temperature.

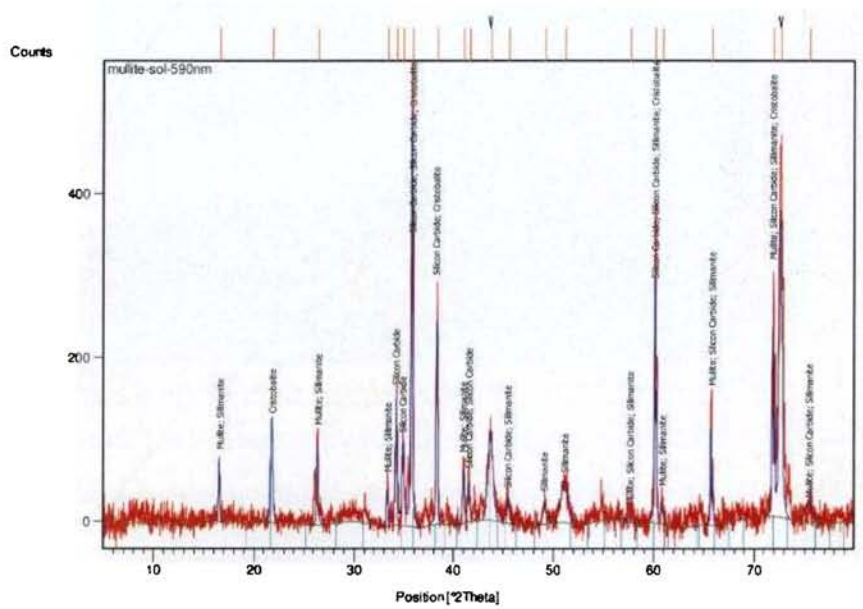

Figure 22. Surface *XRD* of mullite coated on SiC substrate fired at 1300 °C

Table 2. XRD pattern list

Ref. Code	Score	Compound Name	Scale Factor	Chemical Formula
00-006-0258	23	Mullite	0.168	3 Al_2O_3 2 SiO_2
00-031-1232	49	Silicon Carbide	0.593	Si C
00-049-1429	23	Silicon Carbide	0.357	Si C

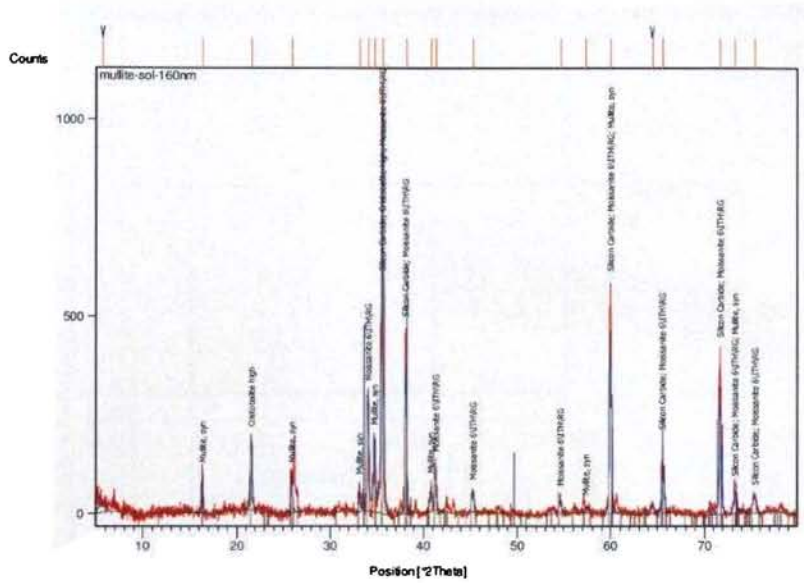

Figure 23. Surface XRD of mullite precursor +10 wt% mullite precursor powder coated on SiC substrate fired at 1300 °C

Table 3. XRD pattern list

Ref. Code	Score	Compound Name	Scale Factor	Chemical Formula
01-089-1396	30	Silicon Carbide	0.559	Si C
01-082-1237	16	Mullite, syn	0.110	Al5.65 Si0.35 O9.175

The SEM micrographs of fractured mullite coated SiC disc clearly indicate the presence of above 3 μm thickness mullite coating on SiC substrate and presented in **Figure 24.** The SEM micrograph also shows the presence of mullite in needle like shapes (**Figure 25.**).

Figure 24. SEM micrograph of mullite coated SiC disc fired at 1300 °C.

Figure 25. SEM micrograph of mullite coated SiC disc fired at 1300 °C

The SEM indicates 2-5 µm long and 0.2-0.4 µm thick mullite needles typical of morphology of mullite derived in presence of silica. The silica originated either from the mullite precursor or from the glassy phase available

on the surface of the sintered SiC as a result of partial oxidation. However, these mullite needles will provide sufficient compressive stress at the coating-SiC interfaces and it could be maintained that the coatings could have adherence. The needle like mullite formation is also dependent on the heat treatment schedule adopted in this work. More importantly, needle like mullite has better thermal shock resistance and mechanical properties than granular mullite because of "jigsaw" bonds among the particles.[44] Okada et al. reported that synthesis of the needle like mullite particle as well as mullite fiber or whisker is strongly dependent upon starting materials and synthesizing methods.[45]

According to literature, the sintering temperature strongly influences the grain shape of mullite.[46] The effects of the initial pH conditions of the sol on the final formation and morphology of mullite were considered based on Ring's study.[47] Ring suggested a model for the effects of initial pH conditions on the gelation and growth of silicon ethoxide in a non aqueous system. In acidic solutions, hydrolysis is achieved by a bimolecular displacement mechanism that substitutes a hydronium ion (H^+) for alkyl, showing rapid hydrolysis, compared to condensation of the hydrolyzed monomers. Therefore, the acidic conditions promote the development of larger and more linear molecules. Under basic conditions, hydrolysis occurs by nucleophilic substitution of hydroxyl ions (OH^-) for alkyl groups. Here hydrolysis is rapid, relative to condensation. Huang et al. reported that the formation of a glass phase at high temperature leads to the formation of rod like mullite grains due

to enhanced the anisotropic grain growth of mullite.[48] Matsuda et al. reported that addition of float glass in a kaolin or kaolin/Al_2O_3 mixture significantly enhanced the formation of needle like mullite grains in the sintered samples.[49] It is also reported that needle like mullite grains increases the mechanical properties of coating.[50]

4.4 Conclusions

The mullite precursor sol was prepared using sol-gel method. The average particle size of boehmite sol and mullite precursor sol was measured and it was found to be 205 nm and 250 nm respectively. The mullite precursor sol was used to coat the as received BHEL SiC disc. The coated samples were further treated at 1300 °C under an inert atmosphere. The SEM observation of coated SiC disc indicated that mullite is coated at the pore channels without crack. Thicker coating in the range 300 nm was also possible over SiC using a modified mullite precursor sol. The morphology of coating was observed under stereo microscope.

The mullite precursor sol having high boehmite content was prepared using sol-gel method. The high solid content boehmite sol was prepared by varying the molar concentration of aluminium nitrate solution and the solid content was increased from 0 .37 g/100 mL to 2.5 g/100 mL. The average particle size of boehmite sol and mullite precursor sol was measured and it was found to be 165nm and 170nm respectively. The SEM analysis shows that the coating appears to be much thicker than the mullite coating using boehmite sol having low solid content. The high solid loading in boehmite sol increases the mullite coating thickness to 3 μm. The gas permeation analysis of mullite coated SiC disc shows that mullite coated on SiC disc results in decrease in pressure.

The particle size of mullite precursor was varied by the addition of mullite precursor powder. The coating thickness was not varied much and high

solid content mullite precursor coating increases the coating thickness of mullite on SiC substrate but the thicker coating peals off during drying. Up to 2 wt% addition of mullite precursor powder will give a smooth coating.

The XRD surface characterisation of mullite coated SiC disc shows that the mullite is coated on the SiC disc. The SEM indicates 2-5 μm long and 0.2-0.4 μm thick mullite needles typical of morphology of mullite derived in presence of silica. These mullite needles impart compressive strength at the coating interface of mullite and SiC particles. Mullite coating thickness of above 3μm was achieved through the present sol-gel method.

References

1. J. Stringer, A. J. Leitch, *J. Eng. Gas Turb. Powder.* **1992,** 114, 371.
2. M. A. Alvin, T. E. Lippert, J. E. Lane, *Am. Ceram. Soc. Bull.* **1991,** 70, 1491.
3. J. E. Oakey, I. R. Fantom, *Mater. High. Temp.* **1997,** 14, 337.
4. M. A. Alvin, *Mater. High. Temp.* **1997,** 14, 355.
5. D. A. Barrow, T. E. Petroff, M. Sayer, *Surf. Coat. Tech.* **1995,** 76-77, 113.
6. P. Greil, *Adv. Mater.* **2002,** 14, 709.
7. J. H. She, Z. Y. Deng, J. D. Doni, T. Ohji, *J. Mater. Sci.* **2002,** 37, 3615.
8. L. Montanaro, Y. Jorand, G. Fantozzi, A. Negro, *J. Eur. Ceram. Soc.* **1998,** 18,1339.
9. X. Zhu, D. Jiang, S. Tan, *Mater. Sci. Eng. A.* **2002,** 323, 232.
10. Z. Shi, J. Lee, D. Zhang, H. Lee, M. Gu, R. Wu, *J. Mater. Tech.* **2001,** 110, 127.
11. W. L. Vaughn, H. G. Maahs, *J. Am. Ceram. Soc.* **1990,** 73, 1540
12. C. E. Ramberg, G. Cruciani, K. E. Spear, R. E. Tressler, C. F. Ramberg, *J. Am. Ceram. Soc.* **1996,** 79, 730
13. O. Lujt, *J. Am. Ceram. Soc.* **1997,** 80, 1544
14. Y. J. Lin, L. J. Chen, *Ceram. Int.* **2000,** 26, 593.
15. J. He, C. B. Ponton, *J. Mater. Sci.* **2008,** 43, 4031.
16. H. Schneider, K. Okada, J. A. Pask, Mullite and Mullite Ceramics. Wiley, New York, **1994.**
17. K. N. Lee, *J. Am. Ceram. Soc.* **1998,** 81, 3392.
18. I. A. Aksay, D. N. Dabbs, M. Sarikaya, *J. Am. Ceram. Soc.* **1991,** 74, 2343.
19. S. Prochazka, F. J. Klung, *J. Am. Ceram. Soc.* **1983,** 66, 874.
20. K. Okada, N. Otsuka, S. Somiya, *Am Ceram. Soc. Bull.* **1991**, *70*, 1633.
21. P. S. Aggrawal, *Glass.Ceram. Bull.* **1975**, *22*, 19.
22. S. Rajendran, H. J. Rossell, J. V. Sanders, *J. Mater. Sci.* **1990**, *25*, 4462.

23. D. Hoffman, R. Roy, S. Komerneni, *J. Am. Ceram. Soc.* **1984**, *67*, 468.

24. S. Komerneni, Y. Suwa, R. Roy, *J. Am. Ceram. Soc.* **1986**, *69*, C155.

25. C. W. Turner, *Am. Ceram. Soc. Bull.* **1991**, *70*, 1487.

26. A. K. Chakravorthy, D. K. Ghosh, *J. Am. Ceram. Soc.* **1988**, *71*, 978.

27. M. G. M. U. Ismail, Z. Nakai, S. Somiya, *J. Am. Ceram. Soc.* **1987**, *70*, C-7.

28. S. M. Zemskova, J. A. Haynes, K. M. Cooley, *J. Phys. IV*, **2001**,11 [PR3], 861.

29. K. L. Luthra, *J. Am. Ceram. Soc.* **1991**, 74, 1095.

30. M. L. Auger, V. K. Sarin, *Int. J. Refract. Met. H.* **2001**, 19, 479.

31. K. N. Lee, R. A. Miller, N. S. Jacobson, *J. Am. Ceram. Soc.* **1995**, 78, 705.

32. T. Damjanovic, C. Argirusis , G. Borchardt , H. Leipner , R. Herbig , G. Tomandl, R. Weiss, *J. Eur. Ceram. Soc.* **2005**, 25, 577.

33. H. K. Varma, T. V. Mani, A. D. Damodaran, K. G. K. Warrier, *J. Am. Ceram. Soc.* **1994**, 77, 1597.

34. G. M. Anilkumar, U. S. Hareesh, A. D. Damodaran, K. G. K. Warrier, *Ceram. Int.* **1997**, 23, 537.

35. ASTM Standards, Standard Test Method for Permeability of Refractories. Annual Book of ASTM Standards (ASTM, Philadelphia, **1999**) 99, C 577.

36. The Physics of Flow through Porous Media, A. E. Scheidegger, University of Toronto Press, Toronto, **1974**.

37. E. A. Moreira, M. D. M. Innocentini, J . R. Coury, *J. Eur. Ceram. Soc.* **2004**, 24, 3209.

38. A. Seal, D. Chattopadhyay, A. Das Sharma, A. Sen, H. S. Maiti, *J. Eur. Ceram. Soc.* **2004**, 24, 2275.

39. X. Y. Chen, S. W. Lee, *Chem. Phys. Lett.* **2007**, 438 279.

40. G. M. Anilkumar, P. Mukundan, K. G. K. Warrier, *Chem. Mater.* **1998**, 10, 2217.

41. M. Kumagai, G. L. Messing, *J. Am. Ceram. Soc.* **1985**, 68, 500.

42 P. Padmaja, G. M. Anilkumar, K. G. K. Warrier, *J. Eur. Ceram. Soc.* **1998,** 18, 1765.

43. W. G. Fahrenholtz, D. M. Smith, *J. Am. Ceram. Soc.* **1993**, *76*, 4333.

44. B. L. Metcalfe, J. H. Sant, *Trans. J. Brit. Ceram. Soc.* **1995,** 74, 193.

45. K. Okada, N. Otuska, *J. Am. Ceram. Soc.* **1991,** 74, 2414.

46. J. Leivo , M. Linden , J. M. Rosenholm, M. Ritola , C. V. Teixeira , E. Levanen , T. A. Mantyla, *J. Eur. Ceram. Soc.* **2008,** 28, 1749.

47. Fundamentals of Ceramic Powder Processing and Synthesis T.A. Ring, Academic Press, New York, **1996,** 340.

48. T. Huang, M. N. Rahaman, T. I. Mah, T. A. Parthasarathay, *J. Mater. Res.* **2000,** 15, 718.

49. O. Matsuda, T. Watari, T. Torikai, Y. Yamasaki, H. Katsuki, *J. Ceram. Soc. Jpn.* **1992,** 100, 725.

50. X. Jin, L. Gao, *J. Am. Ceram. Soc.* **2004,** 87, 706.

SUMMARY

Ceramic matrix composites combine reinforcing ceramic phase with a ceramic matrix to create materials with new and superior properties. The primary goal of the ceramic reinforcement is to enhance characteristics such as toughness, electrical conductivity, thermal conductivity, thermal expansion coefficient, thermal shock resistance and hardness. The combination of these characteristics makes ceramic matrix composites attractive alternatives to traditional ceramic materials and often substitute conventional metal matrix such as high alloy steels and refractory metals. The increasing industrial application of nanocomposites in the field of thermal, electronic, machinable and biological fields have generated considerable interest in developing nanocomposites. One of the recent approach to achieve uniform dispersion of minor constitutes in ceramic composite systems, is by sol-gel core shell approach in addition to the conventional route based on solid state method. The alumina-aluminium titanate composite exhibits functional as well as structural properties for application such as low thermal expansion, high thermal shock, thermal barrier coating, exhaust filter components for diesel engines and high temperature ceramic substrates. Due to the nearly similar thermal expansion coefficients of Al_2O_3 and $LaPO_4$, their composites were widely investigated for applications like machinability and were found to be chemically inert. The thesis entitled **"Sol-Gel Alumina Nano Composites for Functional Applications"** investigates sol-gel methods for the synthesis of alumina

nanocomposites with special reference to alumina-aluminium titanate and alumina-lanthanum phosphate composites.

Formation of aluminium titanate (AT) has been achieved at a low temperature of 1320 °C through sol-gel process using boehmite and titanium hydroxide as precursors by controlling the particle size at nano scale followed by in-situ peptisation. DTA and XRD analysis have been performed to confirm the formation of AT. Aluminium titanate having 94% relative density was obtained at 1550 °C with controlled grain size in the range 2-3 μm.

A simple sol-gel based core-shell approach for the synthesis of alumina-aluminium titanate composite was successfully developed where alumina is the core and titania is the shell. The coating of titania has been performed in aqueous medium on alumina particle by means of heterocoagulation of titanyl chloride. Further heat treatment results in low temperature formation of aluminium titanate as well as low temperature sintering of alumina-aluminium titanate composites. The lowering of the reaction temperature can be attributed to the maximization of the contact surface between the reactants due to the core-shell approach involving nano particles. The mechanism of formation of aluminium titanate and the densification features in the present process are compared with that of mixture of oxides under identical conditions. The sintered alumina-aluminium titanate composite has an average grain size of 2 μm. The composite can be sintered at 1350 °C to 98% density with 1.5 to 2.0 μm grain size. Other composites containing 5-50 wt% aluminium titanate were also sintered at a low temperature. The thermal shock resistance of in situ-

formed alumina –AT composites was evaluated by water-quenching technique. Alumina with 20wt% addition of aluminium titanate shows excellent thermal shock resistance as indicated by critical temperature differential without fracture.

Machining is emerging as an inevitable requirement for flexible use of advanced ceramics, especially for structural ceramics. However, the extremely high hardness of ceramics makes conventional machining very difficult or even impossible. The synthesis of grain size controlled Al_2O_3-$LaPO_4$ has been done by sol-gel method. The low temperature sintering of Al_2O_3-$LaPO_4$ is achieved at 1450 °C. The strength and hardness Al_2O_3-$LaPO_4$ composite decreases with increasing the addition of $LaPO_4$. In the grinding tests on the Al_2O_3, Al_2O_3-30$LaPO_4$, $LaPO_4$, show that the mean surface removal rate for the $LaPO_4$ is the highest. The mean surface removal rate for Al_2O_3-30$LaPO_4$ is higher compared to Al_2O_3 by a factor of 2. This was a good indication of better machinability of alumina-lanthanum phosphate compared to alumina.

Films and coatings represent the earliest commercial use of sol-gel processing. Sol-gel films can be deposited by spraying, dip coating, and spin coating. Sol-gel techniques offer the following advantage in coating, control of microstructure, pore size and surface area. By controlling these parameters, the film properties can be tailored. Irregularly shaped surface can also be coated. Porous film can be prepared by changing the reaction conditions and the amount of porosity in a sol-gel derived film can be controlled by the pH. A dense mullite coating having thickness of 3 μm on SiC porous substrates was

successfully produced by coating a sol-gel mullite precursor at low temperature heat treatment at 1300 °C. The low tempearture formation of mullite was characterised by XRD. Mullite grains formed on the SiC have needle like morphology. The mullite formation has been explained on the basis of reaction between the silica-alumina nano precursor and the needle like morphology has been similar to that formed from a liquid phase. The gas permeation analysis showed that there is considerable difference between gas pressure while using SiC substrate before and after coating and hence clearly indicated reduction in pore size.

The thesis covers a systematic investigation of sol-gel core shell approach for the preparation of ceramic matrix composites for various applications like alumina-aluminium titanate composite for low thermal expansion, high thermal shock and alumina-lanthanum phosphate composite for machinable ceramic. Sol-gel mullite coating on SiC substrate for hot gas filtration applications is also investigated. The products developed as part of the investigation are shown below.

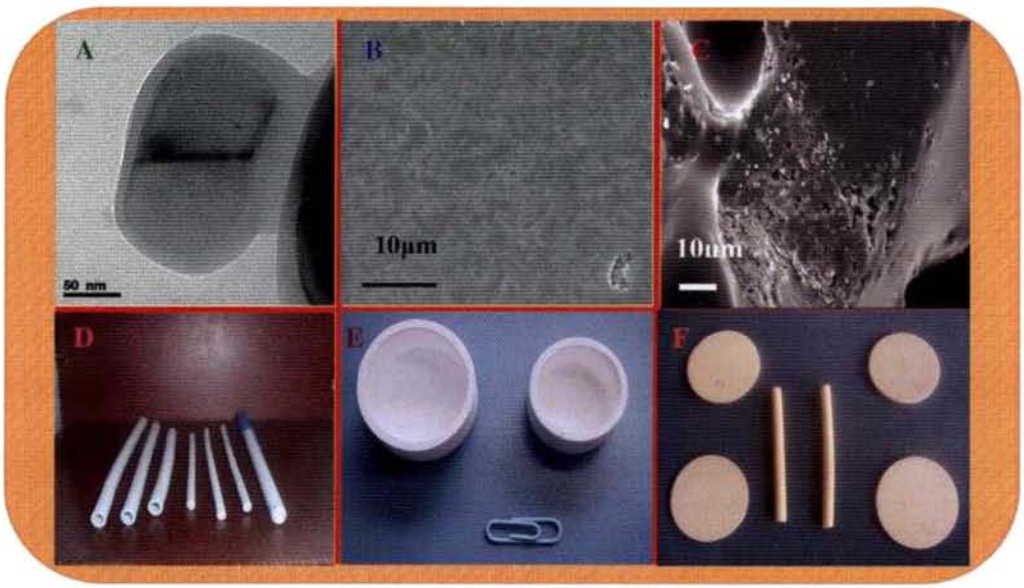

(A) Titania coated alumina particle (B) Grinded Al_2O_3- $LaPO_4$ composites (C) Mullite coated SiC (D) Al_2O_3-AT tubes (E) Al_2O_3-AT crucibles (F) Al_2O_3-AT disc and rods

List of Publications

1. **M. Jayasankar**, S. Ananthakumar, P. Mukundan, W. Wunderlich, K. G. K. Warrier, Al_2O_3 @ TiO_2- A simple strategy to synthesis low temperature sintered alumina-aluminium titanate composite through core-shell approach, **Journal of Solid State Chemistry,** 181 (2008) 2748.
2. **M. Jayasankar**, S. Ananthakumar, P. Mukundan, K. G. K. Warrier, Low temperature fine grained alumina-aluminium titanate composites produced from a titania coated alumina precursor, **Journal of American Ceramic Society,** 90 (2007) 3091.
3. **M. Jayasankar**, S. Ananthakumar, P. Mukundan, K. G. K. Warrier, Low temperature synthesis of aluminium titanate by an aqueous sol-gel route, **Material Letters,** 61 (2007) 790.
4. S. Ananthakumar, **M. Jayasankar**, K. G. K. Warrier, Microstructure mechanical and thermal characterisation of sol-gel derived aluminium titanate-mullite composites, **Acta Materialia,** 54 (2006) 2965.
5. K. Rajesh, K. V. Baiju, **M. Jayasankar,** K. G. K. Warrier, A facile aqueous sol-gel process for the synthesis of alumina-lanthanum phosphate nanocomposites, **Journal of American Ceramic Society,** 91 (2008) 2415.
6. S. Ananthakumar, **M. Jayasankar**, K. G. K. Warrier, Microstructure and high temperature deformation characteristic of sol-gel derived aluminium titanate-mullite composites, **Material Chemistry and Physics,** 117 (2009) 359.

Conference Papers and Posters

1. M. Jayasankar, S. Ananthakumar, P. Mukundan, K. G. K. Warrier, Fine grained aluminium titanate and alumina matrix composite for low thermal expansion and thermal Shock applications, In National Metallurgists Day Annual Technical Meet 2004 held at Triruvanathapuram.
2. K. Rajesh, K.V. Baiju, M. Jayansankar, P. Mukundan, K.G. K. Warrier Nanosize rare earth phosphate particulates for versatile applications, paper presented in National Seminar on Nanotechnology, All Saints College, Trivandrum, India, 17-18th August, 2006.
3. M. Jayasankar, K Rajesh, S. Ananthakumar, P. Mukundan, K. G. K. Warrier, Development of high thermal shock resistance alumina composites by in-situ formation of aluminium titanate phase, International Seminar on Ceramics, CeraTec 2007, Visakhapatnam, India 8th to 10th January 2007. **Best poster award**
4. M. Jayasankar, S. Ananthakumar, P. Mukundan, K. G. K. Warrier, Sol-gel process for the synthesis in-situ formed alumina-aluminium titanate composites with high thermal shock resistance, Oral presentation. National Seminar, IIM TVM chapter, 1-2 March. 2007.
5. Athira N. Raj, M. Jayasankar , K. Rajesh , P. Mukundan, K. G. K. Warrier, High density nanocrystalline $LaPO_4$:Y_2O_3 composite for high temperature application by room temperature aqueous sol-gel process, Indian Ceramic Society Conference at Jaipur 2009 **Best poster award**
6. M. Jayasankar, S. Ananthakumar, P. Mukundan, K. G. K. Warrier Low temperature sintered alumina-aluminium titanate composite through sol-gel coating technique, Indian Ceramic Society Conference at Trivandrum 2009 **Best poster award**